Development of UoYTube Detector for Ionising Radiation

Jennifer Louise Corkhill

Master of Science by Research

University of York

Physics

September 2016

Abstract

This thesis describes the testing of several prototype detectors, designed to be used in a radiation detector called the UoYTube. This detector can be used to detect charged particles emitted in fusion evaporation reactions.

In this work, several UoYTube prototypes were designed, fabricated and characterised/tested. These included prototypes with different scintillator crystals (Caesium Iodide and plastic), prototypes with different geometries (truncated pyramid and cuboid), and prototypes that included different types of light guides (Acrylic and 3D Printed).

These prototypes were characterised in terms of the signal-to-noise ratio, the optimum bias value, the energy resolution, the Acrylic versus 3D-Printed light guides, the number of counts and the optimum amplifier shaping time. Two different methods used to fabricate light guides (one 3D Printed and the other with the HURCO VMX60m Machining Centre), are also described. The light guides were then characterised and compared to each other in terms of their light output, energy resolution, and the optimum shaping time.

Using these results, it was inferred that the plastic scintillator (with a truncated pyramid geometry) demonstrated the highest signal-to-noise ratio. The plastic scintillator (with a truncated pyramid geometry) and Caesium Iodide scintillator (with a truncated pyramid geometry), demonstrated a range of the optimum bias values, over which there was little variation in the measured signal-to-noise ratio. The Caesium Iodide scintillator (with a truncated pyramid geometry), demonstrated good energy resolution. The transmittance of light from the spectrometer through the 3D Printed light guide was significantly poorer than that of the acrylic light guide. The difference in recorded energy resolution between the light guides was not very significant. The recorded number of counts was greater for the Acrylic light guide, when compared to the 3D Printed light guide. It was also concluded that both the acrylic and 3D Printed light guided prototypes should be operated with the highest values of shaping time, corresponding to the best resolution. These results were then used to decide upon the optimum design for the next generation UoYTube detector.

Contents

List of Figures

List of Tables

Acknowledgements

I would like to thank my supervisor Professor David Jenkins for his support with this research. I also acknowledge Dr Pankaj Joshi, Mr Bob Hide, Mr Dave Coulthard and Mr Jason Flatt, who helped with the experimental work. Thanks are also due to Miss Laura Sinclair, who gave constructive feedback on the write-up of this thesis. I would also like to thank my second supervisor Professor Robert Wadsworth and my internal examiner Professor Michael Bentley, who both gave meaningful feedback on my thesis write-up, which was very important when considering how my work could be improved. Thanks are also due to Mr James Cubiss, who helped with my calculations and the analysis of my data sets.

Declaration of Authorship

I hereby declare that the thesis entitled “Development of UoYTube detector for Ionising Radiation” has been carried out in the Department of Physics, at the University of York, in the United Kingdom, under the guidance of Professor David Jenkins and Professor Robert Wadsworth. The work is original and has not been submitted in part or full by myself for any degree or diploma at any other University.

I further declare that the material obtained from other sources has been duly acknowledged in the thesis.

1. Introduction and Motivation

The radiation detector which will be the subject of this thesis is called the University of York Tube, or UoYTube. The purpose of the UoYTube is to detect charged particles emitted in fusion evaporation reactions. The original UoYTube was developed in 2013 [1] and consisted of 96 CsI (Tl) scintillators crystals, arranged as shown in Figure 1: -

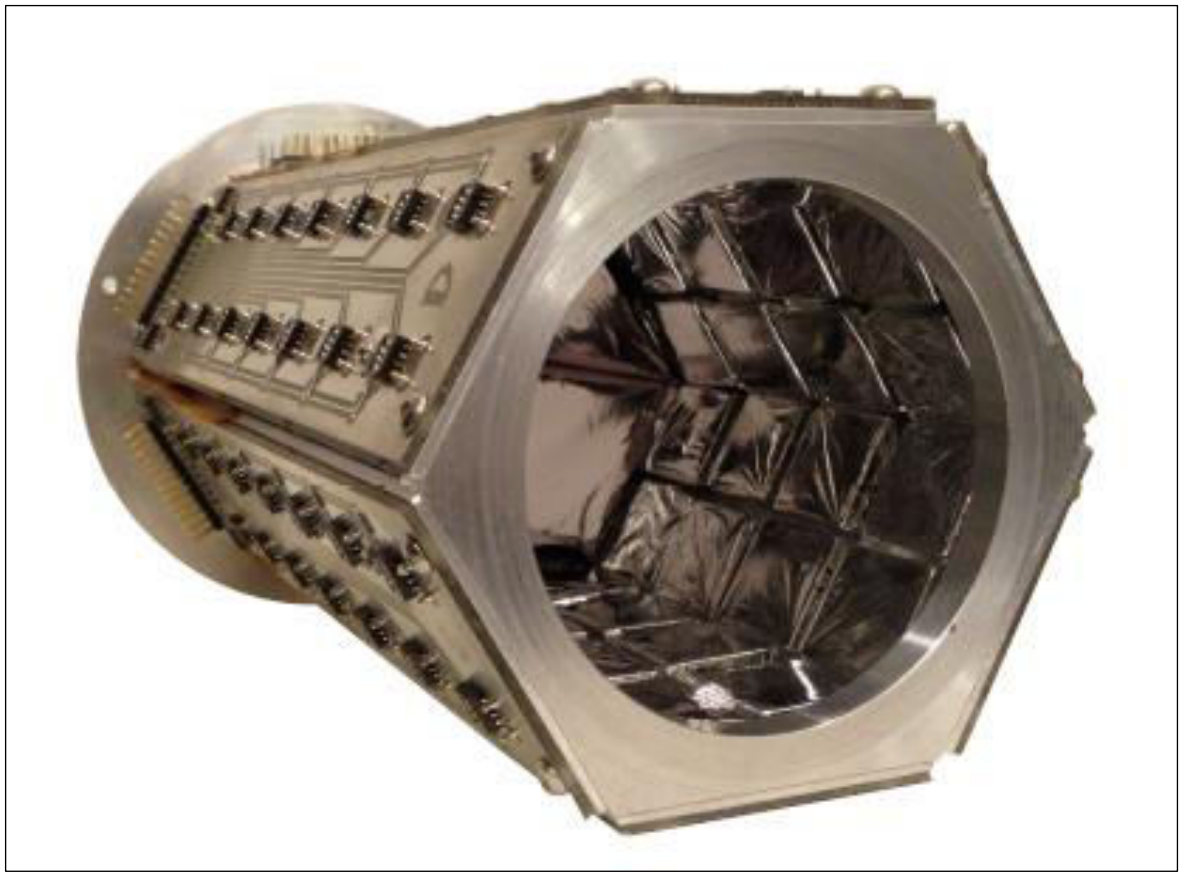

Figure 1: The original UoYTube consisted of 96 CsI (Tl) scintillators crystals, arranged as shown. The dimensions of each of the scintillator crystals were $20 \times 20\,\mathrm{mm}^2$ and $2\,\mathrm{mm}$ thick. The light output from the scintillator crystal was measured by PIN diodes [1].

The dimensions of each of the scintillator crystals were $20 \times 20\,\mathrm{mm}^2$ and $2\,\mathrm{mm}$ thick. The light output from the scintillator crystal was measured by PIN diodes. The UoYTube was originally designed to be used for the study of exotic proton-rich nuclei [1]. The motivation for constructing a new UoYTube is to improve its performance in terms of the efficiency of detection of charged particles emitted in fusion evaporation reactions.

The main aims of this thesis are to design and fabricate several UoYTube prototype detection systems and to then test the performance of these in order to try to establish which prototypes demonstrate the optimum performance. There are several different prototypes which will be tested. These include prototypes with different scintillator crystals (Caesium Iodide and plastic), prototype scintillators with different geometries (truncated pyramid and cuboid), and prototype detection systems that include different types of light guides (Acrylic and 3D Printed). The prototypes will then be characterised in terms of the signal-to-noise ratio, the optimum operating bias value, the energy resolution and the optimum spectroscopy amplifier shaping time. The results will then be used to inform upon the optimum design for the UoYTube detector.

The UoYTube is designed to measure radiation; in this case, the radiation type will principally be protons and alpha particles. Protons and alphas interact with the scintillator crystals in the UoYTube and this occurs by way of the coulomb interaction between their positive charge and the negative charge of the scintillator's atoms [2]. In this thesis, two different types of scintillators are tested; Caesium Iodide and plastic.

The scintillation process itself produces light that is measured by Silicon Photomultipliers, or SiPMs. In a SiPM, the incident photons transfer their energy onto electrons that are positioned in the valance band. The result of this is that the electrons gain energy and move to the conduction band. This process generates an electron-hole pair. If a reverse bias is applied to the SiPM, the incident photons generate a net current through the semiconductor and when the electric field is high enough, the electrons and holes are accelerated and collide with other charge carriers by way of an avalanching process. The result of this is that the charge is amplified to the point at which it can be measured macroscopically [3].

2. Background/Particle Detection Methods

The UoYTube is a detector that is designed to measure ionising radiation such as alpha particles and conversion electrons. Each individual UoYTube cell is constructed from three key components. These are a scintillator, a light guide and a Silicon Photomultiplier (or SiPM).

A scintillator is a material that produces light when exposed to ionising radiation. Examples of scintillators include Sodium Iodide, Caesium Iodide, Plastic and Lanthanum Bromide. Ideally, a scintillator should have the following characteristics: -

1. It should be transparent to its own light.
2. The scintillation efficiency should be high.
3. The light yield should be proportional to the energy of the ionising radiation [2].

Light guides are optical components that are designed to channel light. The light is transmitted via the process of total internal reflection and the light guide should ideally transmit the light with as little loss of photons as possible. Light guides are typically manufactured from Acrylic Resin and glass [4]. In the UoYTube, the light guide is used to channel the light that is generated by the scintillator and focus it onto the SiPM, where it is measured.

A Silicon Photomultiplier is a semiconductor device that is used in the UoYTube to detect the photons emitted from the scintillator. In a SiPM, the incident photons transfer their energy onto electrons that are positioned in the valance band. The result of this is that the electrons gain energy and move to the conduction band. This process generates an electron-hole pair. If a reverse bias is applied to the SiPM, the incident photons generate a net current through the semiconductor and when the electric field is high enough, the electrons and holes are accelerated and collide with other charge carriers by way of an avalanching process. The result of this is that the charge is amplified to the point at which it can be measured macroscopically [3].

3. Experimental Method

a. UoYTube – Construction of the individual cells

In the UoYTube detector, the scintillator crystal, light guide and SiPM are connected together to form an individual cell, as shown in Figure 2: -

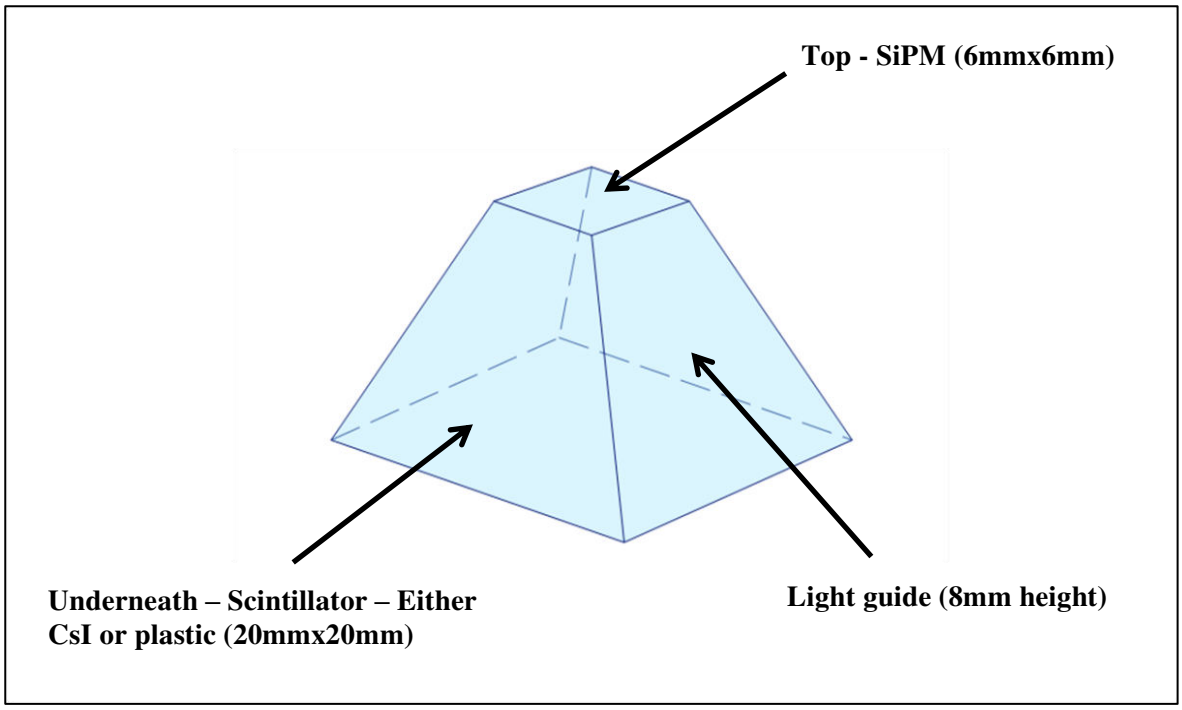

Figure 2: A schematic showing the geometry of each individual UoYTube cell. It is constructed from a scintillator, a light guide and a Silicon Photomultiplier.

To fabricate an individual cell, the method is as follows: -

1. Bind the scintillator crystal to the light guide using glue.
2. Wire up the silicon photomultiplier. There should be two wires; one is the anode and the other is the cathode.
3. Bind the silicon photomultiplier to the other side of the light guide using glue. Ensure that the front of the SiPM faces the light guide. The wires should face outward, away from the light guide.
4. Wrap the entirety of the detector in white insulating tape, but ensure that the wires are not covered.
5. Using a scalpel, cut into the white insulating material where the scintillator crystal face is positioned. Be careful not to scratch the scintillator with the scalpel.
6. Clean the Mylar with isopropanol. Position two pieces of the Mylar material on top of the scintillator and attach using the white insulating tape.
7. Cover the entirety of the detector (but excluding the Mylar covered surface) with the silver tape.

Then, ninety-six of these individual cells are arranged in a frame to form the entirety of the detector. The arrangement of these components is as shown in Figure 3: -

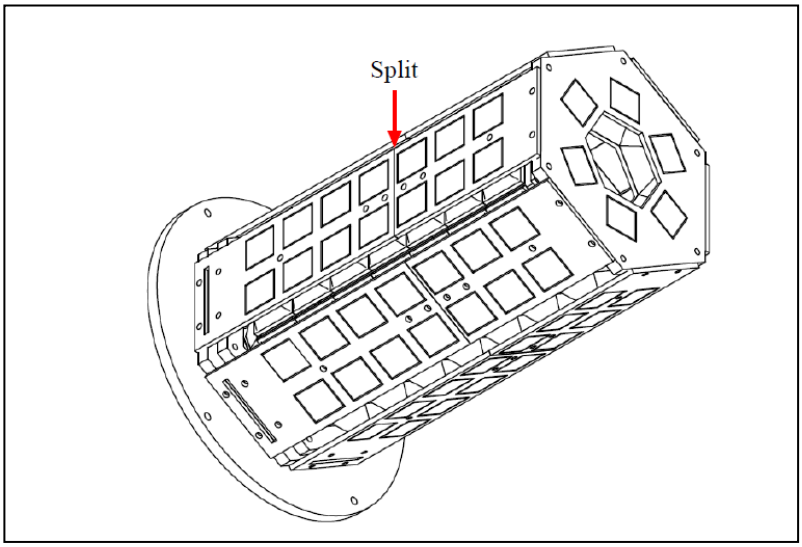

Figure 3: A schematic showing how the ninety-six individual cells are arranged in a frame to form the previous generation of the UoYTube detectors' structure [5].

b. Calibration with Alpha and Conversion Electron Sources

The UoYTube prototypes will each be characterised in terms of several parameters which include the signal-to-noise ratio, the optimum bias value, the energy resolution and the optimum shaping time. These experiments will be conducted in vacuum conditions.

To ensure these parameters are measured and calculated correctly, it is first necessary to calibrate the detector. The calibration process allows the data and the spectrum produced from it to be fully understood and for parameters such as energy to be identified [6].

The computer programme that is used in the laboratory to collect the experimental data is called MAESTRO®. MAESTRO is a Multichannel Analyser (MCA) which when used alongside MCB hardware and a computer, can be used to process the nuclear data and present it in graphical form for analysis [7]. When the data are displayed on the computer screen, they are initially displayed such that the horizontal x axis is the Channel Number and the vertical y axis is the Number of Counts.

To calibrate the data, it is necessary to describe the relationship between the Channel Number and Energy. To do this, you must begin by identifying the known decay products of the radioactive species which will be used as the source. For example, in these experiments the source used is a composite source, consisting of Plutonium-239, Americium-241 and Curium-244 (Serial Number NY332) [8]. Using the data sheets, [9] it is possible to infer that the decay products for the source will be three alpha particles with energies of 5156.59 keV, 5585.56 keV and 5804.77 keV. Therefore, the spectrum should show three characteristic peaks, each one corresponding to a different energy alpha particle. The spectrum for this source is as shown in Figure 4:-

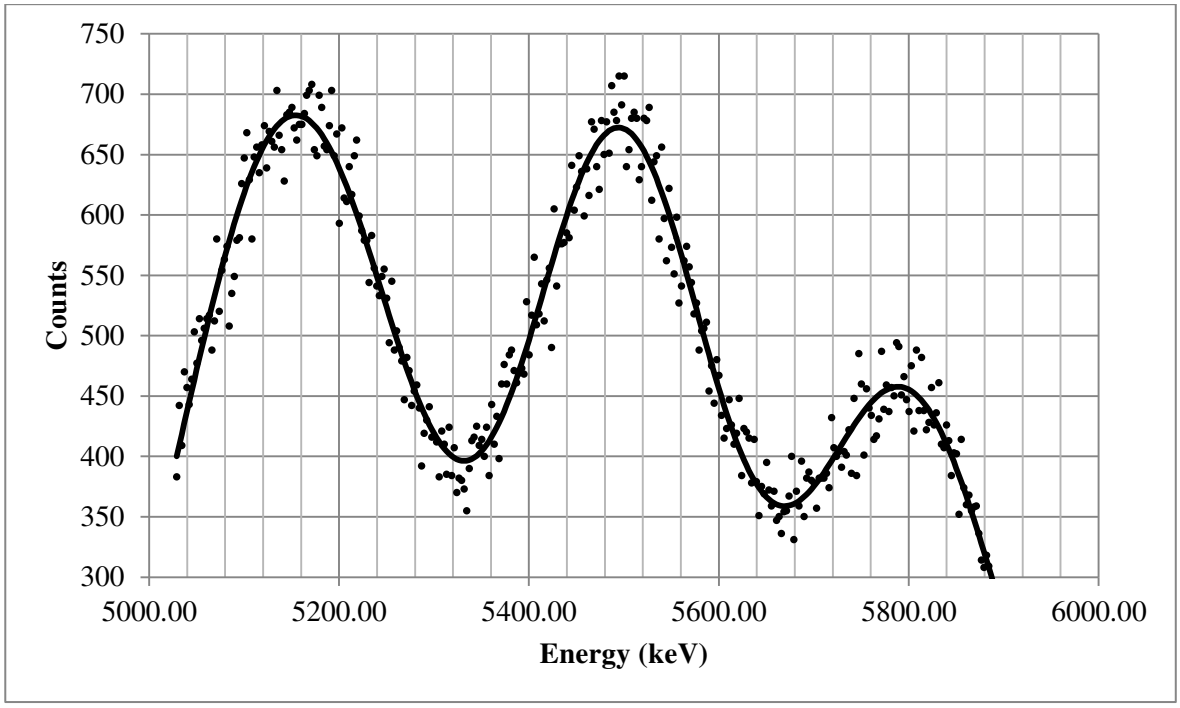

Figure 4: A graph showing the spectrum obtained for the triple alpha source. There are three characteristic peaks, each one corresponding to a different kinetic energy alpha particle. Peak 1 is the Pu-239 alpha, Peak 2 is the Am-241 alpha and Peak 3 is the Cm-244 alpha.

Once this is identified, it is then possible to use MAESTRO to select each of the peaks in turn and input their corresponding energies. Then, the scale is properly calibrated and the spectrum can be interpreted.

To calibrate the data set with a conversion electron source instead of an alpha particle source, it is necessary to once again describe the relationship between the Channel Number and Energy by identifying the known decay products of the radioactive species which will be used as the source. In this case, the source used is a conversion electron source named Bismuth-207 (Serial Number SU486) [8]. The Bi-207 source has four conversion electron peaks and two gamma ray peaks which are normally visible in the spectrum [10]. One peak was visible in this spectrum, but unfortunately it is unclear as to which of the decay products this corresponds to. The spectrum for this source is as shown in Figure 5:-

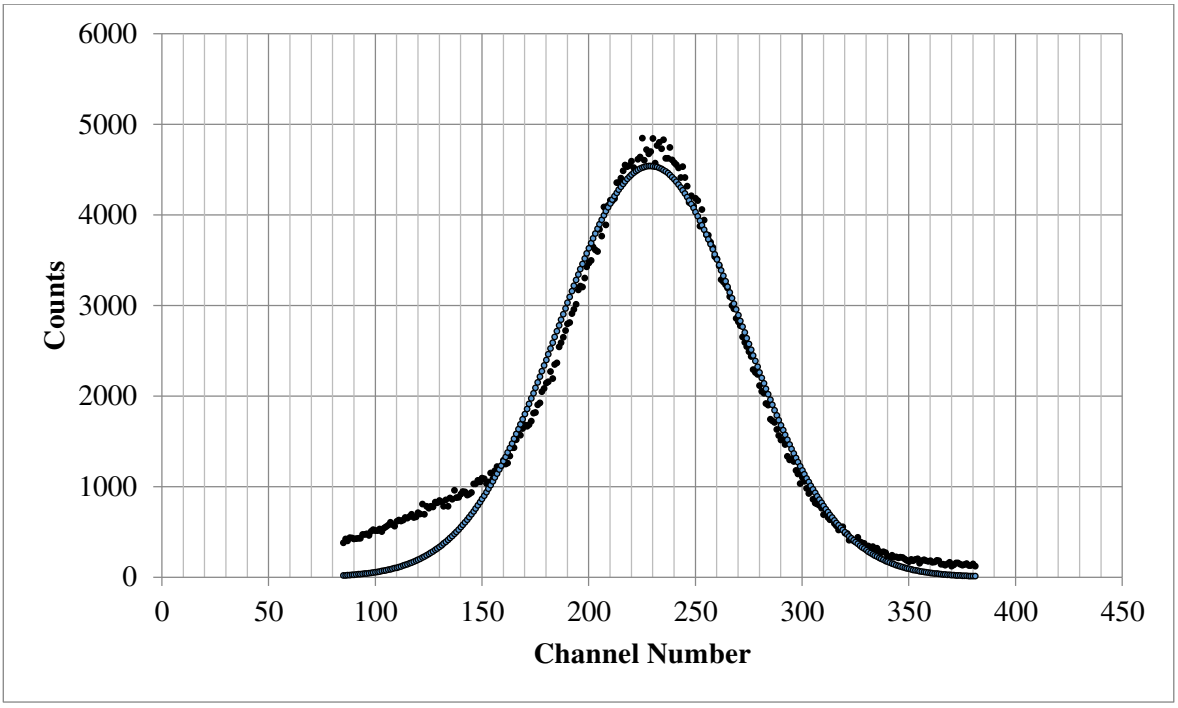

Figure 5: A graph showing the spectrum obtained for the conversion electron source Bi-207. The Bi-207 source has four conversion electron peaks and two gamma ray peaks which are normally visible in the spectrum [10]. One peak was visible in this spectrum, but unfortunately it is unclear as to which of the decay products this corresponds to.

c. Experimental method used to characterise the UoYTube prototypes

To characterise the UoYTube prototypes, a particular experimental method was followed. The equipment was set up as shown in Figure 6:-

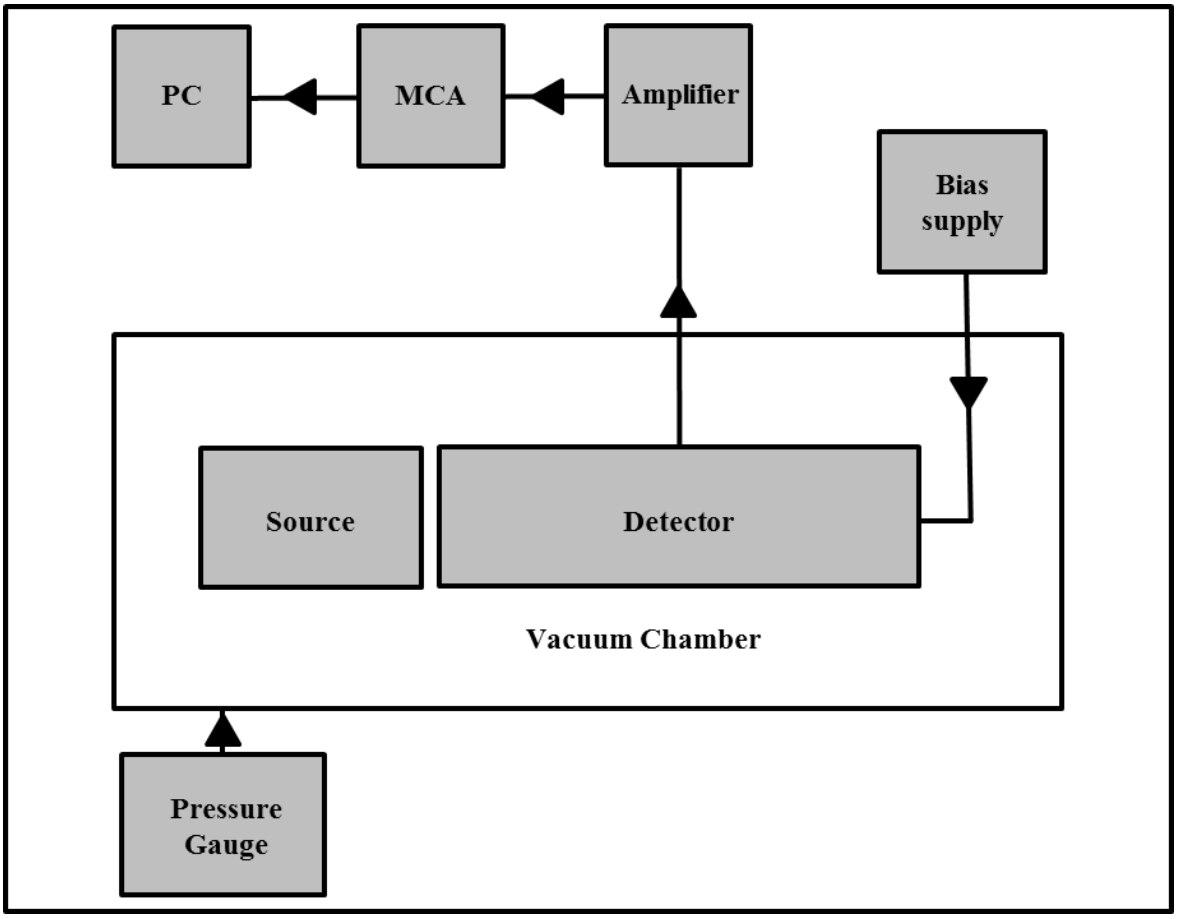

Figure 6: The experimental set-up used to measure the signal-to-noise and optimum bias values. The set-up includes the detector prototype, a radioactive source, the bias supply and the processing electronics.

In these experiments, the radioactive source was first placed into the holder (using forceps) and then screwed into place. Then, the source was placed into a retort stand with two clamps. The source was then positioned on the bottom clamp. The prototype was then wrapped in bubble wrap (so it was not damaged by the clamp) and positioned on the top clamp, approximately 5cm away from the source. The scintillator was facing the source. The retort stand was then placed inside the vacuum chamber.

The prototype has two connections, a blue wire and a yellow wire. The blue wire was attached to the bias supply and the yellow wire was connected to the port next to the bias supply (working

anticlockwise). These ports were located at the top of the vacuum chamber. The door of the vacuum chamber was then closed and the pressure set so that it was of the order of 0.1mbar.

The signals from the silicon photomultiplier are amplified and processed by the Amplifier and the MCA respectively and then read at the computer terminal.

In these measurements, the bias value is varied and spectra are taken at each different bias value. After the bias value is changed, the position of each of the three peaks will change. To compensate for this, after every change in the bias value, the fine and coarse gain settings on the electronics must be changed. This was to ensure that the peaks are always in the same position and that calibration of the x axis is the same for each of the spectra. This also ensures that a direct comparison between each of the spectra is possible.

d. Experimental method used to fabricate the light guide – 3D Printed

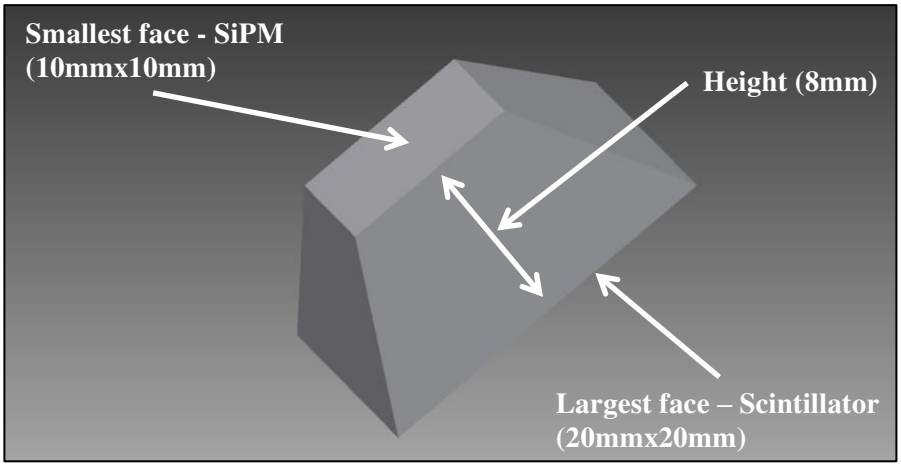

Figure 7: A drawing constructed in AutoCAD Inventor that shows the truncated pyramid geometry of the 3D printed light guide. The largest face measures 20mmx20mm, the smallest face measures 6mmx6mm and the height is 8mm.

In Figure 7, the largest face (where the scintillator will be positioned) measures 20mmx20mm. The smallest face (where the Silicon Photomultiplier will be positioned) measures 6mmx6mm. The height of the light guide (length from the largest face to the smallest face) is 8mm. This drawing is then imported into the PreForm Software 1.8.2 [11] which allows you to change several printing parameters such as the orientation of the light guide, the type of resin, the thickness of each layer and the number of light guides arranged on the tray. In this experiment, the type of resin that was used was the "Clear Resin" which has the greatest optical transparency, the layer thickness was 0.1mm and one light guide was arranged on the tray.

The 3D printer is able to print the desired geometry by using a laser beam to set the photosensitive resin [12]. The resin is set using incremental layers of 0.1mm each and these are built up to form the truncated pyramid shape of the light guide. Once the light guide print was completed, it was then washed with water and Isopropanol and also polished (with a high grade sandpaper and metal polish) to give a smooth surface.

e. Experimental method used to fabricate the light guide – Bulk Acrylic

The device which was used to fabricate the light guides is called the HURCO VMX60m Machining Centre [13]. The first stage in this fabrication process is to use a drawing package such as AutoCAD Inventor which takes the scale drawings of the light guides and convert them into a 3D models. Then, a Computer Aided Manufacturing Programme, in this case HyperMILL®, [14] is used to convert the 3D model into another file type that the HURCO VMX60m can read and interpret. This new file translates the 3D model into a set of movements that the machining centre can use to gradually file down the acrylic (with a slot drill) and form the shape required for the light guide. To ensure that the light guide is fabricated correctly, a vacuum pump was also used. This guaranteed that the acrylic stayed stationary whilst it was being machined. Once the light guide has been machined, it also needs to be polished with high grade sandpaper, to ensure that the surface is smooth and that the light transmission is maximised.

f. Experimental method used to characterise the light guides

To characterise the light guide, the FILMETRICS® F10-RT spectrometer [15] was used to measure the Reflectance and Transmittance of light, recorded as a function of Wavelength. The first step when using this spectrometer, was to acquire data from two baseline samples, which could be used for the purposes of calibration. This data was collected using the spectrometer's propriety software. In this case, as the light guides are made from plastic, the BK7 plastic sample was used as the first calibration data set. The second calibration set was from the background (this is, with no sample in the beam). Then, the spectrometer's wavelength was varied from 200-1100nm and the Reflectance and Transmittance of the light through the light guide was recorded.

4. Error Analysis

Experimental error is defined as the deviation from the "true value" which occurs as a result of the measurement process [16]. These errors are inherent in the process of measurement and can be classified into two categories: systematic errors and random errors [17]: -

g. Systematic and Random Errors

A Systematic Error is one which affects accuracy. These can originate from for example, an incorrect calibration of a measuring device or an incorrect reading of the device, made by the user. Random Errors are those that affect precision. These can originate from a fluctuation in a measurement (making it difficult to read) or the difficulty associated with reading a measurement which lies between two increments on a measuring scale [17].

It is possible to specify the uncertainty for a given measurement, by considering these errors. This is advantageous, as error analyses identify ways in which an experiment can be redesigned to reduce errors and allow direct comparison between different values, so confidence can be stated in the conclusions being made [16].

There are two different techniques used for error analysis. The first, referred to as the Type A mode of analysis, involves using statistics to analyse errors in the measurements. The second, referred to as a Type B mode of analysis, involves using known quantities, such as the resolution of a particular instrument, to analyse errors in the measurements. To calculate the error using this method, it is first necessary to establish the resolution of the instrument that is being used to make the measurement. This information can be inferred by examining the manufacturer's specifications or by inspecting the instrument directly to establish the minimum increment [16]. These values are then displayed on the graphs as the plus and minus error bars for the data points.

h. Parameters calculated in MATLAB

Once the data are collected, there is a requirement to fit the data to a particular distribution and extract values which describe how successful the fitting process it is. The following list describes the different fitting procedures which have been used, as well as parameters of interest, measured by MATLAB and Microsoft Excel, that describe how consistent the experimental results are with the fitting: -

i. Gaussian Distribution

A Gaussian distribution is described by three values in MATLAB [18] : A (the peak height), $\bar{x}$ (the mean value) and σ (the standard deviation). These values can then be used in the mathematical expression for a Gaussian distribution, as shown below: -

$$f(x) = A \times \exp\left(-\frac{1}{2}\left(\frac{x - \bar{x}}{\sigma} \right)^2 \right)$$

ii. Full Width Half Maximum

The Full Width at Half-Maximum is described via the following expression [19]: -

$$FWHM = 2\sqrt{2\ln 2} \times \sigma$$

iii. Energy Resolution

The energy resolution of a detector can be calculated using the following equation [20]: -

$$Energy\,Resolution = FWHM \div Peak\,Centroid$$

Both the FWHM and Peak Centroid are measured in units of energy or channels. Thus, their units are either keV or Channels. The energy resolution can also be expressed as a percentage, by multiplying the above equation by 100. The energy resolution and FWHM will be calculated for each of the three different UoYTube prototypes and when using two different radioactive sources,

the Pu/Am/Cm triple alpha source (Serial Number NY332) and the Bi-207 conversion electron source (Serial Number SU486). This is as described in sections x, xii and xiii.

iv. A1/B1/C1 Lower and Upper Bounds

The lower and upper bounds of A1, B1 and C1 in a Gaussian distribution, as calculated by MATLAB, corresponding to values within 95% confidence. This is because MATLAB automatically sets the errors to be within two-sigma. These are expressed as the plus and minus error bars for A1, B1 and C1.

v. Confidence Bound CB (%)

A confidence bound is used to specify the width of an interval and the corresponding lower and upper values of that interval. By default, the confidence bound value is set at 95% by MATLAB. This indicates that there is a 5% probability that the fit will make an incorrect prediction and that there is a 95% probability that a prediction will be within the lower and upper bounds. This can also be referred to as the two sigma limit [21].

vi. Sum of Squares Due to Error (SSE)

This value is a measure of how much the fit calculated by MATLAB, deviates from the actual experimental data. The SSE value should ideally be as close to zero as possible. This would imply that the random errors are smaller and that the fit is as more effective tool for prediction. It is defined in equation form as [22]: -

$$SSE = \sum_{i=1}^{n} w_i \left(y_i - \hat{y}_i\right)^2$$

vii. R-Square (R-sq) and Adjusted R-Square (Adj R-sq)

The R-Squared (R-sq) value outlines the extent to which the fit is able to describe the variation in the experimental data. This value ranges from 0 to 1. This value should ideally be close to one; this would demonstrate that the fit is able to accommodate a larger proportion of the variance in the data. The Adjusted R-Squared (Adj R-sq) value uses the R-squared value and corrects it to

compensate for the number of residual degrees of freedom. This value can be any value less than or equal to one. This value should ideally be close to one; this would demonstrate that the fit is more accurate [22].

viii. Root Mean Squared Error (RMSE)

The Root Mean Squared Error (RMSE) describes the standard deviation of the random aspect of the experimental data and should be as close to zero as possible. This would mean that the fit can be used more accurately when making predictions [22].

i. Error Propagation for the parameters of interest

In this section, the specific methods used to analyse errors in the UoYTube characterisation process will be described. This will include the specific error values used in the data, how these were deduced from reference materials and/or MATLAB and how these errors were propagated through to the final results for the parameters of interest.

The specific error values used for the data in this thesis are as follows in Table 1: -

Parameter	Unit	Error	Explanation/Reference
Bias	Volts	±0.01	Resolution of the digital multimeter
Counts	No Units	Various	A1 values, calculated by MATLAB [21]
Angle of Polariser	Degrees	±3	An estimate, based on inspection
Wavelength	nm	±2.5	Resolution of the spectrometer [23]
Transmittance	Percent	±0.02	Resolution of the spectrometer, for all wavelengths [23]
Reflectance	Percent	±0.002	Resolution of the spectrometer [23]
Shaping Time	Percent	±5	Based on the same MCA, in a different experiment [24]
A1/B1/C1 (LB and UB)	Various	Various	Calculated by MATLAB [21]
Signal-to-Noise Ratio	No Units	Various	A1 values, calculated by MATLAB [21]
FWHM	keV	Various	The LB and UB values, as calculated by MATLAB
Energy Resolution	Percent	Various	The LB and UB values, as calculated by MATLAB

Table 1: This table lists the specific error values used for the data in this thesis. The table includes the name of the parameter, the unit of measurement, the error value, an explanation as to where the value comes from and a reference.

Some of the errors depend on more than one measured parameter. This means that in order for them to be calculated, an error propagation must be performed. In this thesis, the parameters that require this type of error propagation are the signal-to-noise ratio, the Full Width Half Maximum and the energy resolution.

ix. Signal-to-Noise Ratio and Optimum Bias

To perform the error propagation for the signal-to-noise ratio, the signal (counts) value and the noise (counts) value were first recorded. These values were calculated using MATLAB and the energy spectra data. Figure 8 demonstrates where the signal and noise values were taken from on the energy spectrum: -

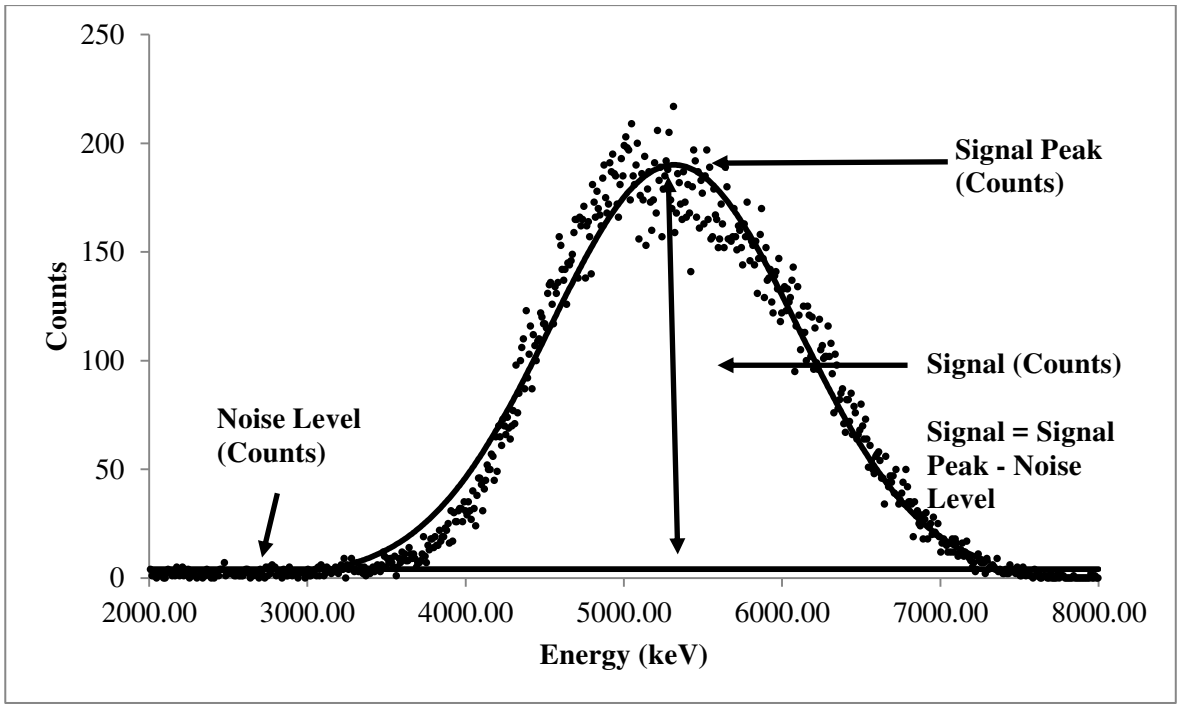

Figure 8: This figure demonstrates how the signal and noise values were taken from the energy spectrum. This Energy spectrum was measured at a bias of 27V. These results are for the UoYTube prototype made from a plastic scintillator (with a truncated pyramid geometry), and include a Gaussian fitted to the Am-241 source peak.

The error for each of these parameters corresponds to the A1 value errors from the energy spectra. These errors are assumed to be within 95 percent confidence, as calculated by MATLAB. This is because MATLAB automatically sets the errors to be within two-sigma [21]. For a two variable function of the form, z = x/y (such as the S/N ratio), the equation for the error in z [25], labelled as Δz, is as follows: -

$$\frac{\Delta z}{z} = \sqrt{\left(\frac{\Delta x}{x}\right)^2 + \left(\frac{\Delta y}{y}\right)^2}$$

In this equation, x is the signal counts, y is the noise counts, Δx is the signal error corresponding to the A1 value errors, Δy is the noise error, also corresponding to the A1 value errors and z is the signal divided by the noise. Using this equation, Δz, the error in the signal-to-noise ratio, can be calculated.

x. Full Width Half Maximum and Energy Resolution

To perform the error propagation for the FWHM and the energy resolution, B1 (the position of the peak centroid on the x axis) and C1 (equal to $\sqrt{2}\sigma$, where σ is the standard deviation) were first recorded. These values were calculated using MATLAB and the energy spectra data. Figure 9 demonstrates where the peak centroid and standard deviation values were taken from on the energy spectrum and how the FWHM and energy resolution values were inferred from the data: -

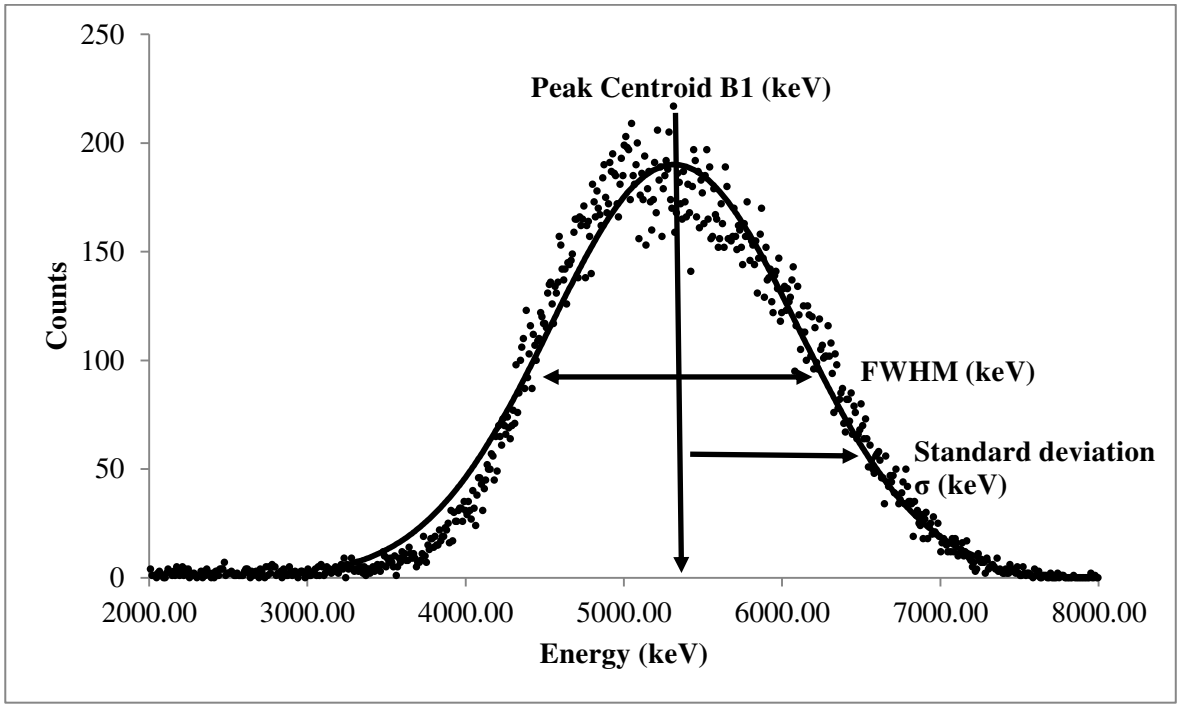

Figure 9: This figure demonstrates where the peak centroid and standard deviation values were taken from on the spectrum and how the FWHM and energy resolution values were inferred from the data. This Energy spectrum was measured at a bias of 27V. These results are for the UoYTube prototype made from a plastic scintillator (with a truncated pyramid geometry), and include a Gaussian fitted to the Am-241 source peak.

The error in C1 was assumed to be plus the Upper Bound and minus the Lower Bound, corresponding to values within 95 percent confidence, as calculated by MATLAB. This is because MATLAB automatically sets the errors to be within two-sigma. Using the error in C1, labelled as ΔC1 and the equation written below, the error in the FWHM [19], labelled as ΔFWHM was calculated: -

$$\Delta\text{FWHM} = \frac{2\sqrt{2\ln 2}}{\sqrt{2}} \times \Delta\text{C1}$$

The errors in B1 were assumed to be plus the Upper Bound and minus the Lower Bound, corresponding to values within 95 percent confidence, as calculated by MATLAB. This is because MATLAB automatically sets the errors to be within two-sigma. Using the errors in B1 and C1, labelled as ΔB1 and ΔC1, and the following equation [19] [25], the error in the energy resolution, labelled as ΔE, was calculated: -

$$\frac{\Delta\text{E}}{\text{E}} = \sqrt{\left(\frac{2\sqrt{2\ln 2}}{\sqrt{2}}\frac{(\Delta\text{C1})}{\text{FWHM}}\right)^2 + \left(\frac{\Delta\text{B1}}{\text{B1}}\right)^2}$$

xi. Analysis of the light output from the light guides

The measurements of reflectance and transmittance will be measured using the FILMETRICS® F10-RT spectrometer [15] and will be for both the Acrylic and 3D Printed light guides. This is as described in section xi. To perform the error analysis for the measurements of reflectance and transmittance, the following error values were used: -

1. Angle of Polariser ±3 degrees, this is an estimate based on how accurately the values could be established by inspection
2. Wavelength ±2.5 nanometres, corresponding to the resolution of the spectrometer according to the manufacturer's specifications [23]
3. Transmittance ±0.02 percent, corresponding to the resolution of the spectrometer according to the manufacturer's specifications, for all wavelengths [26]

4. Reflectance ±0.002 percent, corresponding to the resolution of the spectrometer according to the manufacturer's specification [26]

xii. Optimum Shaping Time

For a Gaussian shaped pulse, shaping time is stated as being the standard deviation of that pulse, when the horizontal axis is measured in time [27]. The optimum shaping time of the amplifier, is defined as the shaping time that corresponds to the highest energy resolution. The measurements of optimum shaping time will be measured using the MCA for both the Acrylic and 3D Printed light guides, using the Pu/Am/Cm triple alpha source (Serial Number NY332). This is as described in section xvii. To perform the error analysis for the measurements of the optimum shaping time, the following error values were used: -

1. Shaping Time ±5 percent, this is an estimate based on the errors associated with the same Multichannel Analyser, but a different pre-amplifier and sensor [24]
2. Energy Resolution various, but as calculated using the methods described in section x

xiii. Energy Resolution as a function of the applied Bias

To perform the error analysis for the measurements of the energy resolution as a function of the applied Bias, the following error values were used: -

1. Bias ±0.01 Volts, corresponding to the resolution of the digital multimeter
2. Energy Resolution various, but as calculated using the methods described in section x

5. Results and Analysis

j. Characterisation of CsI and Plastic prototypes – S/N and Optimum Bias

The experimental method used for these measurements, is as described in section c. The error analyses for these measurements, are as described in ix. The first parameter which will be used to characterise the UoYTube cells is the signal-to-noise ratio. The signal-to-noise ratio is defined as the signal height (in mV or counts) divided by the noise signal height (in mV or counts) [28]. Ideally, the signal-to-noise ratio should be as high as possible. Once the signal-to-noise ratio is measured, it will be then used to infer which of the bias values applied to the silicon photomultiplier, is the optimum value.

There are three different UoYTube prototypes which were characterised in this experiment. In each case, the triple alpha Pu/Am/Cm source was used, (Serial Number NY332), where their kinetic energies are 5156.59 keV, 5585.56 keV and 5804.77 keV respectively. These prototypes are distinguished by the scintillator crystal used and their geometries. The three prototypes are: -

1. Plastic scintillator (with a truncated pyramid geometry)
2. Caesium Iodide scintillator (with a truncated pyramid geometry)
3. Plastic scintillator (with a cuboid geometry)

The results for the plastic scintillator (truncated pyramid geometry) are as shown in Table 2:-

Scintillator	Source Peak	Bias (V)	Signal (Counts)	Noise (Counts)	S/N Ratio
Plastic scintillator (truncated pyramid)	Am-241	27.00±0.01	183±3	7±3	26±9
Plastic scintillator (truncated pyramid)	Am-241	28.00±0.01	236±3	5±3	47±28
Plastic scintillator (truncated pyramid)	Am-241	29.00±0.01	128±2	5±2	26±10
Plastic scintillator (truncated pyramid)	Am-241	30.00±0.01	268±3	23±3	12±1
Plastic scintillator (truncated pyramid)	Am-241	31.00±0.01	304±3	42±3	7±0

Table 2: A table showing how the signal-to-noise ratio varies as the bias across the SiPM is changed. These results are for the prototype with a plastic scintillator (truncated pyramid geometry), acrylic light guide and the Am-241 source peak (of energy 5585.56 keV), from the triple alpha source. The Am-241 peak was used because this prototype has low energy resolution, and so only one peak is visible, even though there are actually three peaks for the triple alpha source.

These results can also be shown in graphical form, as in Figure 10:-

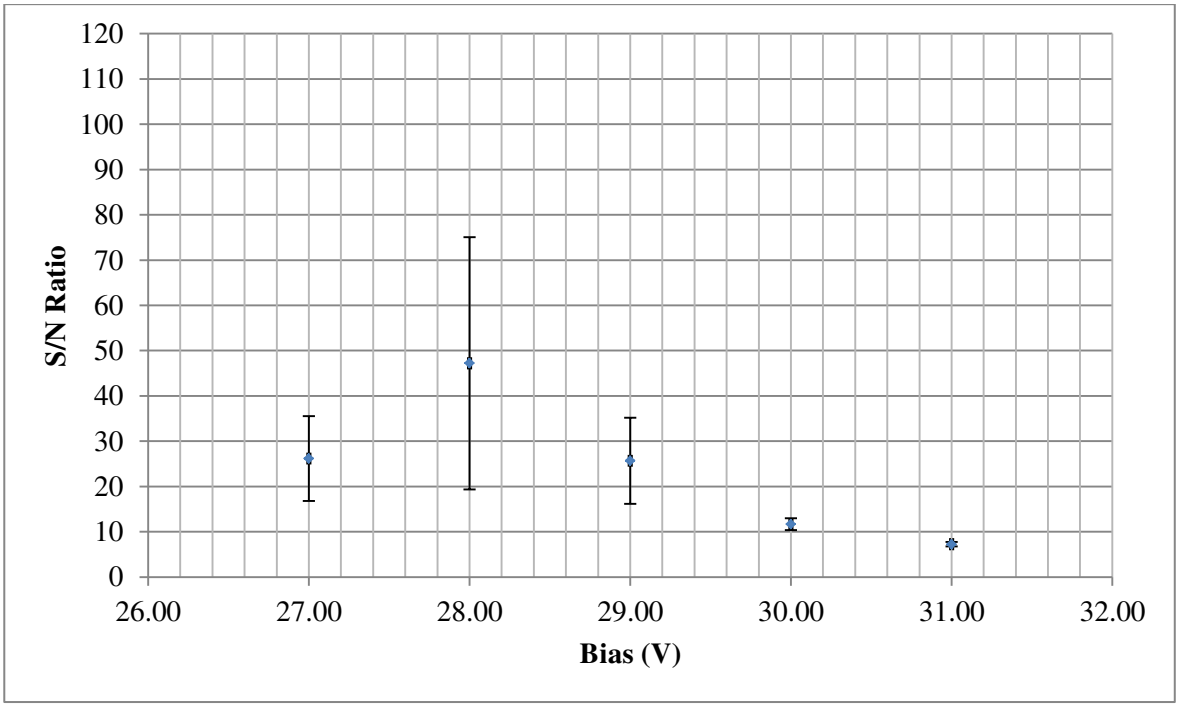

Figure 10: A graph showing how the signal-to-noise ratio varies as the bias across the SiPM is changed. These results are for the prototype with a plastic scintillator (truncated pyramid geometry), acrylic light guide and the Am-241 source peak, (of energy 5585.56 keV), from the triple alpha source. The Am-241 peak was used because this prototype has low energy resolution, and so only one peak is visible, even though there are actually three peaks for the triple alpha source.

The results for the Caesium Iodide scintillator (truncated pyramid geometry) vary depending upon which source peak is used to calculate the signal-to-noise ratio. The results for each of the three different source peaks are as shown in Table 3, Table 4 and Table 5:-

Scintillator	Source Peak	Bias (V)	Signal (Counts)	Noise (Counts)	S/N Ratio
Caesium Iodide scintillator (truncated pyramid)	Pu-239	27.00±0.01	645±7	36±7	18±4
Caesium Iodide scintillator (truncated pyramid)	Pu-239	28.00±0.01	595±7	38±7	16±3
Caesium Iodide scintillator (truncated pyramid)	Pu-239	29.00±0.01	721±7	31±7	23±5
Caesium Iodide scintillator (truncated pyramid)	Pu-239	30.00±0.01	816±9	40±9	20±5
Caesium Iodide scintillator (truncated pyramid)	Pu-239	31.00±0.01	746±8	33±8	23±6

Table 3: A table showing how the signal-to-noise ratio varies as the bias across the SiPM is changed. These results are for the prototype with a Caesium Iodide scintillator (truncated pyramid geometry) and the Pu-239 source peak.

Scintillator	Source Peak	Bias (V)	Signal (Counts)	Noise (Counts)	S/N Ratio
Caesium Iodide scintillator (truncated pyramid)	Am-241	27.00±0.01	618±8	36±8	17±4
Caesium Iodide scintillator (truncated pyramid)	Am-241	28.00±0.01	572±6	38±6	15±2
Caesium Iodide scintillator (truncated pyramid)	Am-241	29.00±0.01	687±7	31±7	22±5
Caesium Iodide scintillator (truncated pyramid)	Am-241	30.00±0.01	816±9	40±9	20±5
Caesium Iodide scintillator (truncated pyramid)	Am-241	31.00±0.01	738±9	33±9	22±6

Table 4: A table showing how the signal-to-noise ratio varies as the bias across the SiPM is changed. These results are for the prototype with a Caesium Iodide scintillator (truncated pyramid geometry) and the Am-241 source peak.

Scintillator	Source Peak	Bias (V)	Signal (Counts)	Noise (Counts)	S/N Ratio
Caesium Iodide scintillator (truncated pyramid)	Cm-244	27.00±0.01	413±7	36±7	11±2
Caesium Iodide scintillator (truncated pyramid)	Cm-244	28.00±0.01	371±7	38±7	10±2
Caesium Iodide scintillator (truncated pyramid)	Cm-244	29.00±0.01	468±7	31±7	15±4
Caesium Iodide scintillator (truncated pyramid)	Cm-244	30.00±0.01	563±9	40±9	14±3
Caesium Iodide scintillator (truncated pyramid)	Cm-244	31.00±0.01	501±9	33±9	15±4

Table 5: A table showing how the signal-to-noise ratio varies as the bias across the SiPM is changed. These results are for the prototype with a Caesium Iodide scintillator (truncated pyramid geometry) and the Cm-244 source peak.

These results can also be shown in graphical form, as in Figure 11, Figure 12 and Figure 13:-

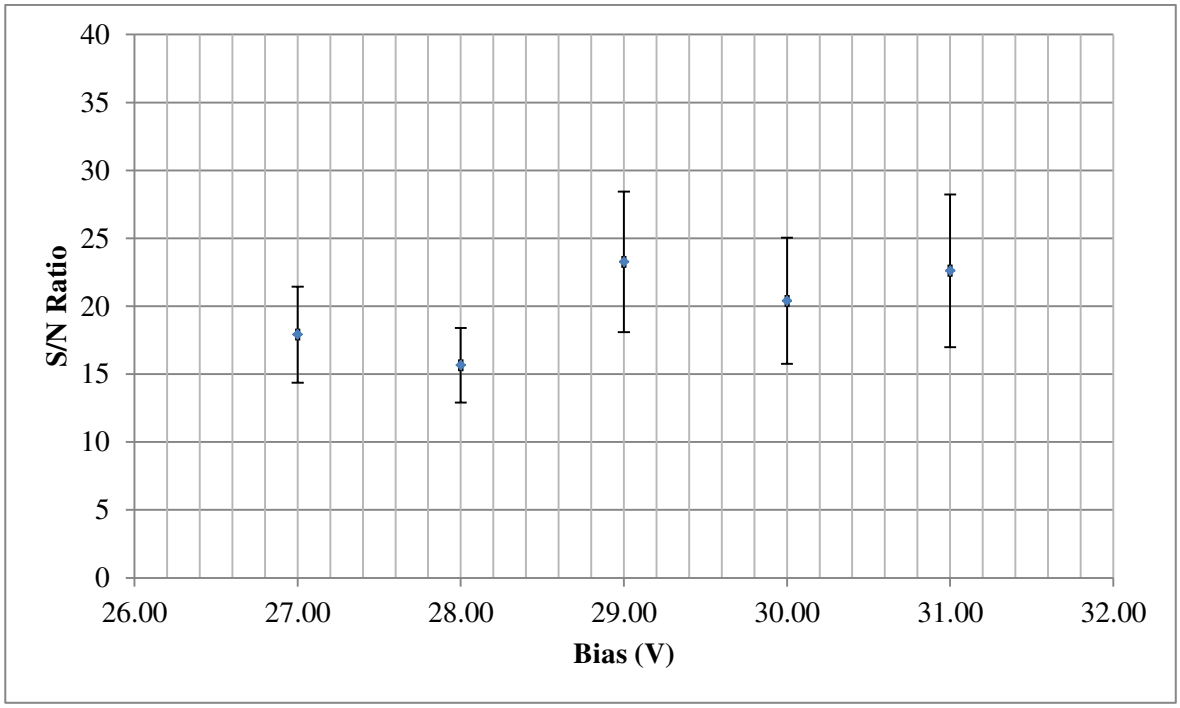

Figure 11: A graph showing how the signal-to-noise ratio varies as the bias across the SiPM is changed. These results are for the prototype with a Caesium Iodide scintillator (truncated pyramid geometry) and the Pu-239 source peak.

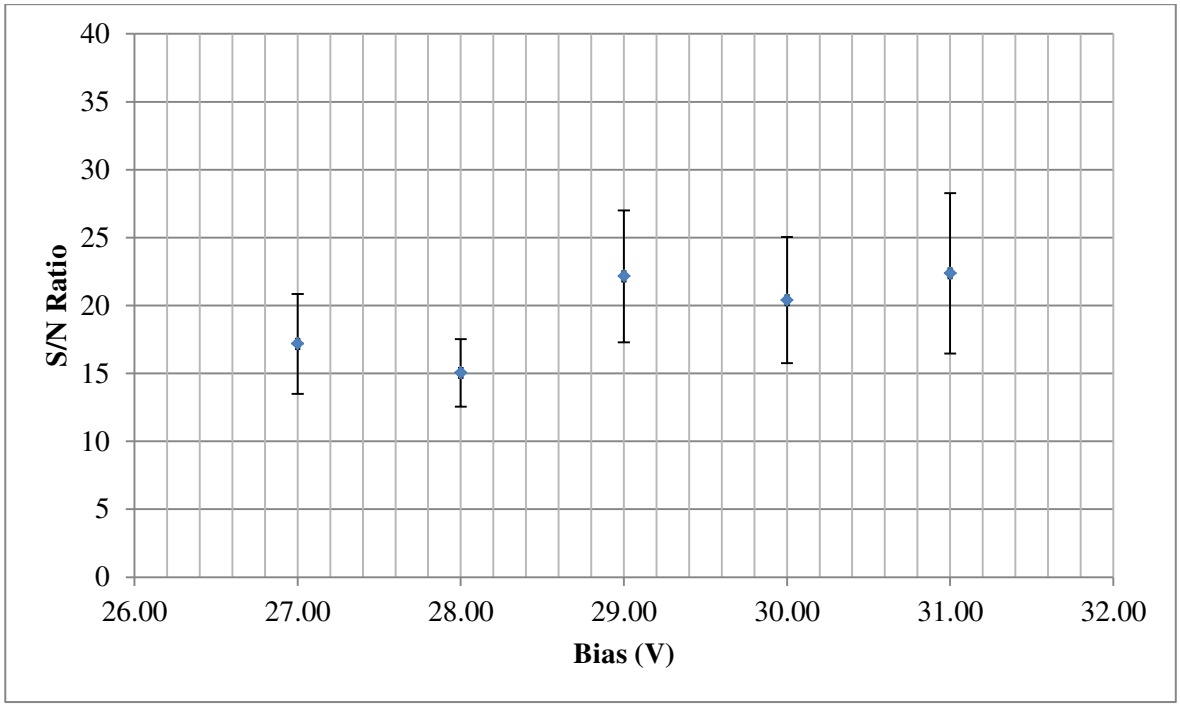

Figure 12: A graph showing how the signal-to-noise ratio varies as the bias across the SiPM is changed. These results are for the prototype with a Caesium Iodide scintillator (truncated pyramid geometry) and the Am-241 source peak.

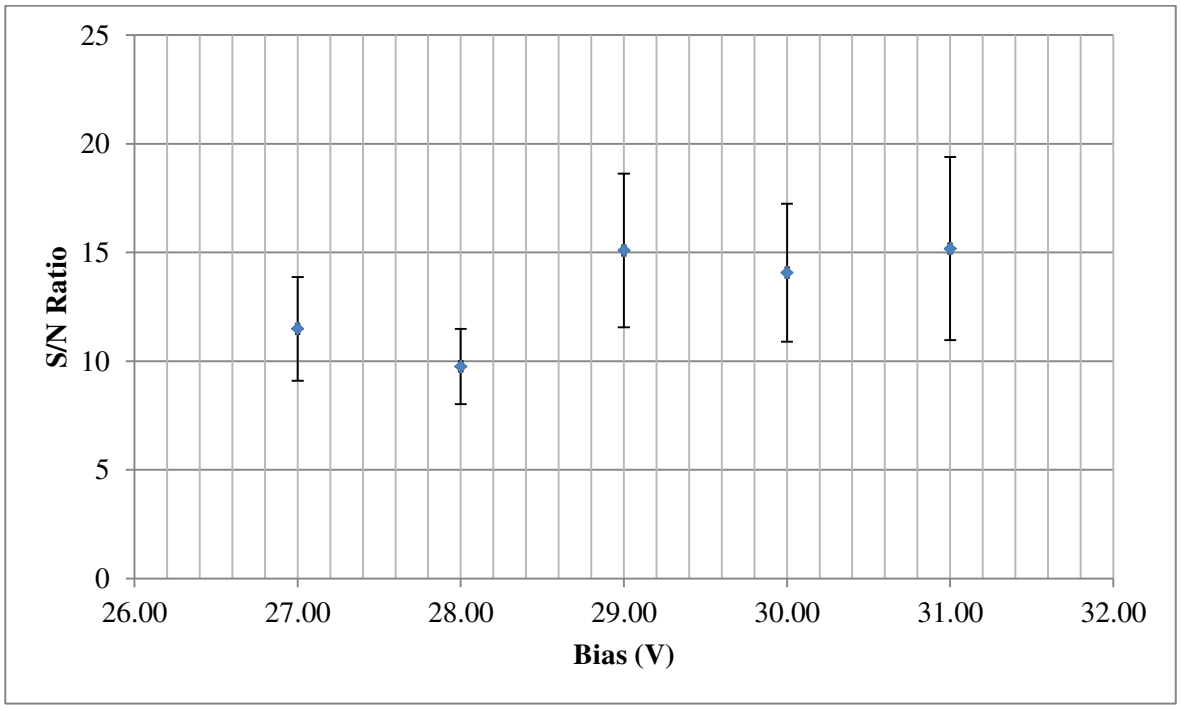

Figure 13: A graph showing how the signal-to-noise ratio varies as the bias across the SiPM is changed. These results are for the prototype with a Caesium Iodide scintillator (truncated pyramid geometry) and the Cm-244 source peak.

The results for the plastic scintillator (with a cuboid geometry) are as shown in Table 6:-

Scintillator	Source Peak	Bias (V)	Signal (Counts)	Noise (Counts)	S/N Ratio
Plastic scintillator (cuboid)	Am-241	27.00±0.01	33±1	2±1	16±7
Plastic scintillator (cuboid)	Am-241	28.00±0.01	20±1	2±1	10±3
Plastic scintillator (cuboid)	Am-241	29.00±0.01	29±1	2±1	15±6
Plastic scintillator (cuboid)	Am-241	30.00±0.01	33±1	2±1	17±7
Plastic scintillator (cuboid)	Am-241	31.00±0.01	33±1	2±1	16±7

Table 6: A table showing how the signal-to-noise ratio varies as the bias across the SiPM is changed. These results are for the prototype with a plastic scintillator (with a cuboid geometry) and the Am-241 source peak, (of energy 5585.56 keV), from the triple alpha source. The Am-241 peak was used because this prototype has low energy resolution, and so only one peak is visible, even though there are actually three peaks for the triple alpha source.

These results can also be shown in graphical form, as in Figure 14:-

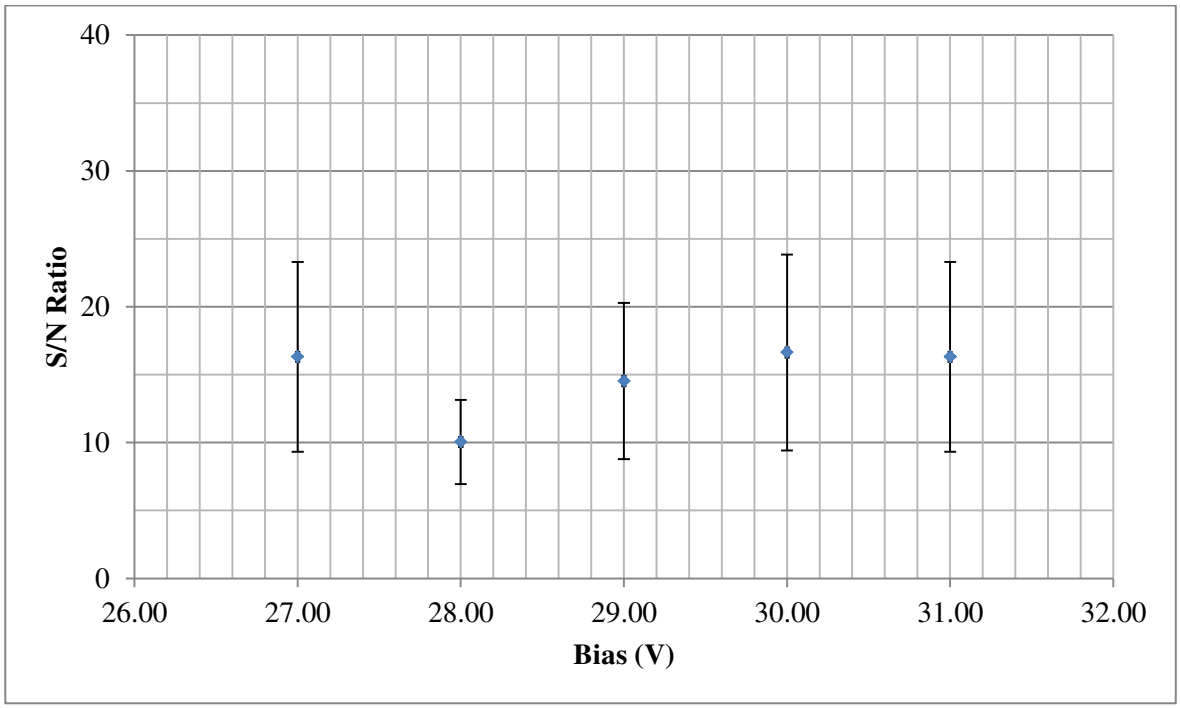

Figure 14: A graph showing how the signal-to-noise ratio varies as the bias across the SiPM is changed. These results are for the prototype with a plastic scintillator (with a cuboid geometry) and the Am-241 source peak.

Table 7 shows a summary of the highest signal-to-noise values for each of the three prototypes and the corresponding optimum bias values: -

Prototype	Scintillator	Geometry	Source Peak	S/N	Optimum Bias Value(s) (V)
1	Plastic	Truncated pyramid	Am-241	26±9	27.00±0.01
				47±28	28.00±0.01
				26±10	29.00±0.01
2a	Caesium Iodide	Truncated pyramid	Pu-239	23±5	29.00±0.01
				20±5	30.00±0.01
				23±6	31.00±0.01
2b	Caesium Iodide	Truncated pyramid	Am-241	22±5	29.00±0.01
				20±5	30.00±0.01
				22±6	31.00±0.01
2c	Caesium Iodide	Truncated pyramid	Cm-244	15±4	29.00±0.01
				14±3	30.00±0.01
				15±4	31.00±0.01
3	Plastic	Cuboid	Am-241	None	None

Table 7: A table showing the signal-to-noise ratio and corresponding optimum bias value for each of the three UoYTube prototypes.

For each of these experiments, it would seem that the trend is such that, as the bias is increased, the signal-to-noise ratio increases. The exception to this is Figure 10, which seems to show the opposite that an increase in bias leads to a decrease in the signal-to-noise ratio. It is unclear as to why this is the case. The optimum bias value is the bias value which yields the highest signal-to-noise ratio. Therefore, for the plastic scintillator (with a truncated pyramid geometry), the optimum bias values are 27.00±0.01, 28.00±0.01 and 29.00±0.01 volts. For the Caesium Iodide scintillator (with a truncated pyramid geometry), there are three peaks visible, and the optimum bias value for this prototype, should be inferred using the results for all three peaks. It should only be one value. Unfortunately, these optimum bias values cannot be said to be distinguishable from each other. Thus, for this prototype, the optimum bias values are 29.00±0.01, 30.00±0.01 and 31.00±0.01 volts. For the plastic scintillator (with a cuboid geometry), the optimum bias value is unknown. This is because the error bars for the signal-to-noise value are too large and therefore, the measurements cannot be said to be distinguishable from each other.

k. Characterisation of CsI and Plastic Prototypes – Energy Resolution

The experimental method used for these measurements, is as described in section c. The error analyses for these measurements, are as described in x. The aim of these measurements is to establish the energy resolution of each of the three UoYTube prototypes. In the following three experiments, the equipment was setup as described in section c. The radioactive source that was used in these experiments was the Am/Cm/Pu composite source. This source has three main characteristic alpha peaks at 5157 keV, 5586 keV and 5805 keV. For each of the three prototypes, spectra were taken at the bias value of 27V. To calculate the energy resolution, each of the alpha peaks were then fitted to Gaussian distributions using MATLAB [18].

A Gaussian distribution is described by three values [19]: A1 (the height of the curve's peak), B1 (the position of the peak centroid on the x axis) and C1 (equal to $\sqrt{2}\sigma$, where σ is the standard deviation). These values appear in the mathematical expression for a Gaussian distribution: -

$$f(x) = A1 \times \exp\left(-\left(\frac{x - B1}{C1}\right)^2\right)$$

The Full Width at Half-Maximum is described via the following expression [19]: -

$$FWHM = \frac{2\sqrt{2\ln 2}}{\sqrt{2}} \times C1$$

The additional factor of $\sqrt{2}$ on the denominator is because the MATLAB Gaussian is missing a root two in its standard equation for the FWHM. Using the expression for the FWHM, the energy resolution can then be calculated using the following equation [20]: -

$$\text{Energy Resolution} = FWHM \div \text{Peak Centroid}$$

Both the FWHM and Peak Centroid are measured in units of energy or channels. Thus, their units are either keV or Channels. The energy resolution can also be expressed as a percentage, by multiplying the above equation by 100. Based on this technique of analysis, the calculations of the energy resolution for each of the three prototypes are as shown in Table 8 and Table 9:-

Prototype	Scintillator	Geometry	Source Peak	A1 (No Units)	B1 (keV)	C1 (keV)
1	Plastic	Truncated pyramid	Am-241	190±3	5317±12	1108±17
2a	Caesium Iodide	Truncated pyramid	Pu-239	681±7	5153±2	170±5
2b	Caesium Iodide	Truncated pyramid	Am-241	654±8	5496±3	142±6
2c	Caesium Iodide	Truncated pyramid	Cm-244	449±7	5791±4	145±9
3	Plastic	Cuboid	Am-241	35±1	5413±18	906±27

Table 8: A table showing A1, B1 and C1 for each of the three UoYTube prototypes.

Prototype	Scintillator	Geometry	Source Peak	Peak Centroid (keV)	FWHM (keV)	Energy Resolution (%)
1	Plastic	Truncated pyramid	Am-241	5317±12	1845±28	35±1
2a	Caesium Iodide	Truncated pyramid	Pu-239	5153±2	283±9	6±0
2b	Caesium Iodide	Truncated pyramid	Am-241	5496±3	236±9	4±0
2c	Caesium Iodide	Truncated pyramid	Cm-244	5791±4	242±14	4±0
3	Plastic	Cuboid	Am-241	5413±18	1536±44	28±1

Table 9: A table showing the Peak Centroid, Full-Width at Half-Maximum (FWHM) and energy resolution for each of the three UoYTube prototypes.

These results can also be shown in graphical form, as in Figure 15, Figure 16 and Figure 17:-

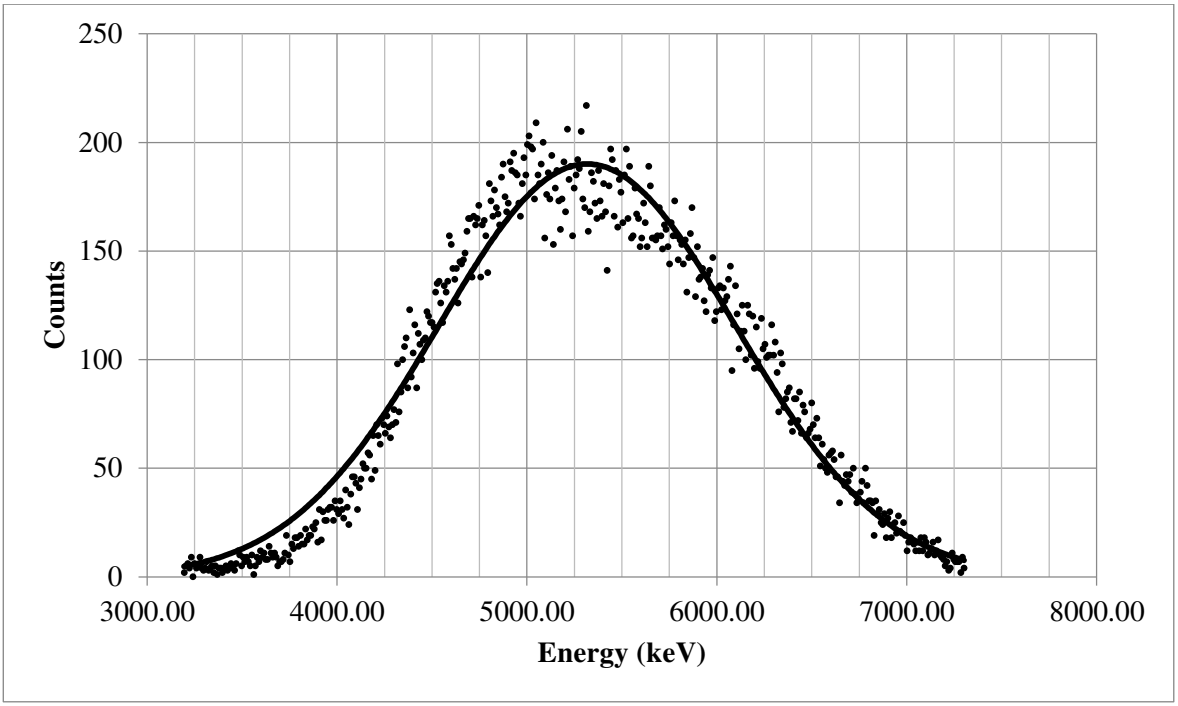

Figure 15: A graph showing the Energy spectrum measured at a bias of 27V. These results are for the UoYTube prototype made from a plastic scintillator (with a truncated pyramid geometry), and include a Gaussian fitted to the Am-241 source peak.

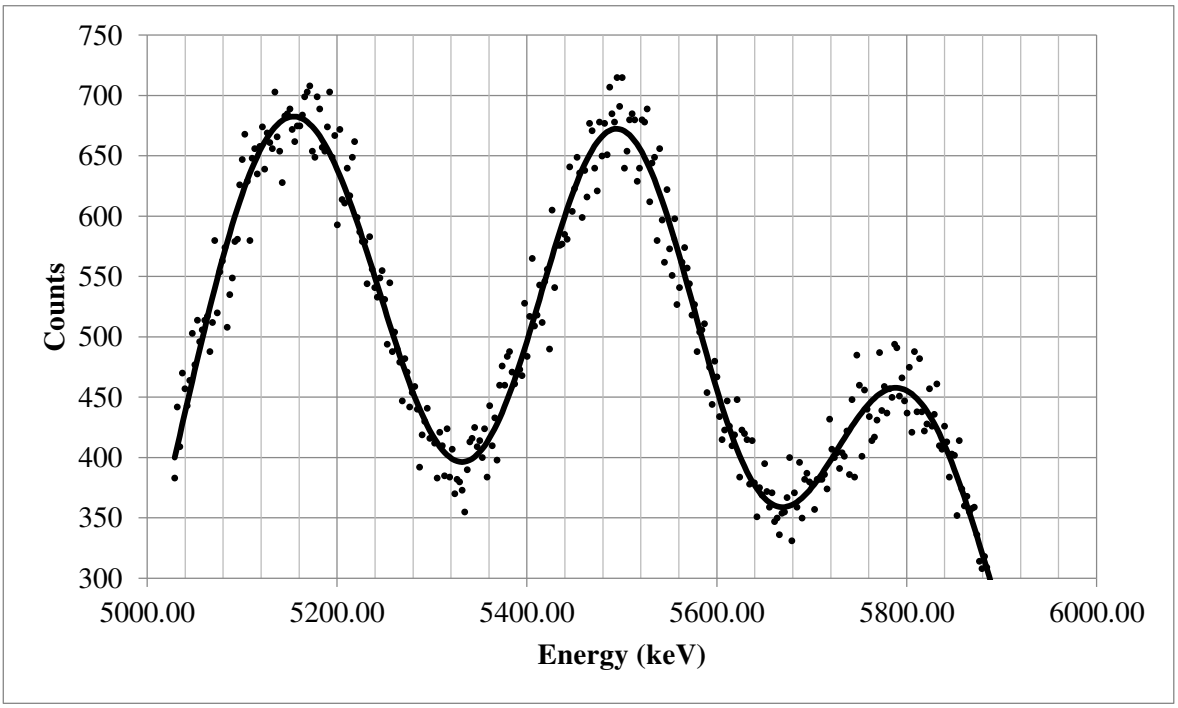

Figure 16: A graph showing the Energy spectrum measured at a bias of 27V. These results are for the UoYTube prototype with a truncated pyramid geometry. The scintillator used in this prototype is Caesium Iodide scintillator. The solid black line represents three fitted Gaussians, one for each of the alpha lines from the mixed Pu-239, Am-241, Cm-244 source.

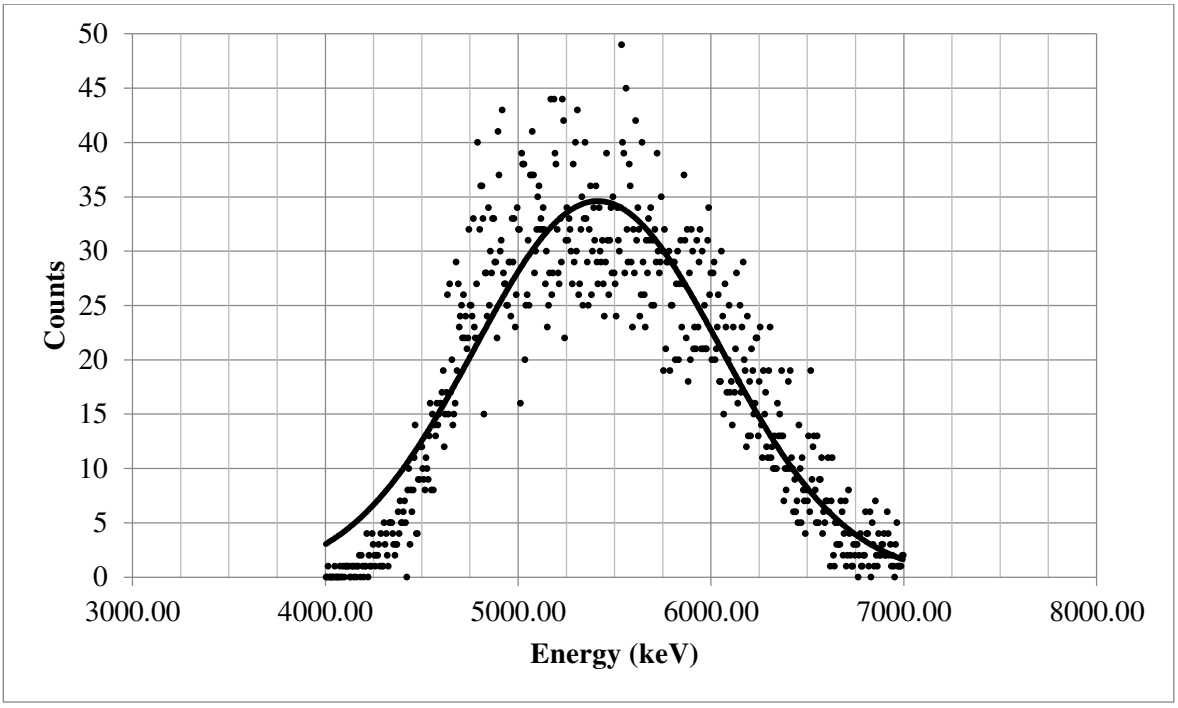

Figure 17: A graph showing the Energy spectrum measured at a bias of 27V. These results are for the UoYTube prototype made from a plastic scintillator (with a cuboid geometry), and include a Gaussian fitted to the Am-241 source peak.

To establish the quality of the fit, the R-Squared and Adjusted R-Squared values can be used. The R-Squared (R-sq) value ranges from 0 to 1. It should ideally be close to one; this would demonstrate that the fit is able to accommodate a larger proportion of the variance in the data. The Adjusted R-Squared (Adj R-sq) value can be any value less than or equal to one. It should ideally be close to one; demonstrating that the fit is more accurate.

The Gaussian fit for Figure 16 seems quite reasonable, given the R-sq and Adj R-sq values of 0.9582 and 0.9571, as shown in section 13, Appendix 2 – Gaussian Distributions. The Gaussian fits for Figure 15 and Figure 17 however, appear by inspection, to be quite poor. This is because it is not possible to resolve the three alpha peaks for the plastic prototypes, as the resolution of these prototypes is too low.

Their R-sq and Adj R-sq values are 0.9639 and 0.9637 for Figure 15 and 0.8412 and 0.8406 for Figure 17. Interestingly, this implies that the fit for Figure 15 is actually better than Figure 16. It also implies (as initially expected) that the fit for Figure 17 is very poor in comparison to Figure 16.

These results also question as to whether the optimum bias value was used; that is, the bias value that produced the best possible energy resolution and the best possible fit, for each of the prototypes. For each of the three prototypes and their corresponding figures, spectra were taken at the bias value of 27V. This was because this was initially believed to be the optimum value for the SiPM. The bias value was varied from 27 to 31 volts. However, the energy resolution as a function of the bias was not calculated for the plastic prototypes. It was however, calculated when comparing the Acrylic and 3D-Printed light guides, with the Bi-207 conversion electron source, and the Caesium Iodide scintillator, as shown in section xix. These results seemed to indicate that an increase in bias, leads to an increase in the energy resolution, but that there is levelling off point after 29 volts. Also, these results are for the Caesium Iodide prototype, so perhaps this is not a fair comparison.

Based on these measurements, the Caesium Iodide scintillator (with a truncated pyramid geometry), is the most suitable for use in the UoYTube, as it has the highest energy resolution. Its energy resolution is calculated as between 4±0 and 6±0 percent, depending upon which source peak is used in the calculation. These values should be all approximately the same, for a given detector, so this indicates that the results are correct.

l. Analysis of the light output from the light guides

The experimental method used for these measurements, is as described in section f. The error analyses for these measurements, are as described in xi. Figure 18, Figure 19, and Figure 20 show the three characteristic spectra (measurements of reflectance and transmittance) which were recorded for the light guides, using the FILMETRICS® F10-RT spectrometer [15]. The first spectrum is only the incident light with no light guide positioned in the path of the beam. The second spectrum is for a light guide made from a bulk Acrylic that was fabricated mechanically by Jason Flatt. In this case, the light guide was positioned in the path of the beam. The third spectrum is for the 3D printed light guide that was fabricated by myself, where the results were recorded with the light guide positioned in the beam. The aim of the measurements was to establish how the reflectance and transmittance varies depending upon the wavelength of the input light, and the type of light guide used. Both the acrylic and 3D printed light guides have the truncated pyramid geometry as described in Figure 7:-

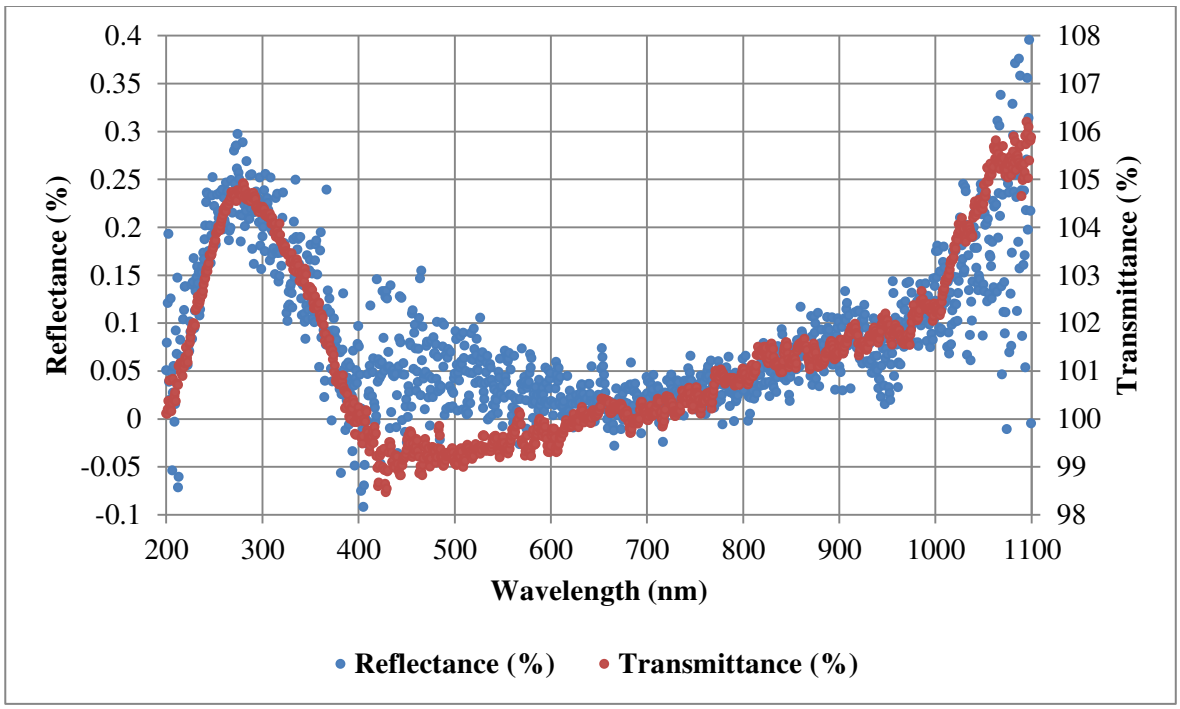

Figure 18: A graph of the Reflectance and Transmittance of light, recorded as a function of Wavelength, using the FILMETRICS® F10-RT spectrometer. This spectrum is with no sample.

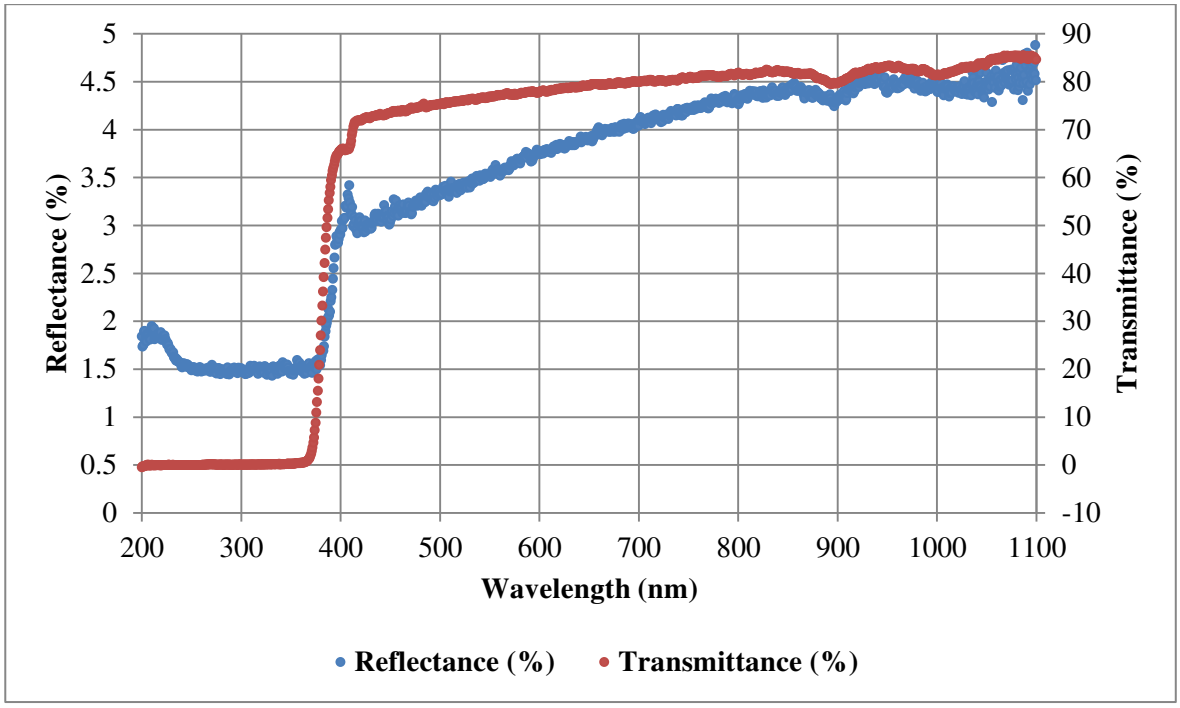

Figure 19: A graph of the Reflectance and Transmittance of light, recorded as a function of Wavelength, using the FILMETRICS® F10-RT spectrometer. This spectrum is for a light guide made from bulk Acrylic.

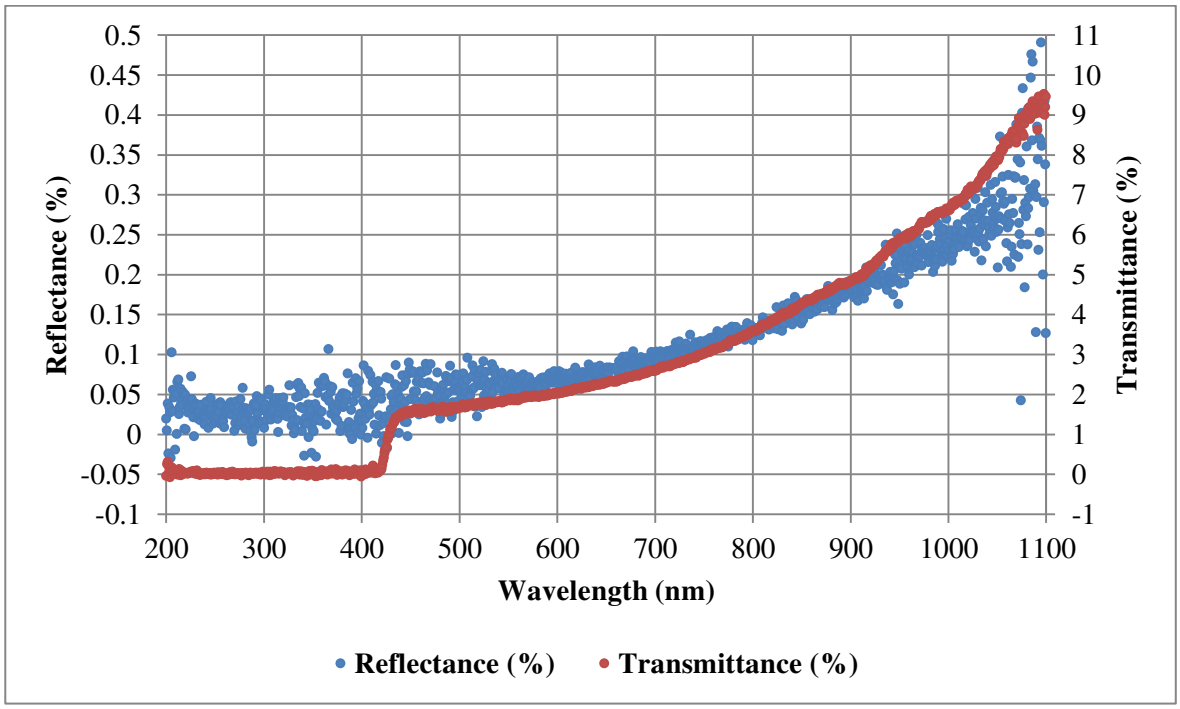

Figure 20: A graph of the Reflectance and Transmittance of light, recorded as a function of Wavelength, using the FILMETRICS® F10-RT spectrometer. This spectrum is for a light guide made using a 3D printer.

The results from the measurements of reflectance and transmittance seem inconsistent. Firstly, the distribution of both the reflectance and transmittance measurements are the same; this is not intuitive, as it should be the case that as one increases, the other should decrease.

Secondly, the addition of reflectance and transmittance should equal 100%. This is not the case for either of the above graphs. This could be attributed to the fact that another parameter, the absorbance is not measured, and that this is required to ensure that the values add up to 100%. It could also be the case that the calibration was performed incorrectly. The calibration process involved the use of a known sample called BK7, which provided a baseline for the spectrometer's software. This may have been an unsuitable sample, in that it may have different optical properties to the light guides. The results may also have been affected by ambient light, which was difficult to shield from the spectrometer during the measurement process. The ambient light would affect the results such that the recorded values would be higher than the actual values.

The Silicon Photomultipliers that are used to detect the light, are designed to operate in the visible part of the electromagnetic spectrum, where the photon detection efficiency is greatest [29] i.e. 400-700nm. Therefore, when measuring the transmission of light guide, this is the region of interest. For the acrylic light guide, the transmission is between 65±0.02 and 80±0.02 percent, for the 400-700nm wavelength region. For the 3D printed light guide, the transmission is between 0±0.02 and 2.5±0.02 percent, again for the 400-700nm wavelength region. This indicates that the acrylic light guide is more suitable for use in the UoYTube when compared to the 3D printed light guide. However, given the distributions observed and the difficulty associated with the calibration of the spectrometer, these values cannot be said with confidence.

It is also unclear as to whether or not the light from the spectrometer is the same as the characteristic light produced by the scintillator (the range of wavelengths and the relative distribution of these wavelengths may be different than those emitted from the spectrometer). To identify if this is the case, if the transmission rate values are correct, the light guides will be attached to a scintillator and compared directly to each other. This will be discussed later in this thesis.

It has been suggested by Professor David Jenkins, that the 3D printed light guide functions poorly as a light guide because it induces a polarisation effect on the input light, which results in a lower transmission rate. To test this hypothesis, a polarising film was introduced into the experiment, positioned directly in front of the light guide. If this light guide is indeed acting as a

polariser, it would be anticipated that as the polariser is rotated (from light to dark) the transmission rate would decrease. Consequently, spectra were recorded at different angles of rotation, to see if the transmission rate changed. The error values in the following figures are assumed to be; angle of polariser ±3 degrees, wavelength ±2.5 nanometres, transmittance ±0.02 percent and reflectance ±0.002 percent. The results are as shown in Figure 21, Figure 22, Figure 23 and Figure 24:-

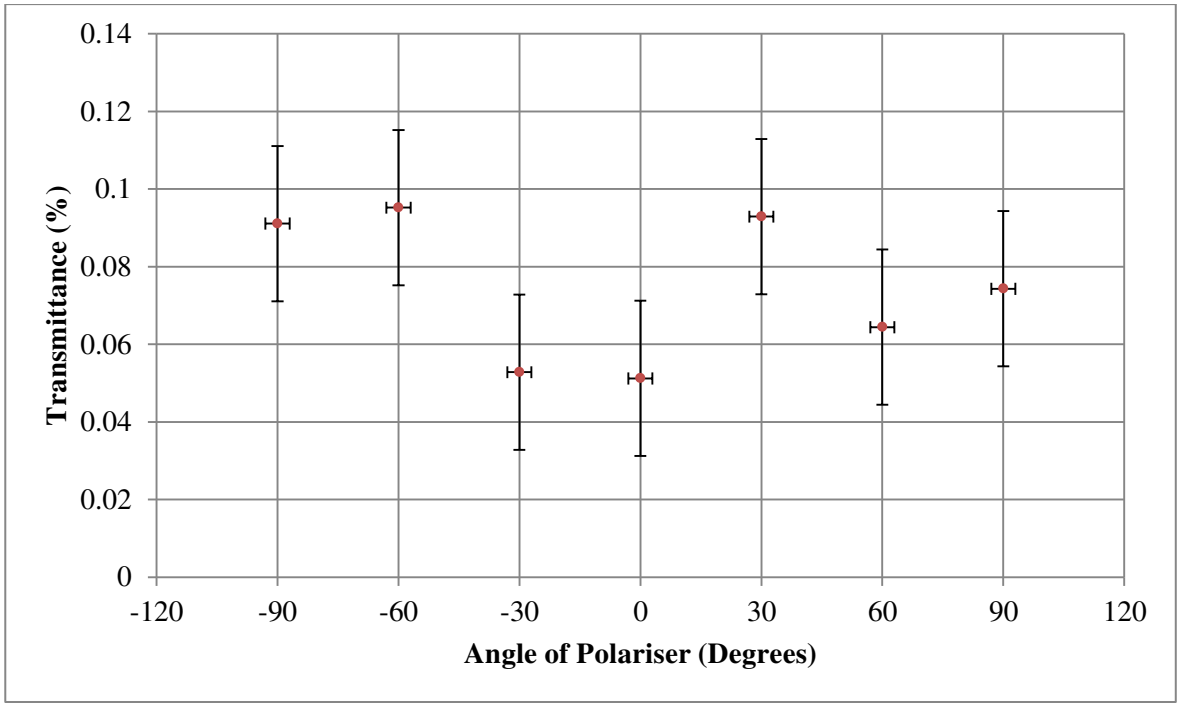

Figure 21: A graph of the transmission rate of the 3D printed light guide as a function of polariser angle of rotation. The wavelength of the light is 400nm.

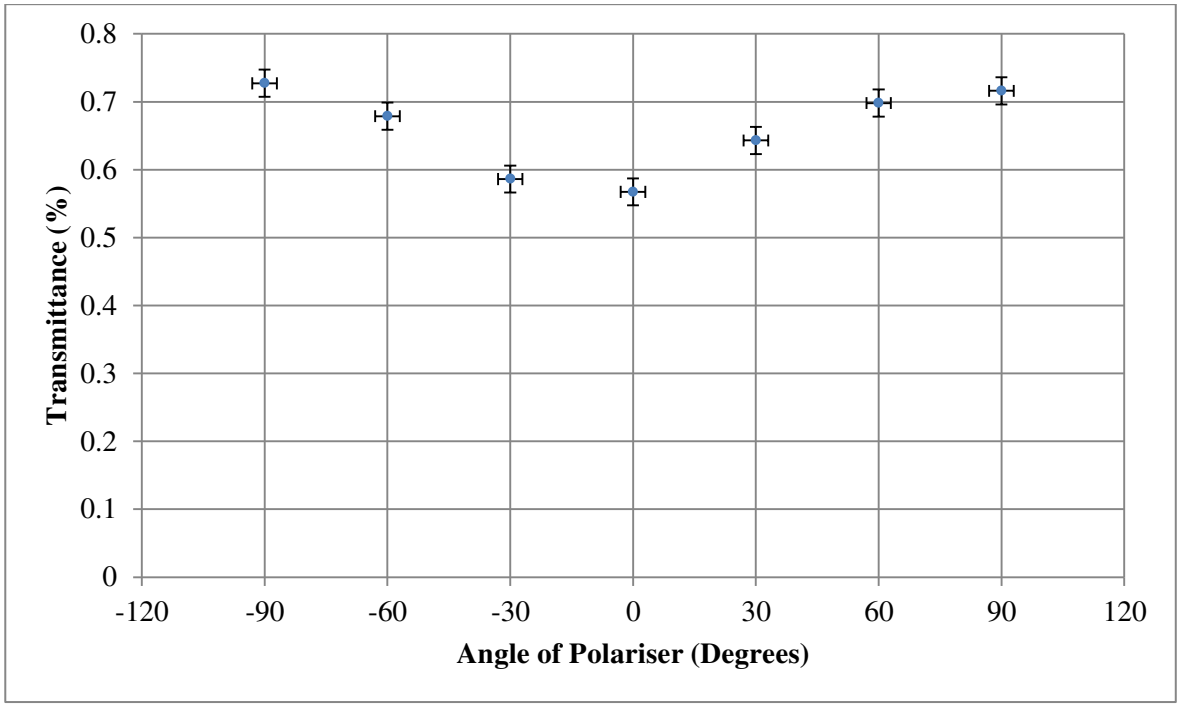

Figure 22: A graph of the transmission rate of the 3D printed light guide as a function of polariser angle of rotation. The wavelength of the light is 500nm.

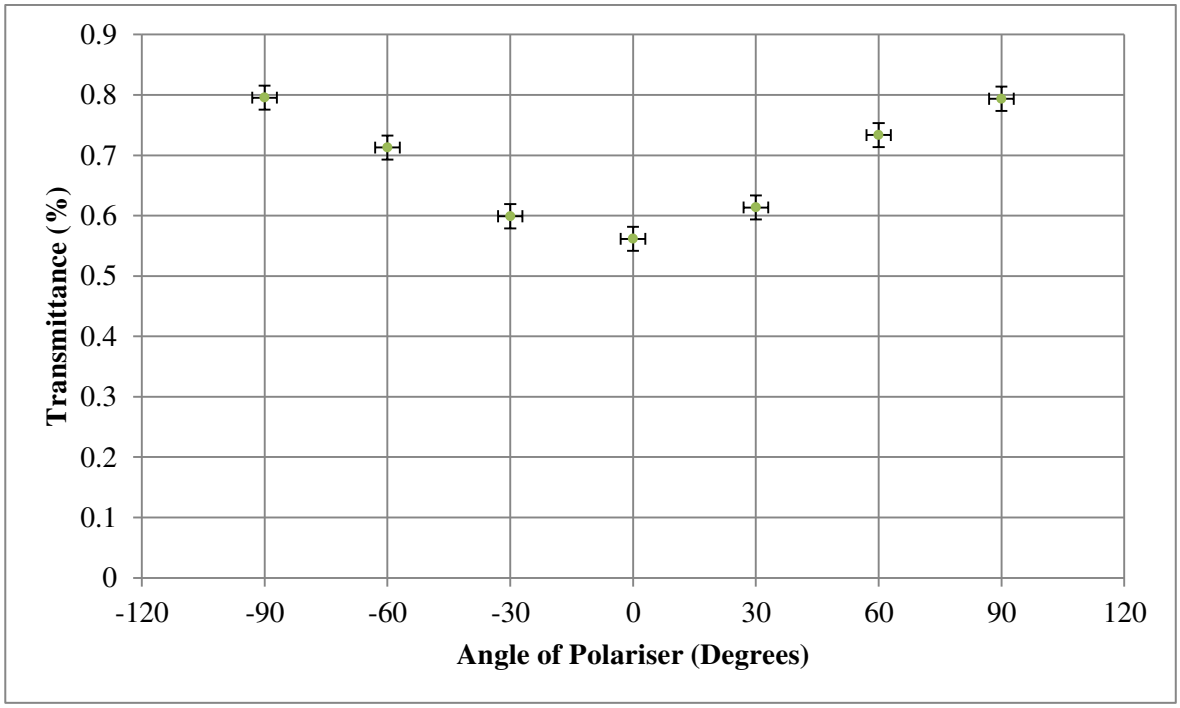

Figure 23: A graph of the transmission rate of the 3D printed light guide as a function of polariser angle of rotation. The wavelength of the light is 600nm.

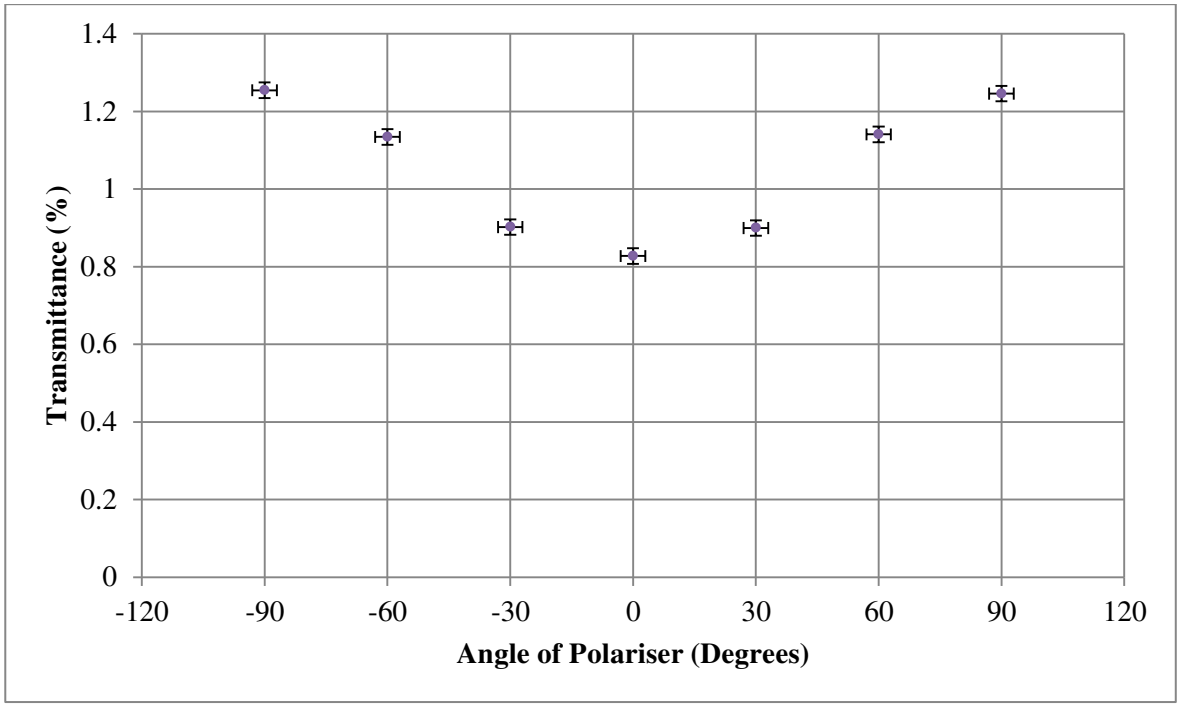

Figure 24: A graph of the transmission rate of the 3D printed light guide as a function of polariser angle of rotation. The wavelength of the light is 700nm.

These results seem to indicate that there is some change in the transmission as the polariser is rotated. The results for the reflectance were also recorded, to see how this parameter changed as a function of polariser angle, as demonstrated in Figure 25, Figure 26, Figure 27 and Figure 28:-

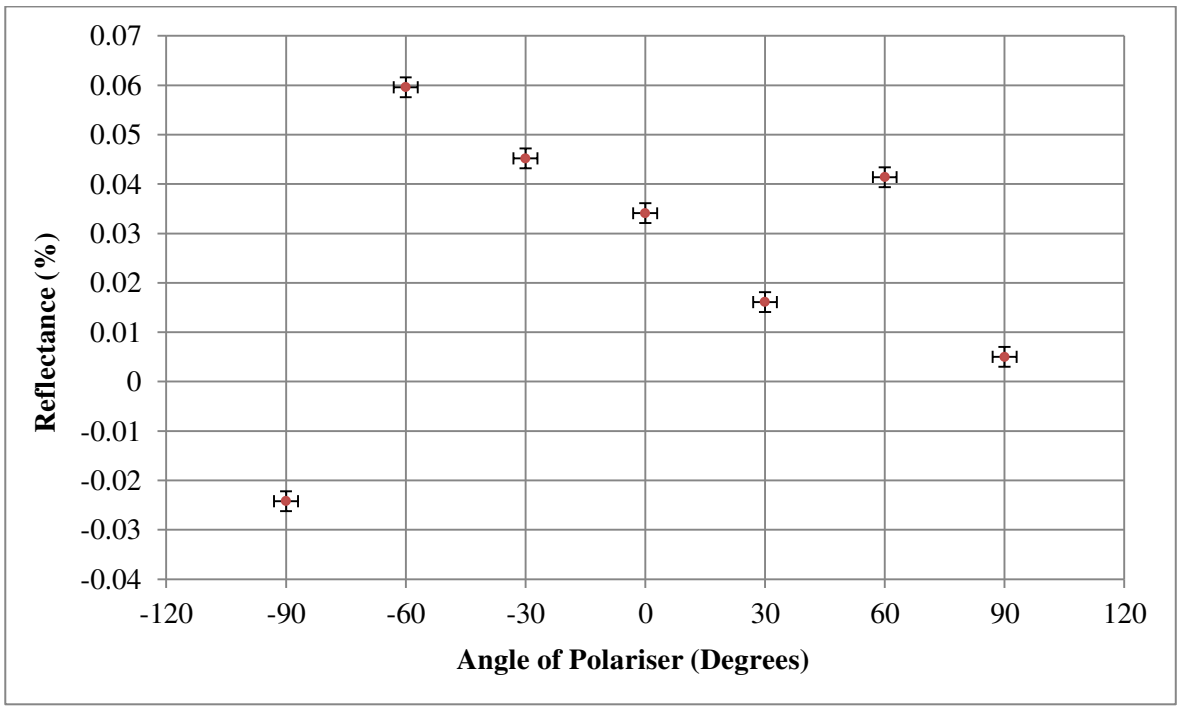

Figure 25: A graph of the reflectance of the 3D printed light guide as a function of polariser angle of rotation. The wavelength of the light is 400nm.

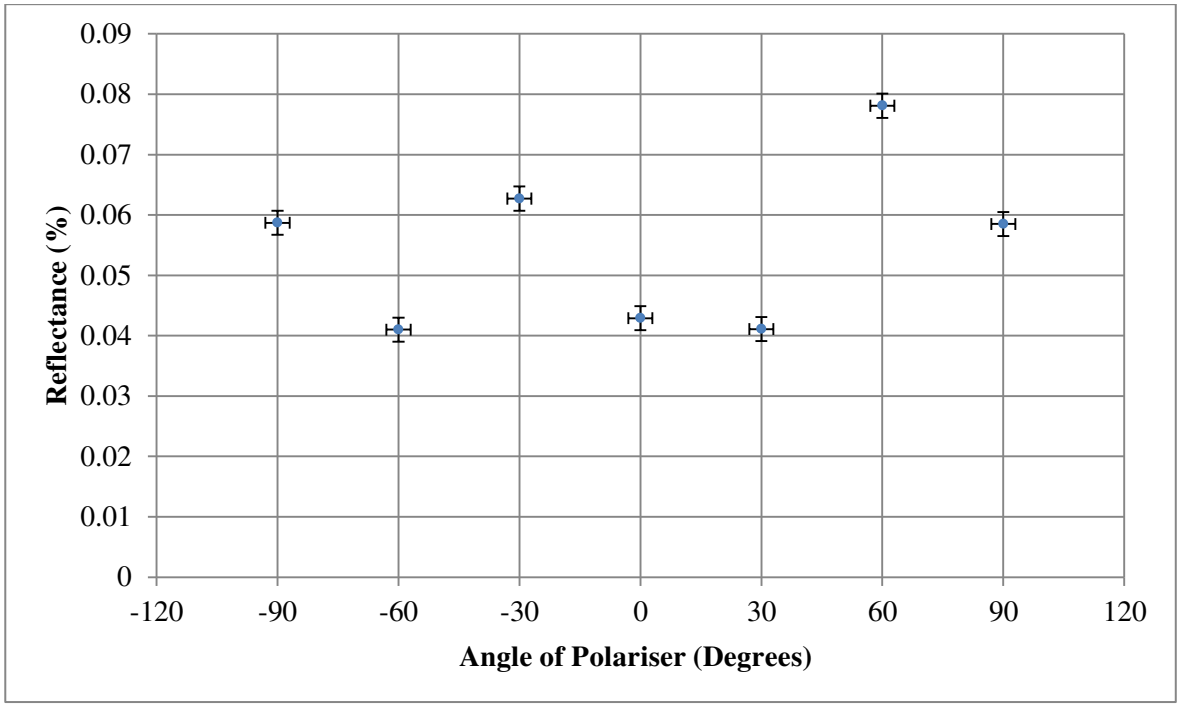

Figure 26: A graph of the reflectance of the 3D printed light guide as a function of polariser angle of rotation. The wavelength of the light is 500nm.

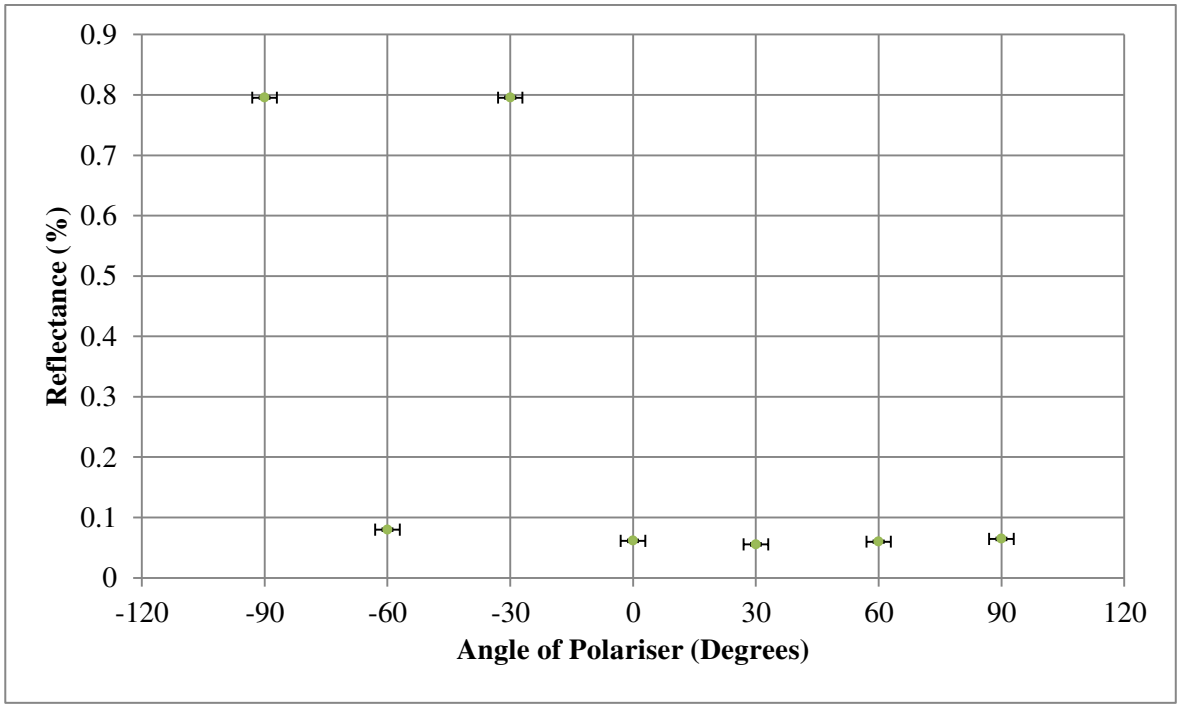

Figure 27: A graph of the reflectance of the 3D printed light guide as a function of polariser angle of rotation. The wavelength of the light is 600nm.

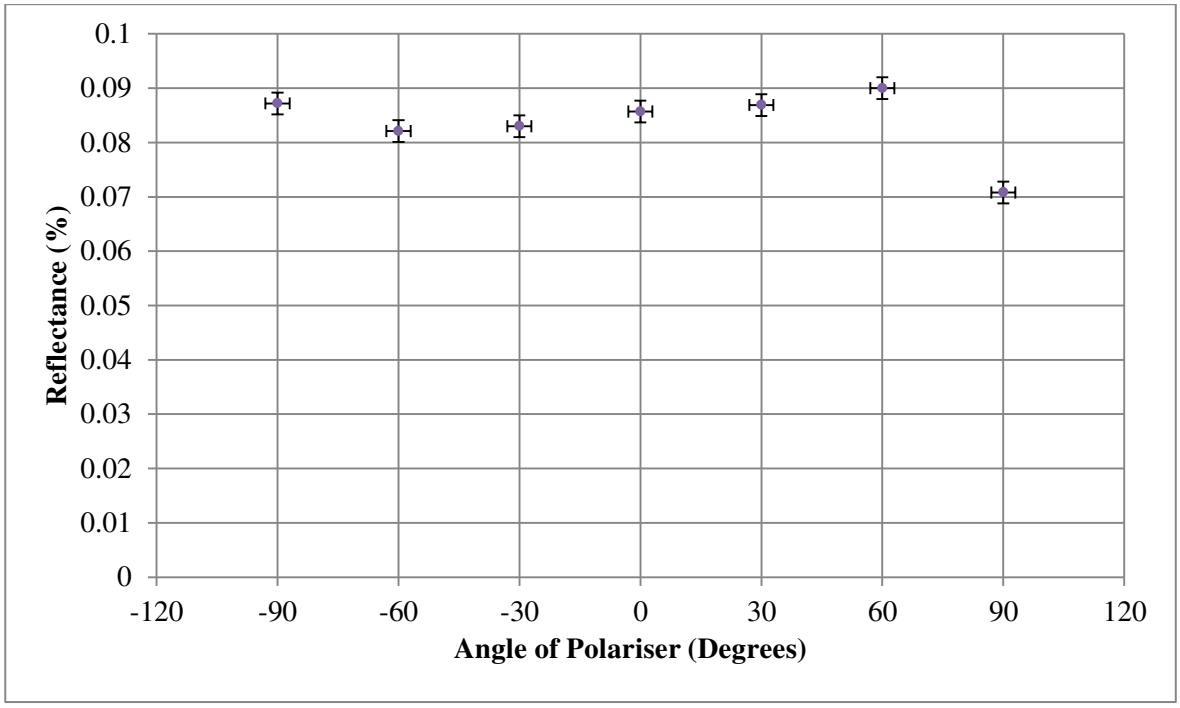

Figure 28: A graph of the reflectance of the 3D printed light guide as a function of polariser angle of rotation. The wavelength of the light is 700nm.

There appears to be no clear trend in the reflectance, as the wavelength and angle of polariser are varied. The errors are as described above, and are determined by the manufacturer's specifications. So, assuming the spectrometer is functioning correctly, these should be correct. However, as stated previously, there were other potential sources of error (calibration, ambient light, use of the BK7 sample), so confidence in these measurements, cannot be guaranteed.

m. Comparison of the 3D Printed and Acrylic light guides (Alpha Source)

The experimental method used for these measurements, is as described in section c. The error analyses for these measurements, are as described in x and xii. The results from the spectrometer suggest that the light transmission from the 3D printed light guide is much poorer than the light transmission from the bulk acrylic light guide. Having said that, in the previous experiments, described in section l, the light guides were not attached to a scintillator crystal; the light source was instead originating from the spectrometers laser beam. The fluorescence radiation from the scintillator crystal has different wavelengths to those provided by the spectrometer, so in these next set of measurements, a scintillator crystal (in this case a Caesium Iodide crystal) will be attached to each of the light guides. This setup was then used to measure spectra from a triple alpha source containing Pu-229, Am-241 and Cm-244, with an activity of 3.85×10^{3} Bq. Using this data, the light guides will be compared to each other in terms of the energy resolution and the optimum shaping time.

xiv. Energy Resolution

The first parameter which will be used to compare the Acrylic and 3D Printed light guide is the energy resolution. The aim of these measurements is to establish whether the observed energy resolution depends upon the material (Acrylic or the 3D Printed), used for the light guide. The spectra for each of the light guides at a bias value of 27 Volts is as demonstrated in Figure 29 and Figure 30:-

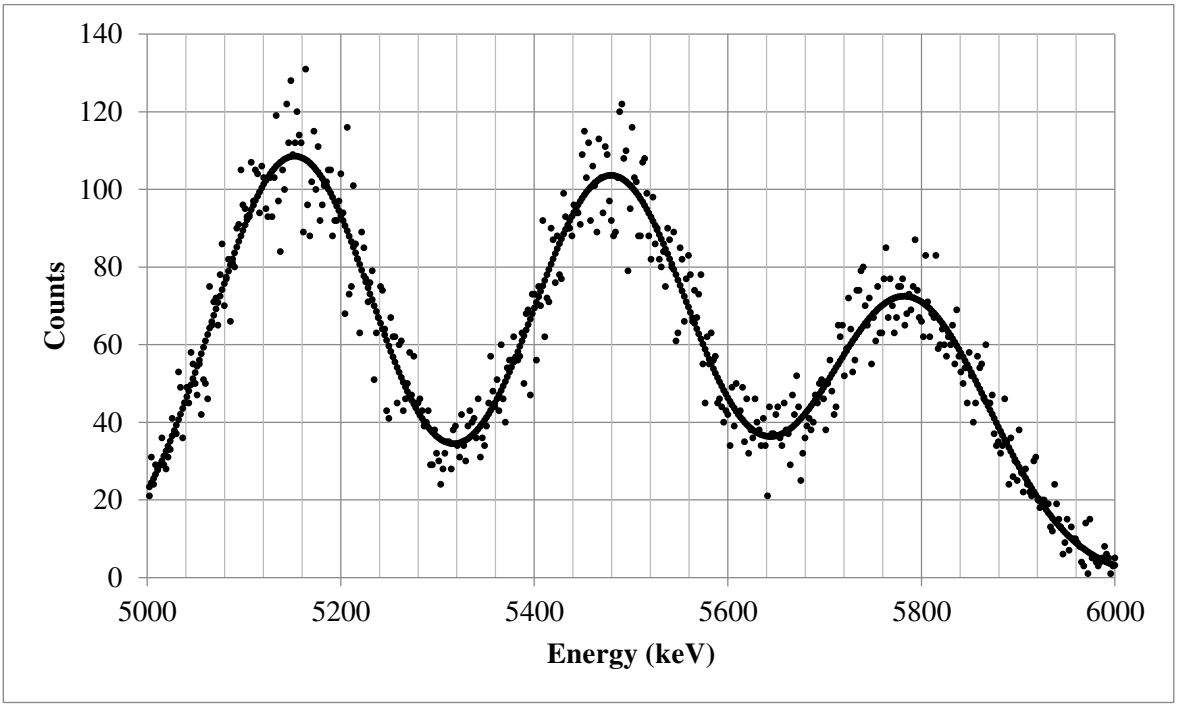

Figure 29: A partial spectrum showing the triple alpha peaks from the mixed alpha source discussed in the text. These results were taken using a bias of 27V and the Acrylic light guide coupled to the UoYTube prototype detector made from a Caesium Iodide scintillator (truncated pyramid geometry). The solid lines show the results of Gaussian fits to each of the Pu-239, Am-241 and Cm-244 principle alpha decay peaks.

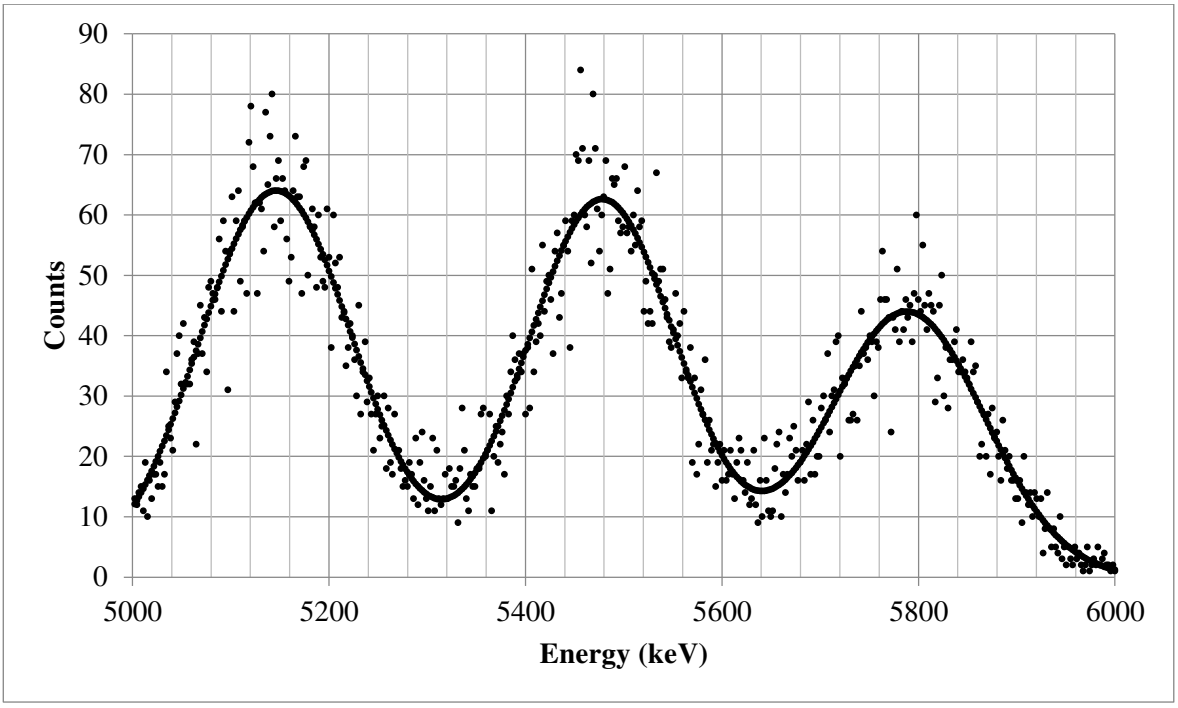

Figure 30: A partial spectrum showing the triple alpha peaks from the mixed alpha source discussed in the text. These results were taken using a bias of 27V and the 3D Printed light guide coupled to the UoYTube prototype detector made from a Caesium Iodide scintillator (truncated pyramid geometry). The solid lines show the results of Gaussian fits to each of the Pu-239, Am-241 and Cm-244 principle alpha decay peaks.

Using these spectra, it is possible to determine the energy resolution. The peaks were fitted to a Gaussian distribution in MATLAB and then A1, B1 and C1 were calculated. The results for the Acrylic and 3D Printed light guides, with a truncated pyramid geometry and operated at a bias value of 27 Volts, are as given in Table 10 and Table 11:-

Scintillator	Geometry	Source Peak	A1 (No Units)	B1 (keV)	C1 (keV)
Caesium Iodide	Truncated pyramid	Pu-239	109±2	5152.00±2.00	120.90±3.75
Caesium Iodide	Truncated pyramid	Am-241	103±2	5479.00±2.50	121.80±4.50
Caesium Iodide	Truncated pyramid	Cm-244	72±2	5783.00±3.50	122.20±5.60
Scintillator	**Geometry**	**Source Peak**	**Peak Centroid (keV)**	**FWHM (keV)**	**Energy Resolution (%)**
Caesium Iodide	Truncated pyramid	Pu-239	5152.00±2.00	201.31±6.24	3.91±0.12
Caesium Iodide	Truncated pyramid	Am-241	5479.00±2.50	202.81±7.49	3.70±0.14
Caesium Iodide	Truncated pyramid	Cm-244	5783.00±3.50	203.48±9.32	3.52±0.16

Table 10: A table showing the A1, B1 and C1 parameters (see section iii) for each of the mixed alpha source peaks for the Acrylic Light guide. The table also shows the Peak Centroid, Full-Width at Half-Maximum (FWHM) in keV and energy resolution, expressed as a percentage.

Scintillator	Geometry	Source Peak	A1 (No Units)	B1 (keV)	C1 (keV)
Caesium Iodide	Truncated pyramid	Pu-239	64±2	5146.00±3.00	111.40±4.10
Caesium Iodide	Truncated pyramid	Am-241	63±2	5478.00±3.00	108.20±4.20
Caesium Iodide	Truncated pyramid	Cm-244	44±2	5788.00±3.50	111.70±5.80
Scintillator	**Geometry**	**Source Peak**	**Peak Centroid (keV)**	**FWHM (keV)**	**Energy Resolution (%)**
Caesium Iodide	Truncated pyramid	Pu-239	5146.00±3.00	185.49±6.83	3.60±0.13
Caesium Iodide	Truncated pyramid	Am-241	5478.00±3.00	180.16±6.99	3.88±0.13
Caesium Iodide	Truncated pyramid	Cm-244	5788.00±3.50	185.99±9.66	3.21±0.17

Table 11: A table showing the A1, B1 and C1 parameters (see section iii) for each of the mixed alpha source peaks for the 3D Printed Light guide. The table also shows the Peak Centroid, Full-Width at Half-Maximum (FWHM) in keV and energy resolution, expressed as a percentage.

The energy resolution values are 3.91±0.12, 3.70±0.14 and 3.52±0.16 percent for the Acrylic light guide and 3.60±0.13, 3.29±0.13 and 3.21±0.17 percent for the 3D Printed light guide. In terms of the energy resolution values themselves, it is apparent that the variation in performance between the light guides is quite small, indicating that they are both are suitable for use in the UoYTube detector, although the 3D Printed light guide is slightly better.

The light guides can also be compared in terms of the number of counts A1 at each of the source peaks. Both experiments were conducted over a time period of five minutes for each bias value. The values are 109±2, 103±2 and 72±2 for the Acrylic light guide and 64±2, 63±2 and 44±2 for the 3D Printed light guide. Therefore, the number of counts is greater in each case, for the Acrylic light guide. This is consistent with the previous measurements of the transmittance. It could be argued that the number of counts is a more important feature than the energy resolution, in this context. This indicates that the Acrylic light guide is more suitable for use in the UoYTube, when compared to the 3D Printed light guide.

xv. Optimum Shaping Time

The third parameter which will be used to describe the performance of the light guides is the optimum shaping time. For a Gaussian shaped pulse, shaping time is stated as being the standard deviation of that pulse, when the horizontal axis is measured in time [27]. This shaping time refers to the shaping time of the amplifier used to process the signal. Optimum shaping time is defined as the shaping time that corresponds to the highest energy resolution. To establish the optimum shaping time, spectra were taken at various shaping time values on the spectroscopic amplifier (ORTEC® EASY-MCA). These were values of 0.5, 1.0, 2.0, 3.0, 6.0 and 10 microseconds. Then, the spectra were analysed in terms of their energy resolution. The optimum shaping time, was then established as the shaping time that corresponded to the highest energy resolution.

Table 12, Figure 31, Figure 32, Figure 33, Figure 34, Table 13, Figure 35, Figure 36, Figure 37 and Figure 38, show how the energy resolution for each of the triple alpha source peaks varies as a function of the shaping time, for both the Acrylic and 3D Printed light guides:-

Shaping Time (µs)	**Energy Resolution (Peak 1) (%)**	**Energy Resolution (Peak 2) (%)**	**Energy Resolution (Peak 3) (%)**	**Average Energy Resolution (%)**
0.5±0.0	4.05±0.36	4.71±0.36	3.74±0.36	4.17±0.36
1.0±0.1	3.95±0.09	3.68±0.11	3.50±0.13	3.71±0.11
2.0±0.1	3.79±0.09	3.58±0.10	3.46±0.13	3.61±0.11
3.0±0.2	3.79±0.10	3.54±0.11	3.42±0.14	3.59±0.12
6.0±0.3	4.15±0.37	4.15±0.37	3.81±0.37	4.03±0.37
10.0±0.5	3.77±0.09	3.64±0.11	3.55±0.13	3.65±0.11

Table 12: A table showing the energy resolution for each of the source peaks with the Acrylic Light guide. The average energy Resolution is also shown.

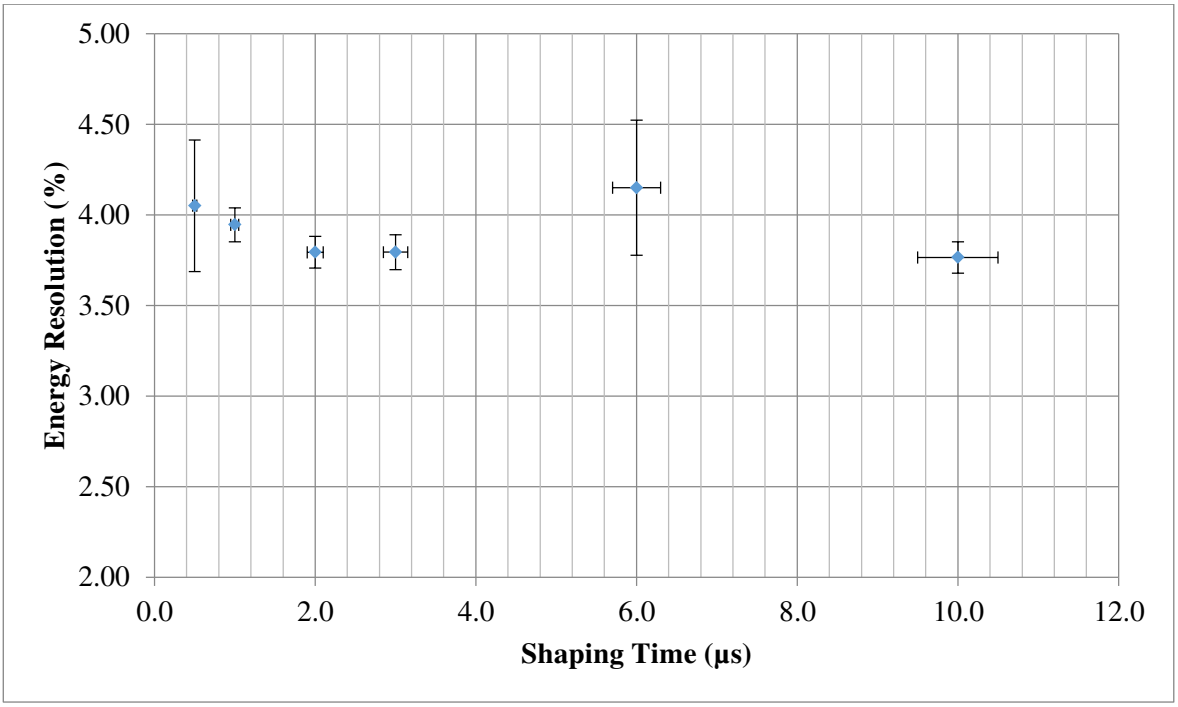

Figure 31: A graph showing the energy resolution as a function of shaping time for the Pu-239 source peak with the Acrylic Light guide.

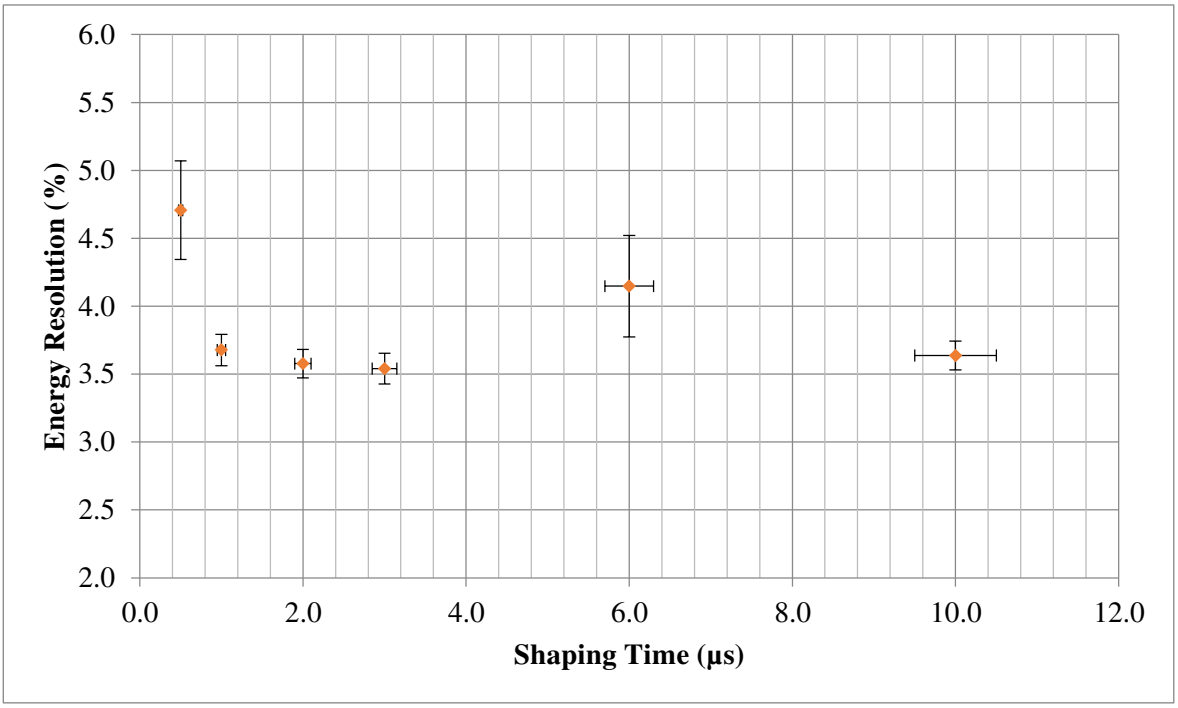

Figure 32: A graph showing the energy resolution as a function of shaping time for the Am-241 source peak with the Acrylic Light guide.

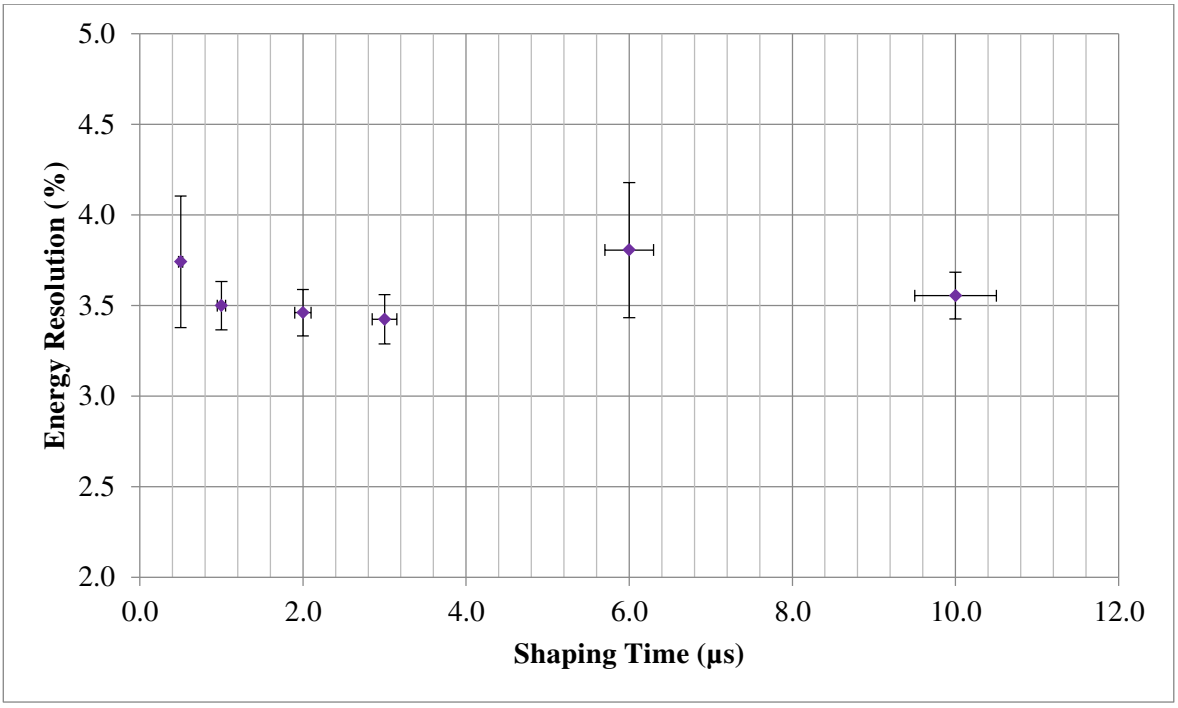

Figure 33: A graph showing the energy resolution as a function of shaping time for the Cm-244 source peak with the Acrylic Light guide.

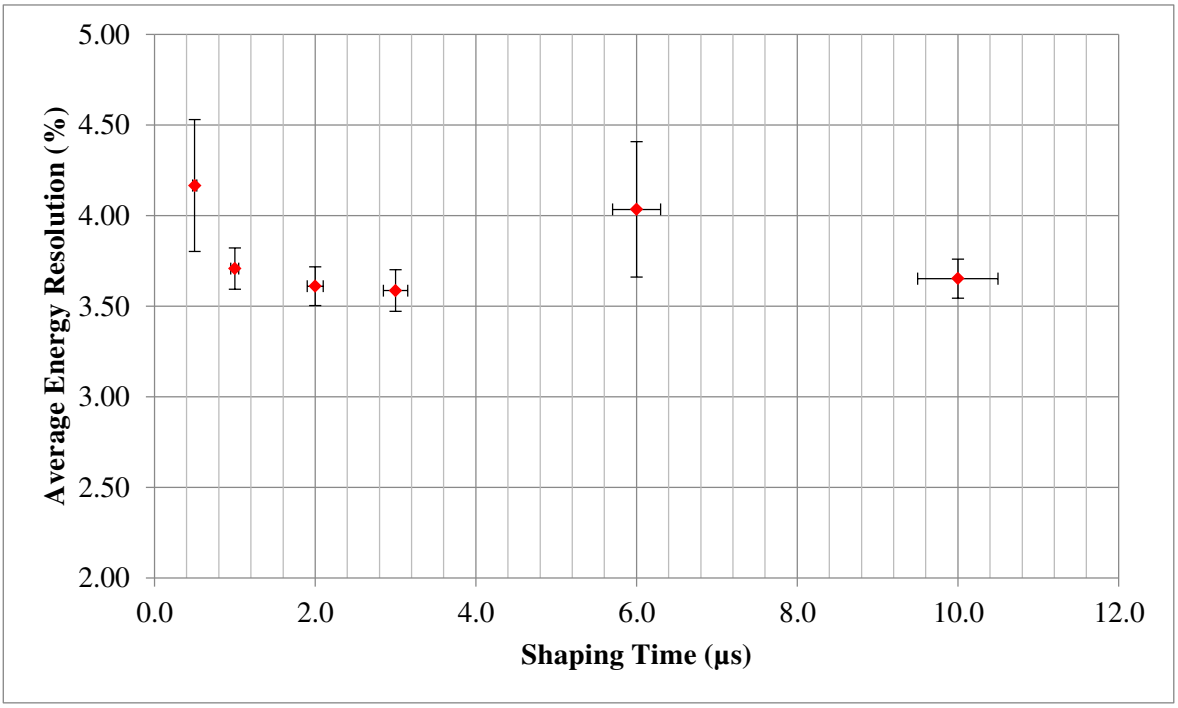

Figure 34: A graph showing the Average energy resolution as a function of shaping time for all of the three peaks, with the Acrylic Light guide.

Shaping Time (µs)	Energy Resolution (Peak 1) (%)	Energy Resolution (Peak 2) (%)	Energy Resolution (Peak 3) (%)	Average Energy Resolution (%)
0.5±0.0	3.82±0.09	3.47±0.09	3.36±0.12	3.55±0.10
1.0±0.1	3.68±0.10	3.36±0.08	3.21±0.12	3.42±0.10
2.0±0.1	3.70±0.08	3.26±0.08	3.06±0.10	3.34±0.09
3.0±0.2	3.62±0.08	3.27±0.08	3.13±0.10	3.34±0.09
6.0±0.3	3.62±0.08	3.26±0.07	3.23±0.10	3.37±0.09
10.0±0.5	3.59±0.07	2.81±0.08	2.32±0.07	2.91±0.07

Table 13: A table showing the energy resolution for each of the source peaks with the 3D Printed Light guide. The average energy resolution is also shown.

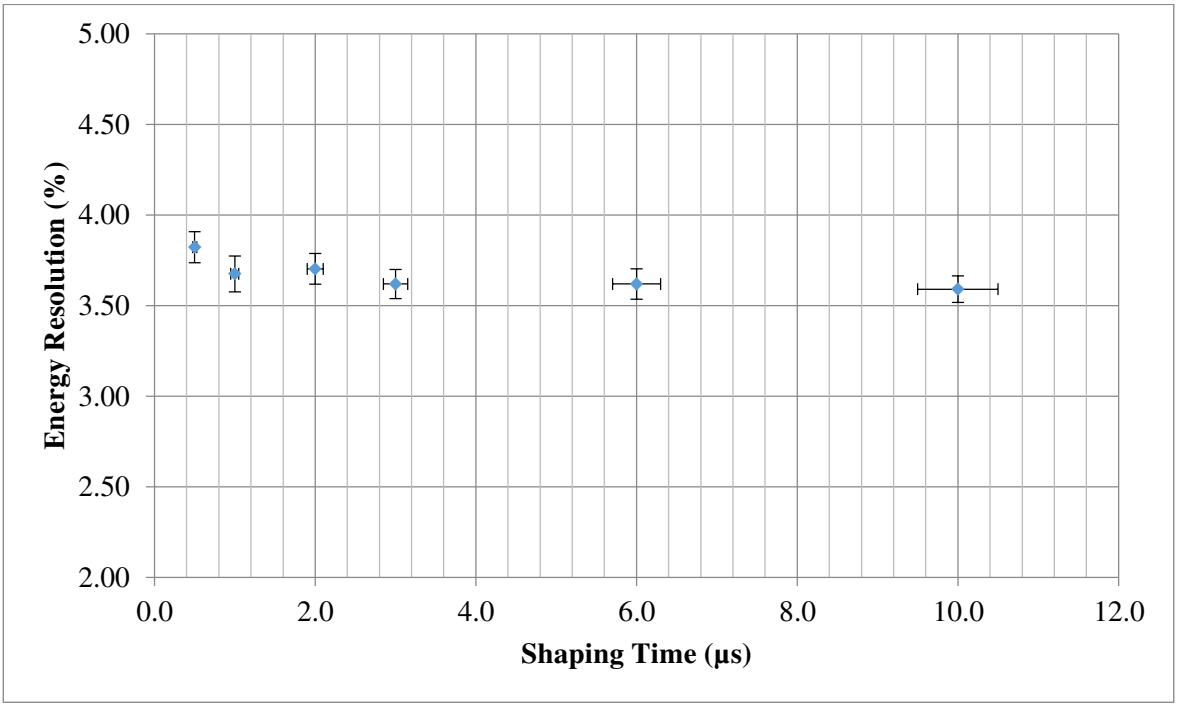

Figure 35: A graph showing the energy resolution as a function of shaping time for the Pu-239 source peak with the 3D Printed Light guide.

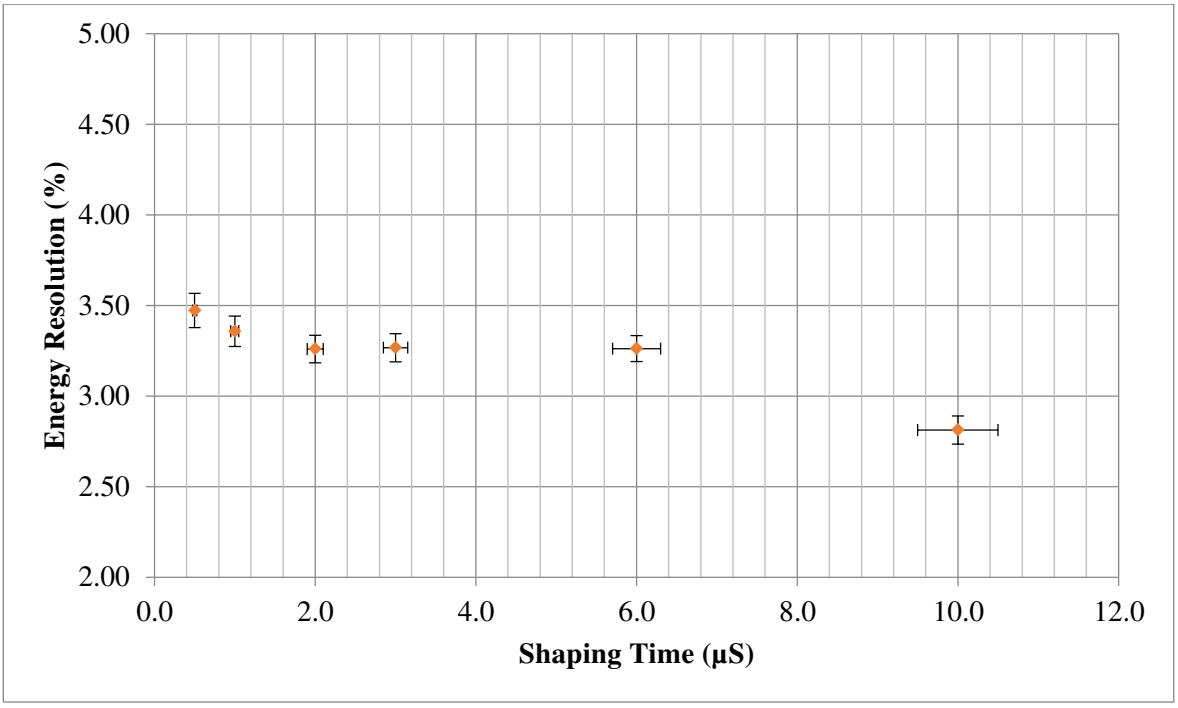

Figure 36: A graph showing the energy resolution as a function of shaping time for the Am-241 source peak with the 3D Printed Light guide.

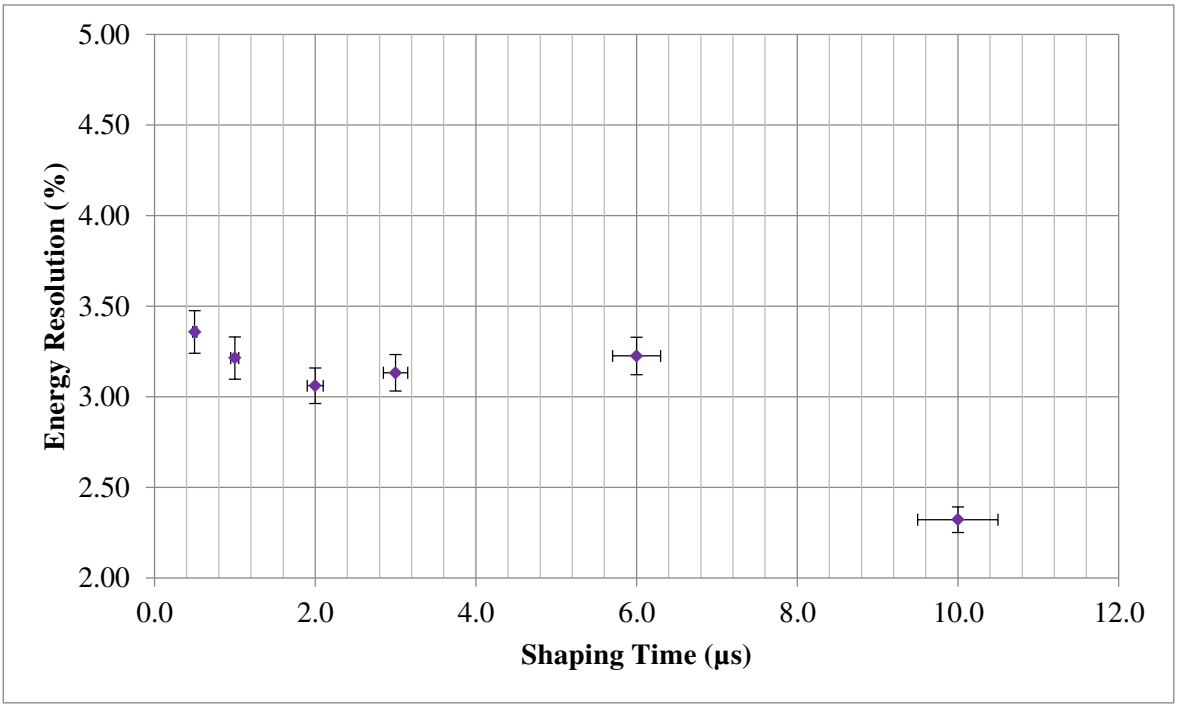

Figure 37: A graph showing the energy resolution as a function of shaping time for the Cm-244 source peak with the 3D Printed Light guide.

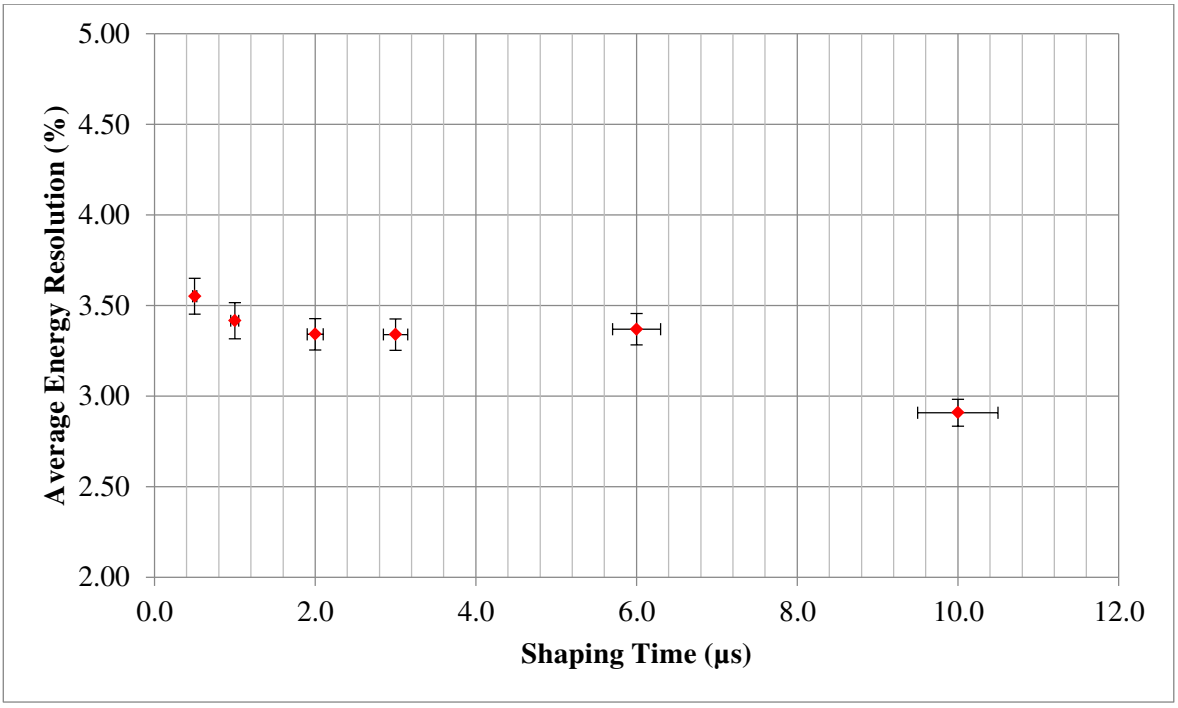

Figure 38: A graph showing the average energy resolution as a function of shaping time for all of the three peaks, with the 3D Printed Light guide.

By considering the error bars, and looking at the trends of all the graphs, it can be concluded that the best resolution is obtained for the highest values of shaping time. The small deviations from this trend at lower shaping times, are not statistically significant when the errors are taken into consideration.

n. Comparison of 3D Printed and Acrylic light guides (Conversion Electrons)

xvi. Signal-To-Noise Ratio and Optimum Bias

The experimental method used for these measurements, is as described in section c. The error analyses for these measurements, are as described in ix. The first parameter which will be used to characterise the UoYTube prototypes with the Bi-207 source, is the signal-to-noise ratio. The Bi-207 source has four conversion electron peaks and two gamma ray peaks which are normally visible in the spectrum [10]. One peak was visible in this spectrum, but unfortunately it is unclear as to which of the decay products this corresponds to. Thus, the calibration of the source and calculation of the parameters of interest, was performed using the channels on the x axis instead of energy.

The results for the Acrylic light guide are as shown in Table 14:-

Scintillator	**Source Peak (CE or γ)**	**Bias (V)**	**Signal (Counts)**	**Noise (Counts)**	**S/N Ratio**
Caesium Iodide scintillator (truncated pyramid)	Bi-207	27.00±0.01	4195±68	344±68	12±2
Caesium Iodide scintillator (truncated pyramid)	Bi-207	28.00±0.01	7344±131	569±131	13±3
Caesium Iodide scintillator (truncated pyramid)	Bi-207	29.00±0.01	5572±100	430±100	13±3
Caesium Iodide scintillator (truncated pyramid)	Bi-207	30.00±0.01	5747±103	445±103	13±3
Caesium Iodide scintillator (truncated pyramid)	Bi-207	31.00±0.01	4917±87	544±87	9±1

Table 14: A table showing how the signal-to-noise ratio varies as the bias across the SiPM is changed. These results are for the prototype with the bulk acrylic light guide, a Caesium Iodide scintillator (truncated pyramid geometry) and the Bi-207 source peak (either CE or γ). These values are taken from the spectra of Bi-207 (Figure 5), with bias values from 27-31 volts.

These results can also be shown in graphical form, as in Figure 39: -

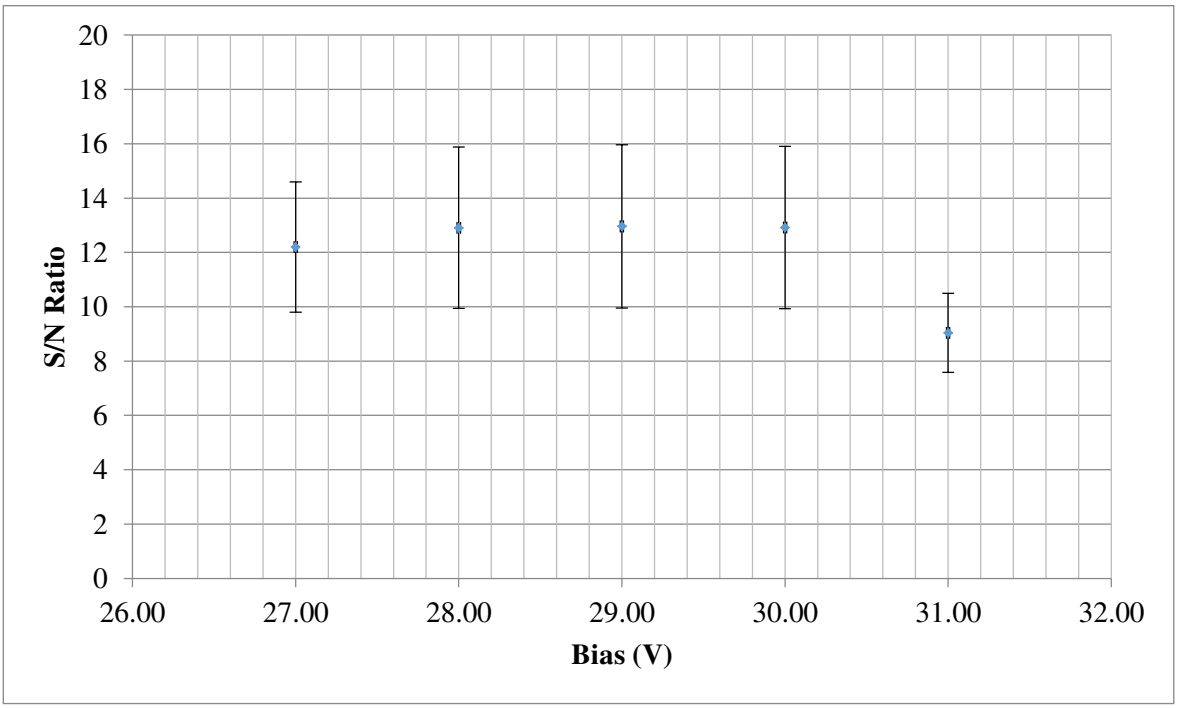

Figure 39: A graph showing how the signal-to-noise ratio varies as the bias across the SiPM is changed. These results are for the prototype with the bulk acrylic light guide, a Caesium Iodide scintillator (truncated pyramid geometry) and the Bi-207 source peak (either CE or γ). These values are taken from the spectra of Bi-207, with bias values from 27-31 volts.

The results for the 3D Printed light guide are as shown in Table 15: -

Scintillator	Source Peak (CE or γ)	Bias (V)	Signal (Counts)	Noise (Counts)	S/N Ratio
Caesium Iodide scintillator (truncated pyramid)	Bi-207	27.00±0.01	3919±70	418±70	9±2
Caesium Iodide scintillator (truncated pyramid)	Bi-207	28.00±0.01	4341±81	302±81	14±4
Caesium Iodide scintillator (truncated pyramid)	Bi-207	29.00±0.01	4095±78	321±78	13±3
Caesium Iodide scintillator (truncated pyramid)	Bi-207	30.00±0.01	3924±74	274±74	14±4
Caesium Iodide scintillator (truncated pyramid)	Bi-207	31.00±0.01	3924±71	210±71	19±6

Table 15: A table showing how the signal-to-noise ratio varies as the bias across the SiPM is changed. These results are for the prototype with the 3D Printed light guide, a Caesium Iodide scintillator (truncated pyramid geometry) and the Bi-207 source peak (either CE or γ). These values are taken from the spectra of Bi-207 (Figure 5), with bias values from 27-31 volts.

These results can also be shown in graphical form, as in Figure 40:-

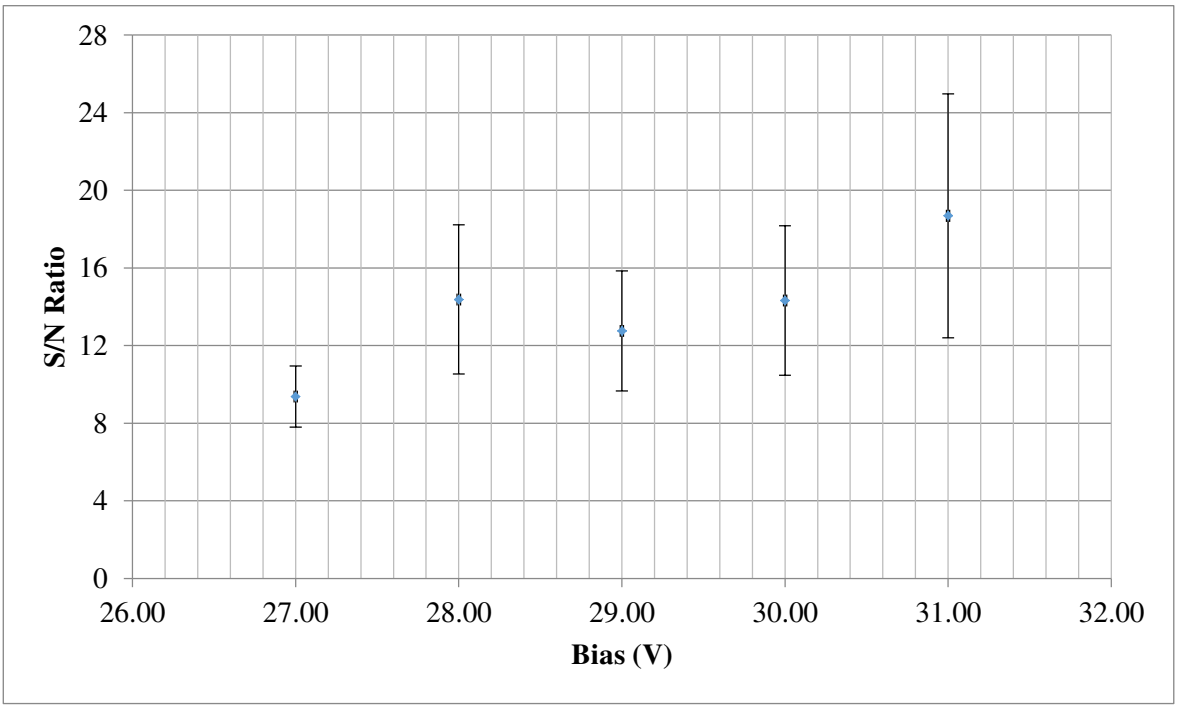

Figure 40: A graph showing how the signal-to-noise ratio varies as the bias across the SiPM is changed. These results are for the prototype with the 3D Printed light guide, a Caesium Iodide scintillator (truncated pyramid geometry) and the Bi-207 source peak (either CE or γ). These values are taken from the spectra of Bi-207, with bias values from 27-31 volts.

The Acrylic light guide seems to show a constant signal-to-noise ratio as the bias value is increased. The 3D Printed light guide seems to show that the signal-to-noise ratio increases as the bias value is increased, although this trend is marginal, so this trend cannot be stated with confidence. This slight difference in trend could be attributed to the fact that the light guides are fabricated using different methods, as well as the difference in the error values. Based on these results, the optimum bias value for the Bulk Acrylic light guide cannot be deduced. This is because there is little variation in the measured signal-to-noise ratio as the bias value is increased and because the error bars are too large. The optimum bias value for the 3D Printed light guide cannot be deduced. This is because as shown with the acrylic light guide, there is little variation in the measured signal-to-noise ratio as the bias value is increased and because the error bars are too large.

xvii. Energy Resolution as a function of the applied Bias

The experimental method used for these measurements, is as described in section c. The error analyses for these measurements, are as described in xiii. The aim of these measurements, is to establish how the energy resolution varies according to the applied bias value, for both the Acrylic and 3D Printed prototypes. The Bi-207 source (Serial Number SU486) has four conversion electron peaks and two gamma ray peaks which are normally visible in the spectrum [10]. One peak was visible in this spectrum, but unfortunately it is unclear as to which of the decay products this corresponds to. Thus, the calibration of the source and calculation of the parameters of interest, was performed using the channels on the x axis instead of energy. For each of the prototypes, spectra were taken with a range of bias values from 27V to 31V. Then, to calculate the energy resolution, the peak was fitted to a Gaussian distribution using MATLAB.

Based on this technique of analysis, the calculation of the energy resolution for the Acrylic prototype at various bias values, is as shown in Table 16 and Table 17:-

Bias (V)	**Scintillator**	**Geometry**	**Source Peak (CE or γ)**	**A1 (No Units)**	**B1 (Channels)**	**C1 (Channels)**
27.00±0.01	Caesium Iodide	Truncated pyramid	Bi-207	4539±68	229±1	61±1
28.00±0.01	Caesium Iodide	Truncated pyramid	Bi-207	7913±131	210±1	51±1
29.00±0.01	Caesium Iodide	Truncated pyramid	Bi-207	6002±100	217±1	52±1
30.00±0.01	Caesium Iodide	Truncated pyramid	Bi-207	6192±103	229±1	55±1
31.00±0.01	Caesium Iodide	Truncated pyramid	Bi-207	5461±87	231±1	58±1

Table 16: A table showing A1, B1 and C1 for the Acrylic light guided prototype. These values are taken from the spectra of Bi-207 (Figure 5).

Bias (V)	Scintillator	Geometry	Source Peak (CE or γ)	Peak Centroid (Channels)	FWHM (Channels)	Energy Resolution (%)
27.00±0.01	Caesium Iodide	Truncated pyramid	Bi-207	229±1	102±2	45±1
28.00±0.01	Caesium Iodide	Truncated pyramid	Bi-207	210±1	85±2	40±1
29.00±0.01	Caesium Iodide	Truncated pyramid	Bi-207	210±1	87±2	40±1
30.00±0.01	Caesium Iodide	Truncated pyramid	Bi-207	229±1	92±2	40±1
31.00±0.01	Caesium Iodide	Truncated pyramid	Bi-207	231±1	96±2	42±1

Table 17: A table showing the Peak Centroid, Full-Width at Half-Maximum (FWHM) and energy resolution for the Acrylic light guided prototype. These values are taken from the spectra of Bi-207 (Figure 5).

These results can also be shown in graphical form, as in Figure 41:-

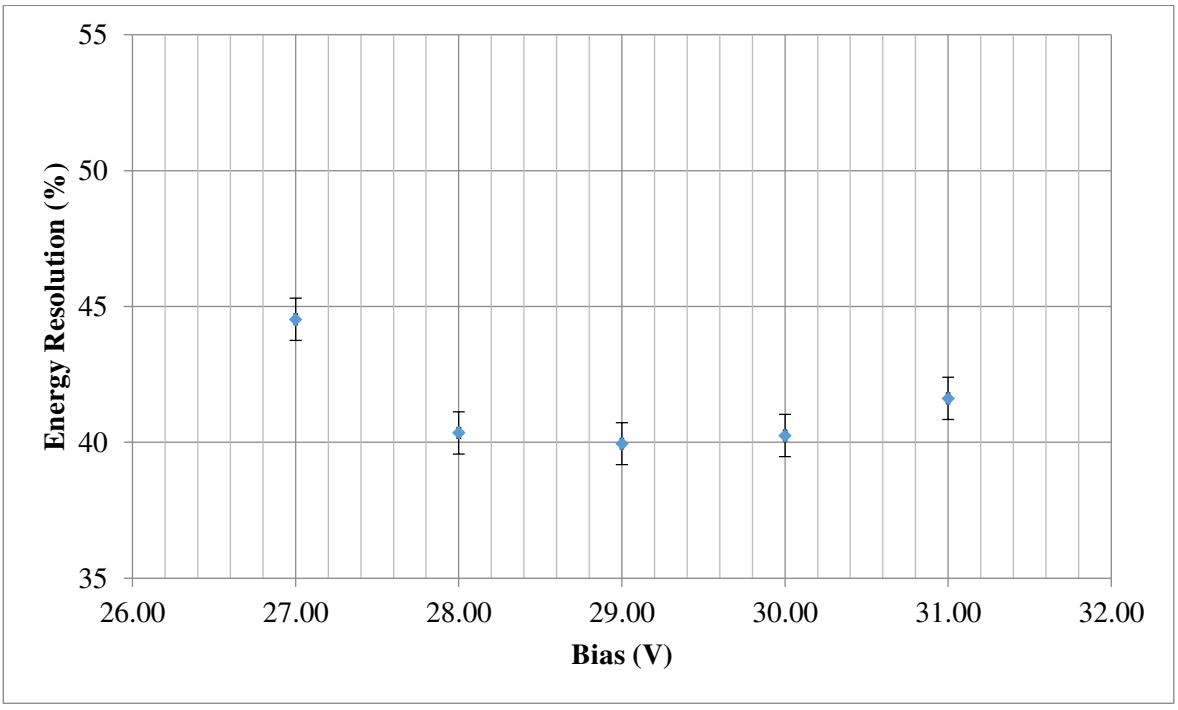

Figure 41: A graph showing how the energy resolution varies as the bias is changed. These results are for the UoYTube prototype with an Acrylic light guide. The scintillator is made from Caesium Iodide (with a truncated pyramid geometry). Any bias between 28 and 30V would seem to be acceptable.

The calculation of the energy resolution for the 3D Printed prototype at various bias values, is as shown in Table 18 and Table 19:-

Bias (V)	Scintillator	Geometry	Source Peak (CE or γ)	A1 (No Units)	B1 (Channels)	C1 (Channels)
27.00±0.01	Caesium Iodide	Truncated pyramid	Bi-207	4337±70	233±1	59±1
28.00±0.01	Caesium Iodide	Truncated pyramid	Bi-207	4643±81	248±1	57±1
29.00±0.01	Caesium Iodide	Truncated pyramid	Bi-207	4416±78	251±1	57±1
30.00±0.01	Caesium Iodide	Truncated pyramid	Bi-207	4198±74	234±1	53±1
31.00±0.01	Caesium Iodide	Truncated pyramid	Bi-207	4134±71	237±1	55±1

Table 18: A table showing A1, B1 and C1 for the 3D Printed light guided prototype. These values are taken from the spectra of Bi-207 (Figure 5).

Bias (V)	Scintillator	Geometry	Source Peak (CE or γ)	Peak Centroid (Channels)	FWHM (Channels)	Energy Resolution (%)
27.00±0.01	Caesium Iodide	Truncated pyramid	Bi-207	233±1	98±2	42±1
28.00±0.01	Caesium Iodide	Truncated pyramid	Bi-207	248±1	95±2	39±1
29.00±0.01	Caesium Iodide	Truncated pyramid	Bi-207	251±1	95±2	38±1
30.00±0.01	Caesium Iodide	Truncated pyramid	Bi-207	234±1	89±2	38±1
31.00±0.01	Caesium Iodide	Truncated pyramid	Bi-207	237±1	92±2	39±1

Table 19: A table showing the Peak Centroid, Full-Width at Half-Maximum (FWHM) and energy resolution for the 3D Printed light guided prototype. These values are taken from the spectra of Bi-207 (Figure 5).

These results can also be shown in graphical form, as in Figure 42:-

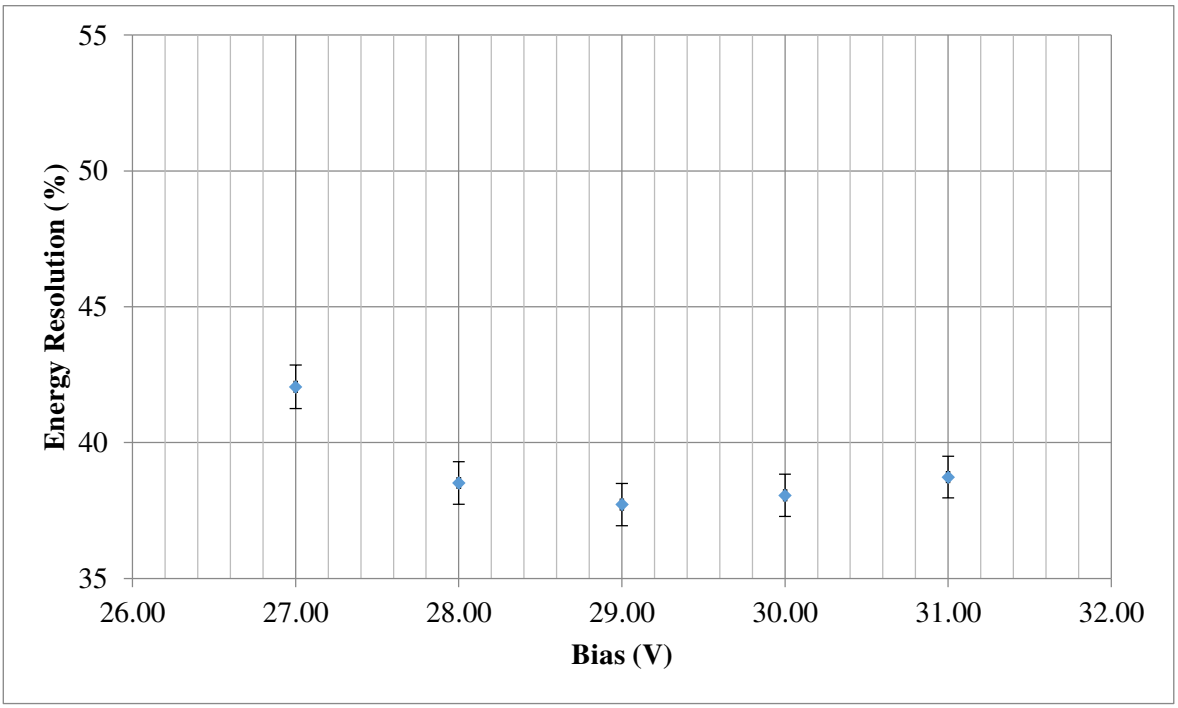

Figure 42: A graph showing how the energy resolution varies as the bias is changed. These results are for the UoYTube prototype with a 3D Printed light guide. The scintillator is made from Caesium Iodide (with a truncated pyramid geometry). Any bias between 28 and 31V would seem to be acceptable.

It is apparent that for the Acrylic light guided prototype, there is a range of optimum bias values. This range is between 28.00±0.01 and 30.00±0.01 volts, where each value corresponds to an energy resolution value of 40±1 percent. For the 3D Printed light guided prototype, there is also a range of optimum bias values. This range is between 28.00±0.01 and 31.00±0.01 volts, where each value corresponds to an energy resolution value of approximately 38±1 percent.

o. Measures of Efficiency

The final parameter which will be discussed to characterise the UoYTube is the detector efficiency. There are three accepted variants of the detector efficiency parameter. These are the absolute, intrinsic and geometrical efficiencies.

1. The absolute efficiency of a detector is determined by the distance of the source to the detector and involves the solid angle covered by the detector. It is defined as [2]: -

$$\varepsilon_{abs} = \frac{\text{number of pulses recorded}}{\text{number of radiation quanta emitted by the source}}$$

2. The intrinsic efficiency of a detector is determined by the detector thickness, the scintillator material and the energy of the source. It is defined as [2]: -

$$\varepsilon_{int} = \frac{\text{number of pulses recorded}}{\text{number of radiation quanta incident on detector}}$$

3. The geometrical efficiency is determined only by the source and detector geometry. It is defined below, where Ω is the solid angle between the source and the detector [30]: -

$$\varepsilon_G = \frac{\text{number of photons emitted towards the detector}}{\text{number of photons emitted by the source}} = \frac{\Omega}{4\pi}$$

4. To calculate the solid angle Ω for a point source and circular shaped detector, the following equation is used, where d is the distance of the detector from the source and r is the radius of the detector [30]: -

$$\Omega = 2\pi\left(1 - \frac{d}{\sqrt{d^2 + r^2}}\right)$$

5. The intrinsic efficiency, absolute efficiency and geometrical efficiency for isotropic sources (radiation which radiates uniformly in all directions) are related according to the following equation [2]: -

$$\varepsilon_{int} = \frac{\varepsilon_{abs}}{\varepsilon_{G}}$$

The geometrical efficiency of the previous generation UoYTube was estimated based on the opening angles at each end and the assumed gaps between detectors. The result of this was that the forward opening angle was reduced to 13.24 degrees and the backward angle was also reduced to 19.98 degrees. Using PACE, it was calculated that the UoYTube would thus, have a coverage of 96.7 percent [5].

The efficiency was estimated by observing the suppression due to the applying of a charged-particle veto. In the ^{70}Kr experiment that ran in September 2014, the UoYTube was able to operate with an efficiency of 73% (one proton detection) and with an efficiency of 99% (for a 3p channel veto) [31]. Unfortunately, no data was taken to enable the actual detector efficiency to be determined.

The geometrical efficiency of the current UoYTube prototype can be calculated using a solid angle calculator [32] [33]. The scintillator crystal is square in shape with a 20mmx20mm size and a thickness of 0.8mm. The alpha source was placed at a distance of 5cm away from the prototype and the conversion electron source was placed on top of the detector prototype, at a distance of 0.5cm. Based on these measurements, the solid angle and geometrical efficiency values for each source are as follows in Table 20: -

Serial Number	**Source**	**Activity (Bq)**	**Scintillator Thickness (mm)**	**Distance to Detector (mm)**	**Solid Angle (sR)**	**Geometrical Efficiency (%)**
NY332	Am/Cm/Pu (α)	3,850	0.8	50	0.154	(0.154/12.56) × 100 = 1.2
SU486	Bi-207 (CE)	32,330	0.8	5	3.709	(3.709/12.56) × 100 = 29.5

Table 20: A table showing the solid angle and geometrical efficiency for the alpha and conversion electron sources.

6. Construction of the UoYTube

Now that the scintillator, light guides and silicon photomultipliers have been characterised, and the method of fabrication decided, the next stage of development is to decide how each of the individual cells are going to be arranged to form the entirety of the UoYTube detector.

Figure 43 shows the geometry of the previous generation UoYTube: -

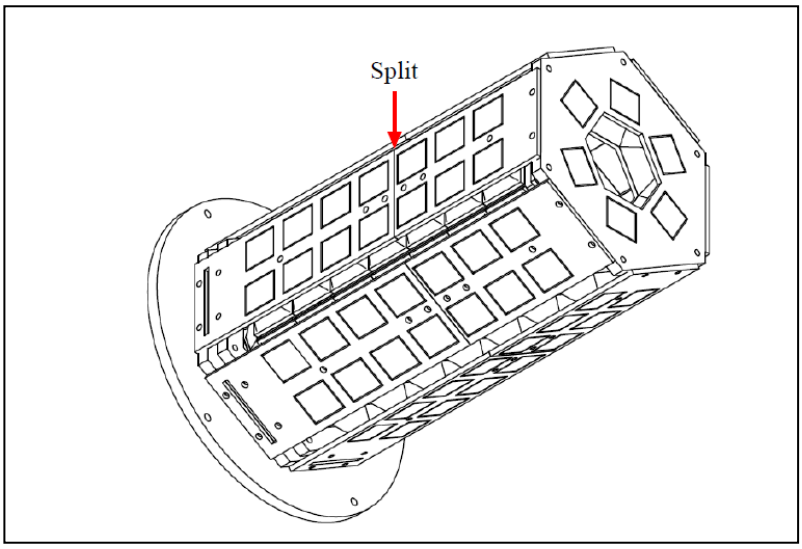

Figure 43: A schematic showing the structure of the previous generation UoYTube. It shows how each of the ninety-six individual cells are arranged in a frame [5].

An idealised design for the UoYTube would have scintillator crystals covering the entirety of the inside of the detector. This would ensure that the detector would have the highest probability of recording an event. Unfortunately, the previous design, is such that the length of the detector is covered well, but the end caps are not covered so well. This was due to restrictions, at that time, of the scintillator and light guide geometries (the scintillators were all of a square geometry and the light guides, all a truncated pyramid geometry).

In this new design, the length of the detector is again covered with the truncated pyramid cells, but the end caps also have diamond-like shaped individual cells as well. This means that the end caps have much better coverage than previously. This is as shown in Figure 44, Figure 45, Figure 46 and Figure 47, which outline the exact measurements of the length, end caps and each

individual cell (truncated pyramid and diamond-like geometries. They also show explicitly how each of the individual cells are arranged in the detector lattice: -

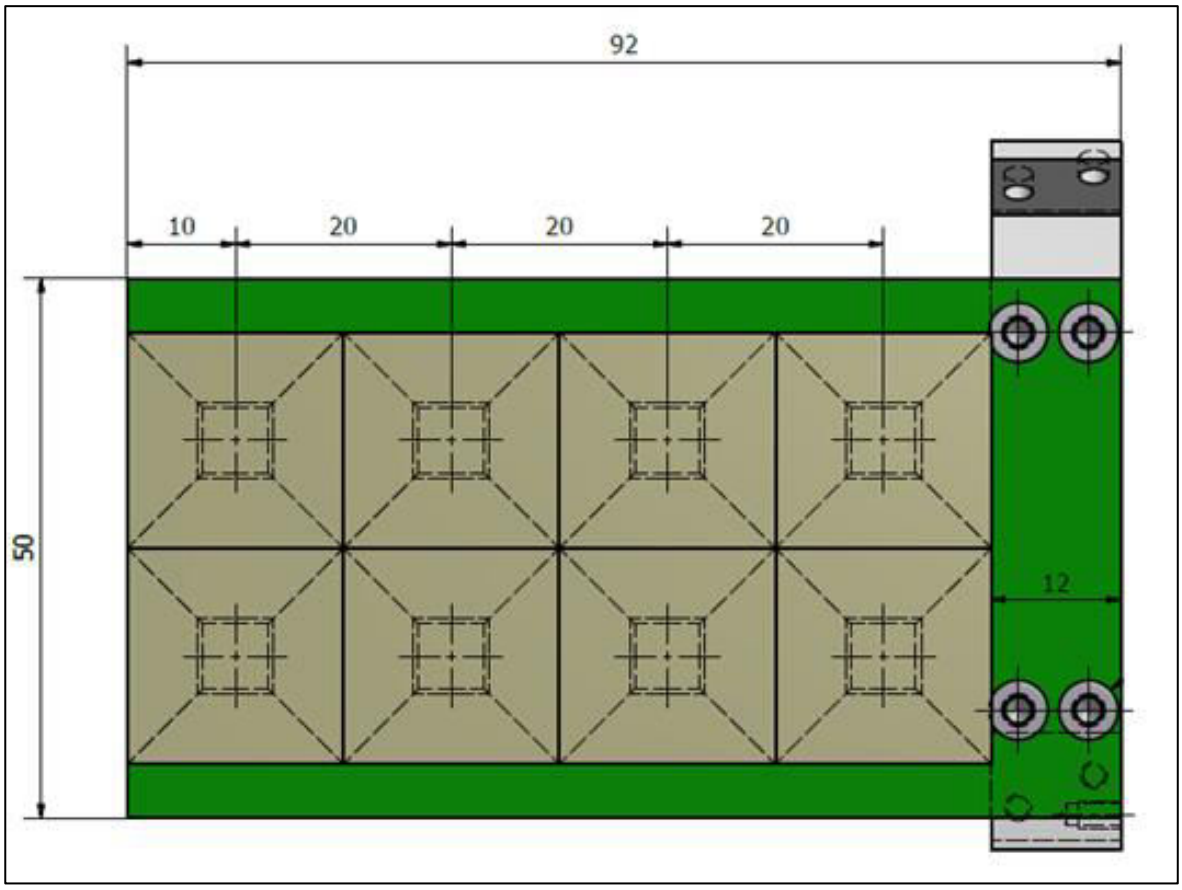

Figure 44: A diagram showing the length of the detector. There are six of these sections, each one corresponding to a different face. Each of these faces has eight UoYTube cells, each with the truncated pyramid geometry. The largest face of the light guide measures 20mmx20mm and the smallest face of the light guide measures 6mmx6mm [34].

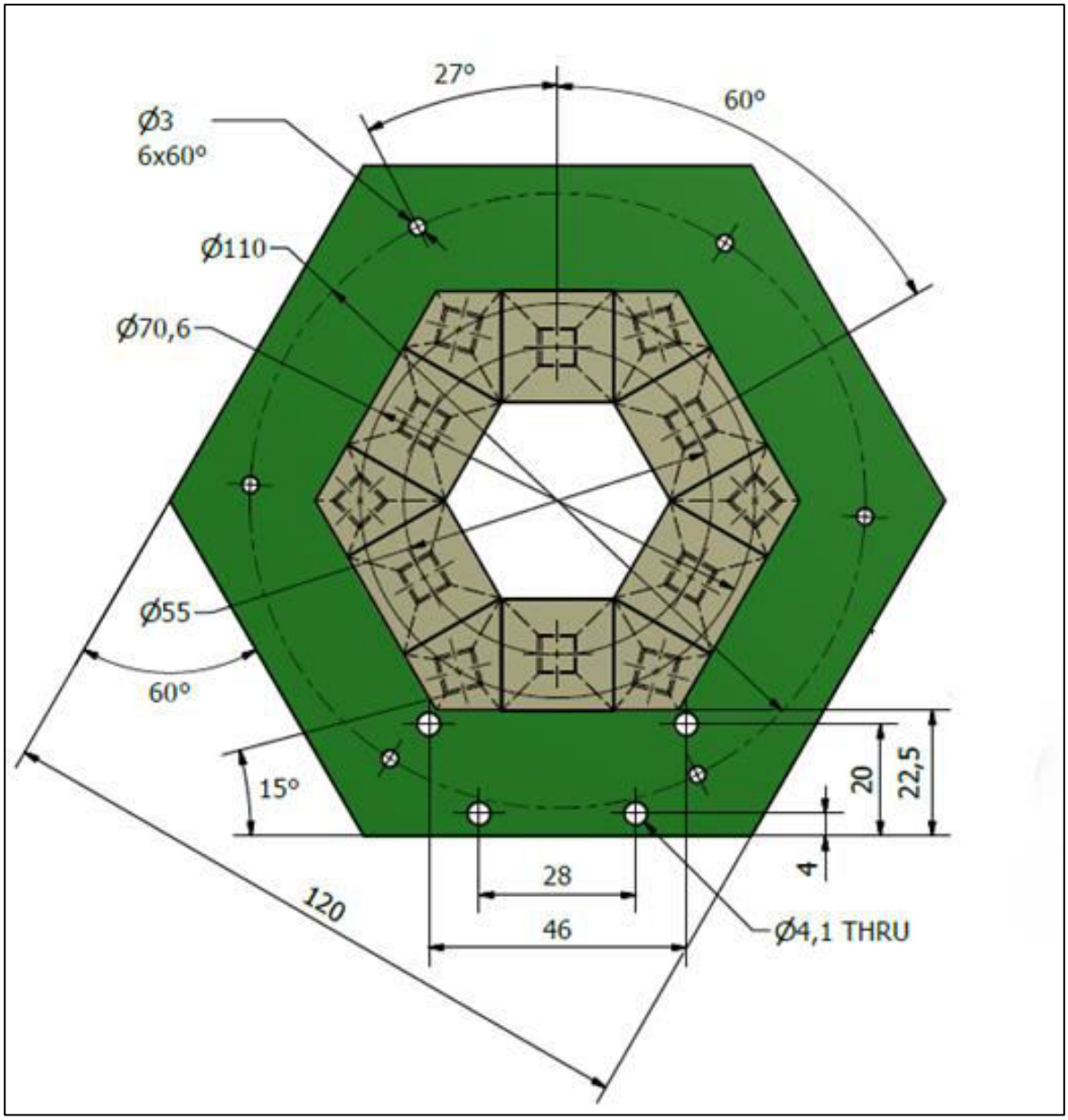

Figure 45: A diagram showing the end caps of the detector. There are two of these, each one corresponding to a different end. Each end cap contains twelve UoYTube cells; six with the truncated pyramid geometry and six with the diamond-like geometry [35].

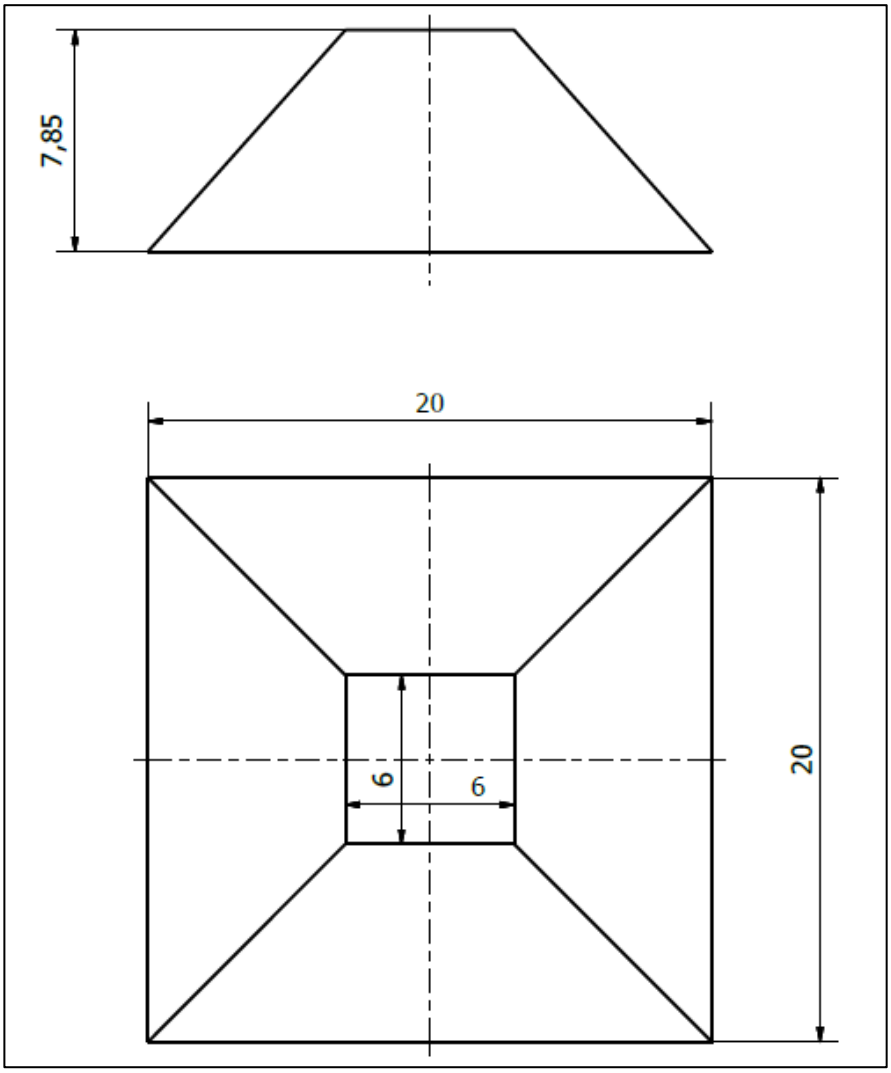

Figure 46: A drawing that shows the geometry of the truncated pyramid light guide. The largest face measures 20mmx20mm, the smallest face measures 6mmx6mm and the height is 7.85mm [36].

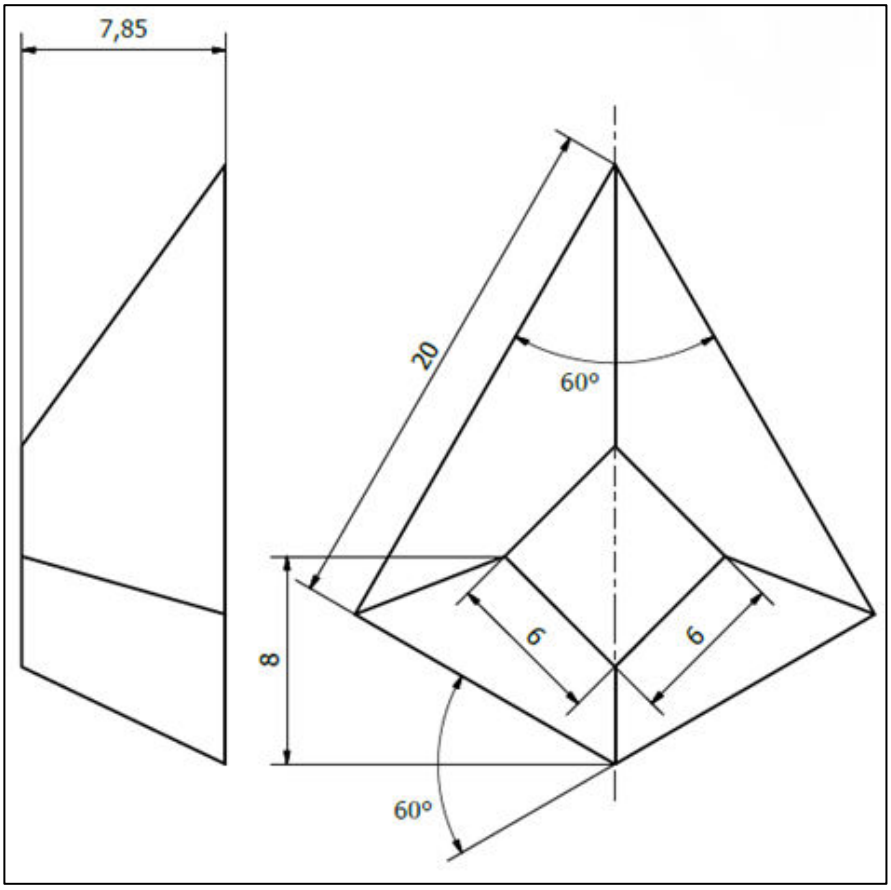

Figure 47: A drawing that shows the geometry of the diamond-like light guide. The smallest face measures 6mmx6mm and the height is 7.85mm [37].

The final stage of the design is to establish how these cells are actually attached to the frame and to the additional electronics which are needed to collect the signals from the SiPMs. The UoYTube is fabricated such that the brackets are attached to the Printed Circuit Board (PCB). The SiPMs are mounted onto the PCB where their signals are collected. The scintillator crystals, light guides and SiPMs (now with the PCB attached) are then bound to each other with glue. Figure 48 describes how each of these components would be arranged and connected in practice: -

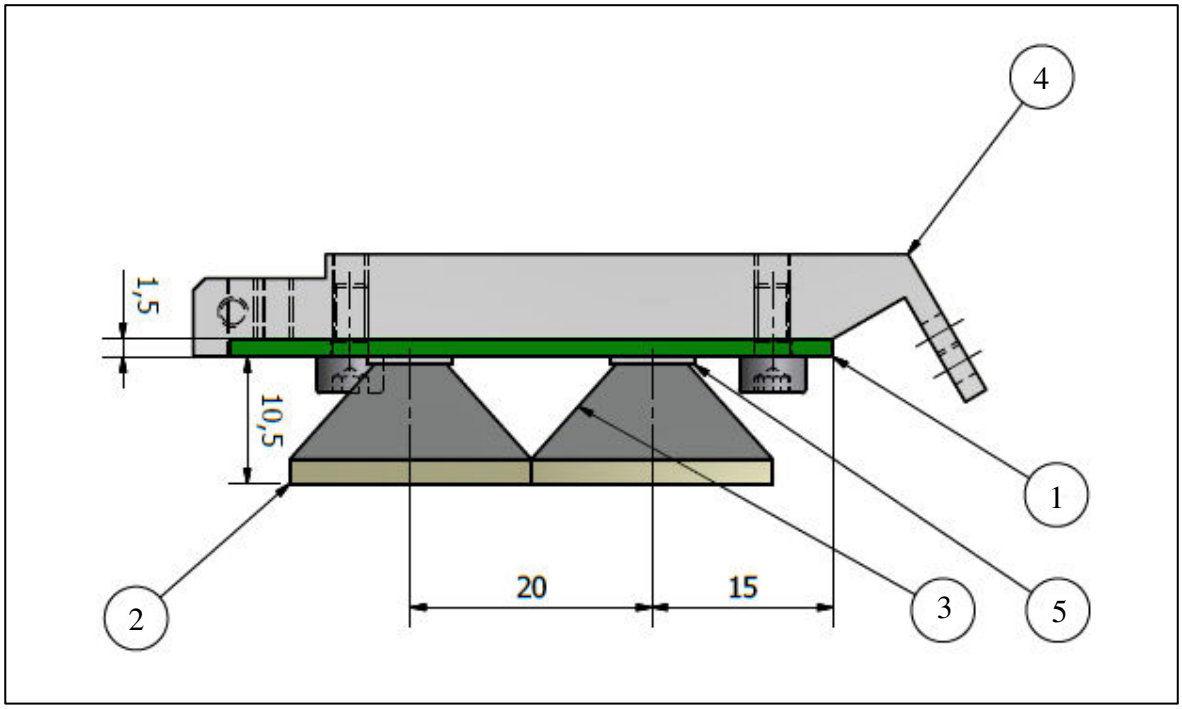

Figure 48: A drawing that shows the geometry of all of the required components. Item 1 is the PCB; Item 2 is the scintillator crystal; Item 3 is the light guide; Item 4 is the bracket; Item 5 is the SiPM. The height of the PCB is 1.5mm. The height of the scintillator, light guide and SiPM is 10.5mm [34].

7. Uses of the UoYTube detector

It has been discussed in section 5 how the UoYTube can be used to detect different types of radiation, including alpha particles and conversion electrons (although it is not technically designed to measure conversion electrons). The main purpose of the UoYTube is to detect charged particles emitted in fusion evaporation reactions. A use for the UoYTube detector will be now be discussed; to study the properties of ^{70}Kr.

The aim of this experiment was to use the recoil-β tagging technique [5], to determine which transitions occur for the ^{70}Kr nucleus, specifically the 2+ and 4+ states. Then, this data was used to identify the triplet energy differences for the isobars of mass 70 [31].

This experiment was conducted at the University of Jyväskylä (JYFL) by other physicists'. I did not conduct this experiment, nor did I analyse any of the experimental results. In this experiment, a beam of ^{32}S was bombarded at a target of natural Calcium. This reaction generated the ^{70}Kr isotope via two neutron evaporation from the compound nucleus [31].

A diagram of the experimental set-up is as shown below, in Figure 49: -

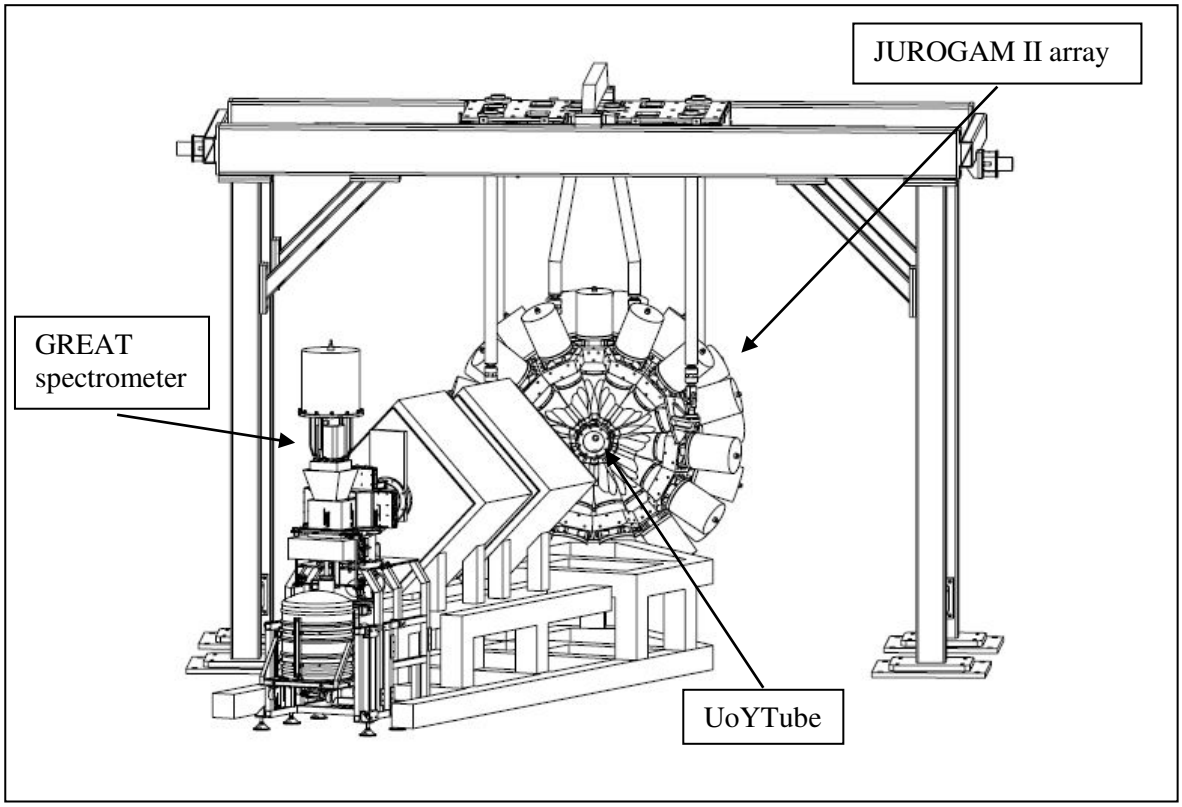

Figure 49: A diagram of the current experimental set-up. This set-up includes the JUROGAM II array, the GREAT spectrometer and the UoYTube. The UoYTube is located inside the JUROGAM II array [38].

There were several detectors in the set-up, including the UoYTube, each with their own role. These detectors are listed below: -

1. The JUROGAM II array (composed of 24 Eurogam II clover detectors [39] and 15 Eurogam phase I/GASP [40] [41] detectors), used to measure prompt gamma rays
2. A Double-sided silicon strip detector (DSSSD), used to measure the recoiled fusion evaporation products. The DSSSD is a component in the Gamma Recoil Electron Alpha Tagging (GREAT) [42] spectrometer
3. A multi-wire proportional counter (MWPC), used to register the recoils being implanted into the DSSSD.
4. The UoYTube, used to veto those events that occur in coincidence, with particles ejected from the fusion evaporation reaction [31]

In this experiment, the UoYTube suppressed those channels, and many others too, corresponding to the ^{69}As (3p evaporation) and ^{70}Se (2p evaporation). This meant that the UoYTube was able to operate with an efficiency of 73% (one proton detection) and with an efficiency of 99% (for a 3p channel veto) [31].

The results of the experiment provided the first identification of two gamma rays in ^{70}Kr (which are assumed to correspond to the $2^+ \rightarrow 0^+$ and $4^+ \rightarrow 2^+$ transitions), thus allowing a first study of the isobaric analogue states in the mass 70 nuclei ^{70}Kr, ^{70}Br and ^{70}Se.

8. Conclusion

This thesis describes the testing of several prototype detectors, designed to be used in a radiation detector called the UoYTube. The objectives in this work were to design and fabricate several UoYTube prototypes. These included prototypes with different scintillator crystals (Caesium Iodide and plastic), prototypes with different geometries (truncated pyramid and cuboid), and prototypes that included different types of light guides (Acrylic and 3D Printed).

These prototypes were then characterised in terms of the signal-to-noise ratio, the optimum bias value, the energy resolution, the Acrylic versus 3D-Printed light guides, the number of counts and the optimum amplifier shaping time. These results were then used to inform upon the optimum scintillation material and light collection materials to be used for the next UoYTube detector design.

A use for the UoYTube in terms of the detection and veto of charged particles emitted in fusion evaporation reactions is briefly described. The specific experiment discussed aimed to identify transitions from the first few Yrast states in the nucleus ^{70}Kr.

Firstly, each of the different components that make up the UoYTube cells (scintillator, light guide and SiPM) were described individually, and then a description of how they were fabricated was presented. Following this, the UoYTube prototypes were characterised in terms of their signal-to-noise ratio. In these experiments, the bias was varied and the signal-to-noise ratio calculated at each different bias value. Then, the optimum bias value was inferred by establishing which bias value corresponded to the highest signal-to-noise. Using these results, it was deduced that the plastic scintillator (with a truncated pyramid geometry) was the best performing in terms of the signal-to-noise ratio.

The optimum bias value corresponded to the highest signal-to-noise ratio. Both the plastic scintillator (with a truncated pyramid geometry) and Caesium Iodide scintillator (with a truncated pyramid geometry), demonstrated a range of the optimum bias values, over which there was little variation in the measured signal-to-noise ratio. For the plastic scintillator (with a cuboid geometry), the optimum bias value was unknown. This was because the error bars for the signal-to-noise values were too large and therefore, each data point was said to not be distinguishable from each other.

The energy resolution for each of the prototypes was then measured using the triple alpha source. The data were fitted to Gaussian distributions by MATLAB. In terms of the energy resolution value achieved, the Caesium Iodide scintillator (with a truncated pyramid geometry), was the best performing and most suitable for use in the UoYTube, as it had good energy resolution.

Two different methods used to fabricate the light guides, one involving the use of a 3D Printer and the other involving the use of the HURCO VMX60m Machining Centre, was then outlined. The light output was analysed with a spectrometer and the Reflectance and Transmittance of light as a function of Wavelength was recorded. The transmittance of light for the 3D Printed light guide was significantly poorer than that of the acrylic light guide. This indicated that the acrylic light guide was more suitable for use in the UoYTube when compared to the 3D printed light guide. Similarly, there was also a direct comparison of the light guides, when the light source originated from a scintillator crystal and not a spectrometer. The light guides were then compared to each other in terms of the energy resolution, number of counts and the optimum shaping time, using the triple alpha source.

In terms of the energy resolution, the variation in performance between the light guides was not very significant. Thus, both can be said to be suitable for use in the UoYTube detector. The light guides were also compared in terms of the number of counts A1 at each of the source peaks. The number of counts was greater in each case, for the Acrylic light guide. This indicated that the Acrylic light guide was more suitable for use in the UoYTube, when compared to the 3D Printed light guide.

The light guides were also characterised in terms of the optimum shaping time, where the optimum shaping time corresponded to the highest energy resolution value. To establish the optimum shaping time, spectra were taken at various shaping time values and then the energy resolution was calculated. Using these results, it was concluded that the best resolution was obtained for the highest values of shaping time. The small deviations from the observed trend at lower shaping times, were not statistically significant when the errors were taken into consideration.

Using the conversion electron source, the Acrylic and 3D Printed prototypes, were characterised in terms of the signal-to-noise ratio, optimum bias value and the energy resolution (as a function of the applied bias). The optimum bias values for the Bulk Acrylic and 3D Printed light guides could not be deduced. This was because there was little variation in the measured signal-to-noise ratio as the bias value was increased and because the error bars were too large. Both the Acrylic and 3D Printed light guided prototypes demonstrated a range of the optimum bias values, over which there was little variation in the measured energy resolution. Thus, both were demonstrated to be suitable for use in the UoYTube.

The geometrical efficiency of the previous generation UoYTube was estimated based on the opening angles at each end and the assumed gaps between detectors. Using PACE, it was calculated that the UoYTube would thus have a coverage of 96.7 percent. The actual efficiency was established by observing the suppression due to the applying of a charged-particle veto. In the experiment that ran in September 2014, the UoYTube was able to operate with an efficiency of 73% (one proton detection) and with an efficiency of 99% (for a 3p channel veto).

The geometry used in the UoYTube was then described, specifically how each of the individual cells fit together and how the geometry was optimised to ensure maximum surface area coverage. It was also established how the cells are attached to the frame and to the additional electronics, which are used to collect the signals from the SiPMs.

A use for the UoYTube was then described; to detect charged particles emitted in fusion evaporation reactions. The aim of this experiment was to use the recoil-β tagging technique, to determine which transitions occur for the ^{70}Kr nucleus, specifically the 2+ and 4+ states. Then, this data was used to identify the triplet energy differences for the isobars of mass 70. These results provided the first identification of two gamma rays in ^{70}Kr (which are assumed to correspond to the $2^+ \rightarrow 0^+$ and $4^+ \rightarrow 2^+$ transitions), thus allowing a first study of the isobaric analogue states in the mass 70 nuclei ^{70}Kr, ^{70}Br and ^{70}Se.

In terms of further work, the UoYTube could be further characterised by calculating the efficiency of the detector in its entirety and also by establishing how well the detector is able to measure other nuclei. I would also be beneficial to characterise the UoYTube performance in terms of its temperature dependence.

9. Health and Safety

When conducting experimental work, Health and Safety procedures should always be considered. In this section of the thesis, an assessment of the risks associated with experimental work will be described, alongside the methods used to reduce these risks.

An aspect of this work which has an element of risk associated with it, is the handling of radioactive sources. The sources used were the composite triple alpha source, consisting of Plutonium-239, Americium-241 and Curium-244 (Serial Number NY332) and the conversion electron source Bismuth-207 (Serial Number SU486) [43]. Both these sources are sealed sources, which means that they are encapsulated in plastic to reduce the risk associated with their handling [44]. It is essential that forceps are used when handling the sources, particularly when they are transferred from their container to the holder used for the testing of the UoYTube prototypes.

To minimise risk further, these sources are stored in a lead-lined box, so the radiation cannot escape. This box is locked with a key, and this key is stored in a password protected safe. This is to ensure that only those who have permission to access these sources, can do so [44]. Also, whilst working in the laboratory, a sign should be positioned next to the source, to indicate that the source is being used nearby.

To reduce risk further, it was also necessary to complete the online training programme. This programme is designed to teach the user about radiation safety including, safe dose limits, the effects of radiation on the body, the different types of radiation used in the laboratory and the University of York's policy on working with radioactive sources [45].

Another risk was the risk associated with working with Isopropanol, when preparing the 3D Printed light guide. Isopropanol is an irritant to the skin and eyes, and so it was necessary to wear gloves when working with this liquid, to reduce the risk of harm [12].

10. Abbreviations used in the Appendices

The following table contains a list of the abbreviations and their corresponding meanings, used in the Appendices of this thesis: -

Abbreviation	Meaning
x	The x variable
y	The y variable
x Error	The error of the x variable
x Units	The unit of measurement for the error of the x variable
y Error	The error of the y variable
y Units	The unit of measurement for the error of the y variable
S/N	The signal-to-noise ratio of the detector
E Res	The energy resolution of the detector
Av E Res	The average energy resolution of the detector
A1	The height of the Gaussian curve's peak as calculated by MATLAB
A1 (Units)	The unit of measurement for the height of the Gaussian curve's peak
A1 LB	The lower bound of the height of the Gaussian curve's peak as calculated by MATLAB
A1 UB	The upper bound of the height of the Gaussian curve's peak as calculated by MATLAB
B1	The position of the peak centroid on the x axis as calculated by MATLAB
B1 (Units)	The unit of measurement for the position of the peak centroid on the x axis as calculated by MATLAB
B1 LB	The lower bound of the position of the peak centroid on the x axis as calculated by MATLAB
B1 UB	The upper bound of the position of the peak centroid on the x axis as calculated by MATLAB
C1	Equal to $\sqrt{2}\sigma$, where σ is the standard deviation, as calculated by MATLAB
C1 (Units)	The unit of measurement for C1 as calculated by MATLAB
C1 LB	The lower bound of C1 as calculated by MATLAB
C1 UB	The upper bound of C1 as calculated by MATLAB
CB (%)	The confidence bounds for a given fit as calculated by MATLAB and expressed as a percentage

SSE	The sum of squares due to error as calculated by MATLAB
R-sq/ Adj R-sq	The R-Squared and degrees of freedom Adjusted R-Squared values as calculated by MATLAB
RMSE	The Root Mean Squared Error as calculated by MATLAB
Reflect/Trans	The Reflectance and Transmittance of light as measured by the spectrometer
AOP	The Angle of the Polariser

11. Appendix 1 – Errors for x and y axes

Figure(s)	x	x Error	x Units	y	y Error	y Units
Figure 4 & Table 8 & Table 9 & Figure 16	Energy	±18	keV	Counts	±18	None
Figure 5	Energy	±17	keV	Counts	±17	None
Table 2 & Figure 10	Bias	±0.01	Volts	S/N	±9, ±28, ±10, ±1, ±0	None
Table 3 & Figure 11	Bias	±0.01	Volts	S/N	±4, ±3, ±5, ±5, ±6	None
Table 4 & Figure 12	Bias	±0.01	Volts	S/N	±4, ±2, ±5, ±5, ±6	None
Table 5 & Figure 13	Bias	±0.01	Volts	S/N	±2, ±2, ±4, ±3, ±4	None

Figure(s)	x	x Error	x Units	y	y Error	y Units
Table 6 & Figure 14	Bias	±0.01	Volts	S/N	±7, ±3, ±6, ±7, ±7	None
Table 8 & Table 9 & Figure 15	Energy	±21	keV	Counts	±21	None
Table 8 & Table 9 & Figure 17	Energy	±23	keV	Counts	±23	None
Figure 18 & Figure 19 & Figure 20	Wavelength	±2.5	nm	Reflect	±0.002	%
Figure 18 & Figure 19 & Figure 20	Wavelength	±2.5	nm	Trans	±0.02	%
Figure 21 & Figure 22 & Figure 23 & Figure 24	AOP	±3	Degrees	Trans	±0.02	%
Figure 25 & Figure 26 & Figure 27 & Figure 28	AOP	±3	Degrees	Reflect	±0.002	%

Figure(s)	x	x Error	x Units	y	y Error	y Units
Figure 29 & Figure 30 & Table 10 & Table 11	Energy	±22	keV	Counts	±22	None
Table 12 & Figure 31	Shaping Time	±0.0, ±0.1, ±0.1, ±0.2, ±0.3, ±0.5	µs	E Res	±0.36, ±0.09, ±0.09, ±0.10, ±0.37, ±0.09	%
Table 12 & Figure 32	Shaping Time	±0.0, ±0.1, ±0.1, ±0.2, ±0.3, ±0.5	µs	E Res	±0.36, ±0.11, ±0.10, ±0.11, ±0.37, ±0.11	%
Table 12 & Figure 33	Shaping Time	±0.0, ±0.1, ±0.1, ±0.2, ±0.3, ±0.5	µs	E Res	±0.36, ±0.13, ±0.13, ±0.14, ±0.37, ±0.13	%
Table 13 & Figure 35	Shaping Time	±0.0, ±0.1, ±0.1, ±0.2, ±0.3, ±0.5	µs	E Res	±0.09, ±0.10, ±0.08, ±0.08, ±0.08, ±0.07	%
Table 13 & Figure 36	Shaping Time	±0.0, ±0.1, ±0.1, ±0.2, ±0.3, ±0.5	µs	E Res	±0.09, ±0.08, ±0.08, ±0.08, ±0.07, ±0.08	%
Table 13 & Figure 37	Shaping Time	±0.0, ±0.1, ±0.1, ±0.2, ±0.3, ±0.5	µs	E Res	±0.12, ±0.12, ±0.10, ±0.10, ±0.10, ±0.07	%

Figure(s)	x	x Error	x Units	y	y Error	y Units
Table 12 & Figure 34	Shaping Time	±0.0, ±0.1, ±0.1, ±0.2, ±0.3, ±0.5	µs	Av E Res	±0.36, ±0.11, ±0.11, ±0.12, ±0.37, ±0.11	%
Table 13 & Figure 38	Shaping Time	±0.0, ±0.1, ±0.1, ±0.2, ±0.3, ±0.5	µs	Av E Res	±0.10, ±0.10, ±0.09, ±0.09, ±0.09, ±0.07	%
Table 14 & Figure 39	Bias	±0.01	Volts	S/N	±2, ±3, ±3, ±3, ±1	None
Table 15 & Figure 40	Bias	±0.01	Volts	S/N	±2, ±4, ±3, ±4, ±6	None
Table 16 & Table 17 & Figure 41	Bias	±0.01	Volts	E Res	±1	%
Table 18 & Table 19 & Figure 42	Bias	±0.01	Volts	E Res	±1	%

12. Appendix 2 – Gaussian Distributions

Figure(s)	Parameters				
Figure 4 & Table 7 & Table 9 & Figure 16 (Peak 1)	**A1±Error**	**A1 Units**	**B1±Error**	**B1 Units**	**C1±Error**
	681±7	Counts	5153.00±2.00	keV	170.10±5.35
	C1 Units	**CB (%)**	**SSE**	**R-sq/Adj R-sq**	**RMSE**
	keV	95	1.71E+05	0.9582, 0.9571	23.14
Figure 4 & Table 7 & Table 9 & Figure 16 (Peak 2)	**A1±Error**	**A1 Units**	**B1±Error**	**B1 Units**	**C1±Error**
	654±8	Counts	5496.00±3.00	keV	141.70±5.50
	C1 Units	**CB (%)**	**SSE**	**R-sq/Adj R-sq**	**RMSE**
	keV	95	1.71E+05	0.9582, 0.9571	23.14
Figure 4 & Table 7 & Table 9 & Figure 16 (Peak 3)	**A1±Error**	**A1 Units**	**B1±Error**	**B1 Units**	**C1±Error**
	449±7	Counts	5795.00±3.50	keV	145.10±8.60
	C1 Units	**CB (%)**	**SSE**	**R-sq/Adj R-sq**	**RMSE**
	keV	95	1.71E+05	0.9582, 0.9571	23.14
Figure 5	**A1±Error**	**A1 Units**	**B1±Error**	**B1 Units**	**C1±Error**
	4539±68	Counts	229±1	Channels	61±1
	C1 Units	**CB (%)**	**SSE**	**R-sq/Adj R-sq**	**RMSE**
	Channels	95	1.77E+07	0.9744, 0.9742	245.60
Table 7 & Table 9 & Figure 15	**A1±Error**	**A1 Units**	**B1±Error**	**B1 Units**	**C1±Error**
	190±3	Counts	5317.00±12.00	keV	1108.00±17.00
	C1 Units	**CB (%)**	**SSE**	**R-sq/Adj R-sq**	**RMSE**
	keV	95	7.26E+04	0.9639, 0.9637	12.73

Figure(s)	Parameters				
Table 7 & Table 9 & Figure 17	**A1±Error**	**A1 Units**	**B1±Error**	**B1 Units**	**C1±Error**
	35±1	Counts	5413.00±18.00	keV	905.70±26.65
	C1 Units	**CB (%)**	**SSE**	**R-sq/Adj R-sq**	**RMSE**
	keV	95	1.35E+04	0.8412, 0.8406	5.03
Figure 29 & Table 10 (Peak 1)	**A1±Error**	**A1 Units**	**B1±Error**	**B1 Units**	**C1±Error**
	109±2	Counts	5152.00±2.00	keV	120.90±3.75
	C1 Units	**CB (%)**	**SSE**	**R-sq/Adj R-sq**	**RMSE**
	keV	95	2.80E+04	0.9270, 0.9257	7.84
Figure 29 & Table 10 (Peak 2)	**A1±Error**	**A1 Units**	**B1±Error**	**B1 Units**	**C1±Error**
	103±2	Counts	5479.00±2.50	keV	121.80±4.50
	C1 Units	**CB (%)**	**SSE**	**R-sq/Adj R-sq**	**RMSE**
	keV	95	2.80E+04	0.9270, 0.9257	7.84
Figure 29 & Table 10 (Peak 3)	**A1±Error**	**A1 Units**	**B1±Error**	**B1 Units**	**C1±Error**
	72±2	Counts	5783.00±3.50	keV	122.20±5.60
	C1 Units	**CB (%)**	**SSE**	**R-sq/Adj R-sq**	**RMSE**
	keV	95	2.80E+04	0.9270, 0.9257	7.84
Figure 30 & Table 11 (Peak 1)	**A1±Error**	**A1 Units**	**B1±Error**	**B1 Units**	**C1±Error**
	64±2	Counts	5146.00±3.00	keV	111.40±4.10
	C1 Units	**CB (%)**	**SSE**	**R-sq/Adj R-sq**	**RMSE**
	keV	95	1.62E+04	0.8999, 0.8981	5.96
Figure 30 & Table 11 (Peak 2)	**A1±Error**	**A1 Units**	**B1±Error**	**B1 Units**	**C1±Error**
	63±2	Counts	5478.00±3.00	keV	108.20±4.20
	C1 Units	**CB (%)**	**SSE**	**R-sq/Adj R-sq**	**RMSE**
	keV	95	1.62E+04	0.8999, 0.8981	5.96

Figure(s)	Parameters				
Figure 30 & Table 11 (Peak 3)	**A1±Error**	**A1 Units**	**B1±Error**	**B1 Units**	**C1±Error**
	44±2	Counts	5788.00±3.50	keV	111.70±5.80
	C1 Units	**CB (%)**	**SSE**	**R-sq/Adj R-sq**	**RMSE**
	keV	95	1.62E+04	0.8999, 0.8981	5.96

13. References

[1] J. Henderson, “Enhancing the sensitivity of recoil-beta tagging,” *Journal of Instrumentation,* vol. 8, 2013.

[2] G. F. Knoll, Radiation Detection and Measurement, 4th ed., United States: John Wiley & Sons, 2010.

[3] SensL Technologies Limited, “SensL Technologies,” October 2011. [Online]. Available: http://www.sensl.com/downloads/ds/TN%20-%20Intro%20to%20SPM%20Tech.pdf. [Accessed 4 December 2015].

[4] Avago Technologies Limited, “Avago Technologies,” 11 December 2006. [Online]. Available: www.avagotech.com/docs/5988-7057EN. [Accessed 4 December 2015].

[5] J. Henderson, Decay tagging of neutron-deficient 73,74Sr, PhD Thesis, York: University of York, 2014.

[6] International Atomic Energy Agency, “Nucleonica,” [Online]. Available: http://www.nucleonica.net/wiki/images/1/17/nutrons1-eriksson-2.pdf. [Accessed 4 December 2015].

[7] AMETEK, Inc, “Ortec Online,” [Online]. Available: www.ortec-online.com/download/MAESTRO.pdf. [Accessed 4 December 2015].

[8] M. Godwin, *Source Info For Jennifer,* York: The University of York, 2016.

[9] A. Rytz, “John Wiley & Sons, Inc,” 1991. [Online]. Available: http://www.wiley-vch.de/books/info/0-471-35633-6/toi99/www/decay/alpha2.pdf. [Accessed 4 December 2015].

[10] F. G. Kondev and S. Lalkovski, “National Nuclear Data Center,” 2011. [Online]. Available: http://www.nndc.bnl.gov/chart/decaysearchdirect.jsp?nuc=207BI&unc=nds. [Accessed 4 December 2015].

[11] Formlabs, “PreForm Software 1.8.2,” USA, 2015.

[12] Formlabs, “Formlabs,” Formlabs, 4 December 2015. [Online]. Available: http://formlabs.com/support/printers/form-2/quick-start-guide/. [Accessed 4 December 2015].

[13] Hurco, “Hurco,” Hurco, [Online]. Available: http://www.hurco.com/en-us/cnc-machine-tools/machining-centers/vertical/Pages/Performance.aspx. [Accessed 4 December 2015].

[14] OPEN MIND Technologies, “hyperMILL®. Version 2016.1,” OPEN MIND Technologies, 2015.

[15] Filmetrics Inc, “http://www.filmetrics.com,” Filmetrics Inc, 2016. [Online]. Available: http://www.filmetrics.com/thicknessmeasurement/f10-rt. [Accessed 11 August 2016].

[16] L. Kirkup, Data Analysis with Excel®: An Introduction for Physical Scientists, Cambridge: Cambridge University Press, 2002.

[17] G. Carlson, “http://www.ece.rochester.edu,” [Online]. Available: http://www.ece.rochester.edu/courses/ECE111/error_uncertainty.pdf. [Accessed 8 July 2016].

[18] The MathWorks, Inc, “UK Mathworks,” [Online]. Available: http://uk.mathworks.com/help/curvefit/gaussian.html#bs41yzj-1. [Accessed 4 December 2015].

[19] K. Krane, Introductory Nuclear Physics, Toronto: John Wiley & Sons, 1988.

[20] University of Nevada, “http://www.unlv.edu/,” [Online]. Available:

http://radchem.nevada.edu/classes/rfss/lectures/Lect%2011%20-%20Radiation%20Detectors.pdf. [Accessed 11 August 2016].

[21] Mathworks, "mathworks.com," Mathworks, [Online]. Available: http://uk.mathworks.com/help/curvefit/confidence-and-prediction-bounds.html?s_tid=gn_loc_drop. [Accessed 7 July 2016].

[22] Mathworks, "mathworks.com," Mathworks, [Online]. Available: http://uk.mathworks.com/help/curvefit/evaluating-goodness-of-fit.html. [Accessed 7 July 2016].

[23] Filmetrics, Inc, "Filmetrics," Filmetrics, 4 December 2015. [Online]. Available: http://www.filmetrics.com/thicknessmeasurement/f10-rt. [Accessed 4 December 2015].

[24] A. Fukabori, "Comparative analysis of scintillation characteristics derived from different emission," *Journal of Applied Physics,* vol. 117, 2015.

[25] V. Lindberg, "Uncertainties and Error Propagation," Rochester Institute of Technology, 1 July 2000. [Online]. Available: http://www.rit.edu/~w-uphysi/uncertainties/Uncertaintiespart2.html#muldiv. [Accessed 25 July 2016].

[26] F. Inc, "F10-RT Thin Film Analyzer," Filmetrics, Inc., San Diego, 2016.

[27] FAST ComTec GmbH, "FAST ComTec," [Online]. Available: http://www.fastcomtec.com/fwww/datashee/amp/cr-200.pdf. [Accessed 4 December 2015].

[28] Cisco Meraki, "Cisco Meraki," Cisco Meraki, [Online]. Available: https://documentation.meraki.com/MR/WiFi_Basics_and_Best_Practices/Wireless_fundamentals%3A_Signal-to-Noise_Ratio_(SNR)__and_wireless_signal_strength. [Accessed 5 August 2016].

[29] SensL Technologies Limited, "SensL Technologies," November 2015. [Online]. Available: http://sensl.com/downloads/ds/DS-MicroCseries.pdf. [Accessed 4 December 2015].

[30] M. C. Lépy, “Laboratoire National Henri Becquerel,” July 2010. [Online]. Available: http://www.nucleide.org/ICRM_GSWG/Training/Efficiency.pdf. [Accessed 1 August 2016].

[31] D. M. Debenham, “Spectroscopy of 70Kr and isospin symmetry in the T=1 fpg shell nuclei,” *Physical Review Letters,* 2016.

[32] N. J. Zaluzec, “Analytical Formulae for Calculation of X-Ray Detector Solid Angles in the Scanning and Scanning/Transmission Analytical Electron Microscope,” *Microscopy and Microanalysis,* vol. 20, p. 1318–1326, 2014.

[33] TelePresence Microscopy Collaboratory, “http://tpm.amc.anl.gov/,” TelePresence Microscopy Collaboratory, [Online]. Available: http://tpm.amc.anl.gov/NJZTools/XEDSSolidAngle.html. [Accessed 31 August 2016].

[34] University of Jyväskylä , “PCB Assembly 1,” University of Jyväskylä , Jyväskylä , 2015.

[35] University of Jyväskylä, “PCB Assembly 2,” University of Jyväskylä, Jyväskylä, 2015.

[36] University of Jyväskylä, “Guide 1,” University of Jyväskylä, Jyväskylä, 2015.

[37] University of Jyväskylä, “Guide 2,” University of Jyväskylä, Jyväskylä, 2015.

[38] D. Seddon, “The University of Jyväskylä,” [Online]. Available: https://www.jyu.fi/fysiikka/en/research/accelerator/nucspec/jurogam/photos/drawings/great-juro-line2.pdf. [Accessed 15 August 2016].

[39] G. Duchêne, “The Clover: A new generation of composite Ge detectors,” *Nuclear Instruments and Methods in Physics Research A,* vol. 432, pp. 90-110, 1999.

[40] C. W. Beausang, “Measurements on prototype Ge and BGO detectors for the Eurogam array,” *Nuclear Instruments and Methods in Physics Research A,* vol. 313, no. 1, pp. 37-49, 1992.

[41] C. Rossi Alvarez, “Unknown,” *Nuclear Physics News,* vol. 3, p. 10, 1993.

[42] R. D. Page, “The GREAT spectrometer,” *Nuclear Instruments and Methods in Physics Research,* vol. 204, p. 634, 2003.

[43] J. Corkhill, “Ionising Radiation: Registration for Work with Ionising Radiation,” The University of York, York, 2014.

[44] J. Corkhill and S. Gillespie, “Prior Risk Assessment for Ionising Radiation (RA1),” The University of York, York, 2014.

[45] The University of York, “Working with Ionising Radiation: General Module and Sealed Sources,” University of York, York, 2014.

[46] K. Krane, Modern Physics, Wiley, 2012.

[47] RP Photonics Consulting GmbH, “RP Photonics,” [Online]. Available: https://www.rp-photonics.com/signal_to_noise_ratio.html. [Accessed 4 December 2015].

[48] J. Lilley, Nuclear Physics: Principles and Applications, Chichester: Wiley-Blackwell, 2001.

[49] Mathworks, “mathworks.com,” [Online]. Available: http://uk.mathworks.com/help/curvefit/polynomial.html?searchHighlight=polynomial%20order%203. [Accessed 7 July 2016].

[50] G. Woodside, Hazardous Materials and Hazardous Waste Management, New York: John Wiley & Sons, 1999.

[51] R. L. Murray, Nuclear Energy: An introduction to the concepts, systems, and applications and nuclear processes, Burlington: Elsevier, 2009.